12-15-2006

Acoustic Seabed and Target Classification using Fractional Fourier Transform and Time-Frequency Transform Techniques

Madalina Barbu
University of New Orleans

Acoustic Seabed and Target Classification using Fractional Fourier Transform and Time-Frequency Transform Techniques

A Dissertation

Submitted to the Graduate Faculty of the
University of New Orleans
in partial fulfillment of the
requirements for the degree of

Doctor of Philosophy
in
Engineering and Applied Sciences

by

Madalina Barbu

B.S./MS, Physics, University of Bucharest, Romania, 1993
MS, Electrical Engineering, University of New Orleans, 2001

December, 2006

To my family

Acknowledgments

I would like to express my appreciation to Dr. Edit Bourgeois and Dr. Russell Trahan for supervising and reviewing the present dissertation. I would also like to thank Dr. Juliette Ioup, Dr. Dimitrios Charalampidis and Dr. Ralph Saxton for serving in the Ph D thesis defense committee. If it were not for the guidance of my committee, excellent education provided through my graduate studies, the patience and support of my family, this dissertation would not exist. I gratefully acknowledge Naval Research Laboratory for providing me data for testing my algorithm. Finally I acknowledge Reverend Cristian Prusan for his encouragement and prayers throughout the research process.

Table of Contents

List of Tables

List of Figures

Abstract

An approach for processing sonar signals with the ultimate goal of ocean bottom sediment classification and underwater buried target classification is presented in this dissertation. Work reported for sediment classification is based on sonar data collected by one of the AN/AQS-20's sonars. Synthetic data, simulating data acquired by parametric sonar, is employed for target classification. The technique is based on the Fractional Fourier Transform (FrFT), which is better suited for sonar applications because FrFT uses linear chirps as basis functions. In the first stage of the algorithm, FrFT requires finding the optimum order of the transform that can be estimated based on the properties of the transmitted signal. Then, the magnitude of the Fractional Fourier transform for optimal order applied to the backscattered signal is computed in order to approximate the magnitude of the bottom impulse response. Joint time-frequency representations of the signal offer the possibility to determine the time-frequency configuration of the signal as its characteristic features for classification purposes. The classification is based on singular value decomposition of the time-frequency distributions applied to the impulse response. A set of the largest singular values provides the discriminant features in a reduced dimensional space. Various discriminant functions are employed and the performance of the classifiers is evaluated. A study of various classifiers' performance is carried-out for the proposed algorithm under two scenarios for determining the impulse response: FrFT method versus standard deconvolution method. Of particular interest for underwater under-sediment classification applications are long targets such as cables of various diameters, which need to be identified as different from other strong reflectors or point targets. Synthetic test data are used to exemplify and evaluate the proposed technique for target classification. The synthetic data simulates the impulse response of cylindrical targets buried in the seafloor sediments. Results are presented that illustrate the processing procedure. An

important characteristic of this method is that good classification accuracy of an unknown target is achieved having only the response of a known target in the free field. The algorithm shows an accurate way to classify buried objects under various scenarios, with high probability of correct classification.

Chapter 1 Introduction

The problem of pattern classification has been addressed in many contexts and different disciplines. Among the most complex and challenging pattern recognition problems are sediment classification and underwater and under-sediment target classification. The complexity of the problem comes from various factors such as the propagating medium, clutter caused by biological sources in the water column or historical data perishability, mainly in the shallow water littoral regions.

The underwater classification problem involves finding a classification algorithm that improves the classification performance over that of standard algorithms. There are many techniques employed to solve this problem among which pattern recognition ones play an important role. The goal of pattern recognition is to build classifiers that automatically assign measurements to classes. The basis of these techniques is to represent the signal in a favorable space by one or more projection methods; feature vectors are then obtained in this space, usually followed by dimensionality reduction methods. The next step is to use a classification method for determining the class that the signal belongs to; this can be either supervised classification or unsupervised classification (i.e. clustering), depending on the nature of the data. In supervised classification, we are provided with a collection of labels (preclassified patterns). In general, the given labeled patterns (training data) are used to learn the descriptors of classes which in turn are used to label new patterns. In the case of clustering, the problem is to group a given collection of unlabeled patterns into meaningful clusters. In a sense, labels are associated with clusters also, but these category labels are data driven. The classification can be carried out in different ways, depending on the application, the nature of the signal and the final objective.

In this dissertation a novel technique is proposed that allows efficient determination of seafloor

bottom characteristics using the backscattered signal as well as buried target classification. The new approach is based on time-frequency techniques that give a better representation of the signal that leads to a good discrimination of the patterns. The method introduced in this work employs the Fractional Fourier Transform (FrFT) (Ozaktas *et al.* , 2001) in order to compute the impulse response of the seafloor. The FrFT is better suited for chirp sonar applications because it uses linear chirps as basis functions. Singular value decomposition of different distributions (e.g. Wigner, Choi-Williams (Cohen, 1995)) applied to the impulse response is then performed. In this way, discriminant features for classification are obtained due to the fact that the singular value spectrum encodes the most relevant features of the signal. The features thus obtained are mapped in a reduced dimensional space, where various classification approaches are considered and their performance are compared.

This Ph.D. dissertation is organized as follows : Chapter 1 provides an introduction to the research performed on the proposed topics as well as related work on sediment classification, underwater buried target classification and sonar signal processing. Chapter 2 describes the systems used in this work: AN/AQS-20 multibeam sonar and parametric sonar (Kaminsky, 2005). The work presented in Chapter 3, 'Sonar Signal Enhancement using Fractional Fourier Transform' was published in the Proceedings of the SPIE Defense and Security Symposium (Barbu *et al.* , 2005b). Chapter 4, 'Fractional Fourier Transform for Sonar Signal Processing' was published in the Proceedings of the Oceans'05 MTS/IEEE Conference (Barbu *et al.* , 2005a). Chapter 5, 'Acoustic Seabed Classification using Fractional Fourier Transform' was published in the SPIE Defense and Security Symposium (Barbu *et al.* , 2006a). The work reported in Chapter 6, 'Acoustic Seabed Classification using Fractional Fourier Transform and Time-Frequency Transform Techniques' was published in the Proceedings of the Oceans'06 MTS / IEEE Conference (Barbu *et al.* , 2006b). In Chapter 7, new results from empirical studies on

sediment classification using real data are presented. Chapter 8, 'A Time-Frequency Method for Underwater Target Classification' (Barbu *et al.* , 2007) has been submitted to the IEEE International Conference on Acoustics, Speech, and Signal Processing'07. Conclusions and future work are covered in Chapter 9.

1.1 Sediment Classification

Acoustic seabed classification is the organization of the sea floor into seabed sediment types or classes based on characteristics of an acoustic response. Accurate seabed classification is critical in many marine activities, such as marine geology, commercial fishing, cable and pipeline laying and underwater warfare.

The physics and nature of the seabed sonar echoes (return signals) are important for understanding the evaluation of methods used for various underwater applications such as seabed and underwater object classification, the main topics of the current author's work.

The interaction of the acoustic wave with the seafloor is more complex than that its interaction with the sea surface. It is frequency dependent for most of the physical processes such as loss of a part of the incident energy due to seabed penetration, higher sediment absorption (only low frequency can penetrate at a specific level) and internal reflections. At high frequency there is less penetration into the sediment, the wavelength ($\lambda = c/f$, where c is the sound velocity in water and f is the frequency) is smaller, and the scattering from small objects is boosted. Therefore, modeling of the seafloor acoustic interaction processes depends on the frequency. At high frequencies, the interaction is mainly limited to the surface and the structure of the relief. On the other hand, at low frequencies, the model has to include the interaction of the wave with all the sediment layers as well as the sound velocity/density profile. In addition, the grazing angle has to be considered in the model (Lurton, 2002).

Bottom scattering depends on the type of sediment and on the surface roughness which is an indication of the amount of consolidation in the sediment. There are two types of bottom

scattering: surface scattering and volume scattering (Lurton, 2002).

Surface scattering, also called interface scattering, is defined as the scattering which takes place only on the border surface between two different but homogeneous media. The direction of scattering depends on the surface roughness: in the case of a smooth surface there will be a specular reflection with a symmetric angle to the incident angle; when surface roughness increases a little, there exists a component of specular reflection and a scattering component. The component of specular reflection is called the coherent component, while that of scattering is called the diffuse or incoherent component (Lurton, 2002). For completely rough surfaces, only diffuse components will remain, without any component of specular reflection.

The interface backscatter is influenced by the incident angle. In (Jackson *et al.* , 1986), the composite roughness model is applied to bottom backscattering in the frequency range 10–100 kHz. The results show that the Kirchhoff approximation has to be used for small angles near nadir and the composite roughness model for large angles.

Echo coherence decreases with frequency because specular coherent reflections require that the roughness be smaller than the wavelength. If all the scattering is diffuse then the scattering amplitude is independent of direction and the surface is called Lambertian (radiation from a Lambertian surface is isotropic). In addition, for diffused scattering, there is less ping to ping variability.

The surface roughness controls the ratio of coherent to incoherent scattered energy, the intensity of diffuse scattering, thus the backscatter intensity away from nadir, and the ping to ping variability.

Echoes are dominated by the interface scattering at high frequencies. At frequencies lower than 50 kHz (dependent on roughness and acoustic impedance), the volume scattering is important and it may be dominant at a few kilohertz.

Volume scattering depends on the characteristics of water-sediment transmission and absorption inside the bottom, as well as on heterogeneities included in the sediment volume (Lurton, 2002).

The contributions of the interface and volume scattering to the echo are related to the following factors (Novarini & Caruthers, 1998), (Sternlicht & de Moustier, 2003b): the sediment geoacoustical properties, the sediment homogeneity, the sediment attenuation, the sonar frequency, the incident angle and thus the beamwidth and time.

The sediment geoacoustical properties are characterized by acoustic seabed parameters such as: the mean grain size (from small to large values, sediment types are: mud, clay, silt, sand, gravel, pebbles, rock, boulders), the porosity, the density, the relative compressional velocity, the absolute compressional velocity, the reflection coefficient at normal incidence, the compressional absorption coefficient, the shear wave velocity, the roughness spectral strength, standard deviation for roughness along a unit distance and the roughness slope standard deviation (in degrees) (Lurton, 2002).

The product of density and sound speed in a medium defines the acoustic impedance of that medium. In the case of surface scattering, the mean amplitude of the echo is proportional to the ratio of the acoustic impedances sediment/water, whereas in the case of volume scattering, the mean amplitude of the echo is proportional to the ratio of the acoustic impedances of sediment and inhomogeneities, and the number of the scattering centers. Inhomogeneities could be produced by inclusions (e.g. shell fragments) or variations of different parameters such as density, sound speed and compressibility with respect to their mean value.

The biggest contributions to the acoustic reflectivity, as inferred from the above parameters, are given by grain sediment size that influences the packing density, chemical components of the sediment grain that will be reflected in the acoustic impedance, and the roughness of the sediment layer interface (Stanley *et al.* , 1996).

The echo energy and shape are influenced by the nature of the sediment and are frequently used in sediment classification. Echo length needs to be considered since it depends on the penetration distance into the sediment, on the speed of sound in water, on the roughness, on the angle, on the duration of the transmitted pulse and on the sonar beamwidth. Short pulses and wide beamwidth give better discrimination between sediment types.

Seafloor classification techniques depend on the type of signals and the nature of the system (sonar).The single beam echo sounder techniques used for sediment classification are either phenomenological (nonparametric measured echo characteristics are identified with core sample and bottom photographs) or physical (sediment characteristics are evaluated by comparing measurements to predictions made with physical models).

Scattering from boundaries, in the case of single beam echo sounders, can be described by measuring the ratio of the acoustic impedances at boundaries. This procedure is used for low sonar frequencies. After a correct calibration, sediments can be categorized and described in useful ways based on the impedance changes at boundaries (Preston, 2005).

Using the phenomenological approach, Pace and Ceen investigate in (Pace & Ceen, 1982) the bottom roughness based on a comparison of the expanded echo duration with the transmitted pulse. The bottom echo's tail could be considered as an indicator of bottom roughness whereas the energy content of the first surface multiple (bottom-surface-bottom) could be considered an indicator of the reflection coefficient (Pace & Ceen, 1982), (Sternlicht & de Moustier, 2003a). Theoretical studies about the interpretation of the results from (Pace & Ceen, 1982) are performed by Heald and Pace (Heald & Pace, 1996), (Heald & Pace, June, 1998). The physical approach is used by Schock et al. (Schock *et al.* , 1989) and LeBlanc et al. (LeBlanc *et al.* , 1992) to estimate coherent reflection coefficients and to obtain information about sediment attenuation properties. Sediment characterization techniques based on echo envelope inversion are reported in (Jackson

et al. , 1986), (Berry, 1973), (Jackson & Nesbitt, 1988). Lurton uses in (Lurton & Pouliquen, 1992) the cumulative function of the echo envelope in order to obtain features that capture echo shape. Sternlicht and de Moustier proposed in (Sternlicht & de Moustier, 2003a) a sediment geoacoustic parameter estimation technique. It is based on a comparison of bottom returns with an echo envelope model based on incoherent backscatter theory and sediment properties. An average echo amplitude matching procedure iterates on the reflection coefficient to match the peak echo amplitude and separate coarse from fine grain sediments. The procedure is validated through an error analysis using Monte Carlo simulations.

Schock introduced a method, based on the Biot model, for estimating the physical and acoustic properties of the surficial ocean sediments from normal incidence reflection data acquired by a chirp sonar (Schock, 2004). Porosity, grain size and permeability are remotely estimated using the inversion method.

Pace and Gao analyze in (Pace & Gao, 1988) the degree to which different seabed types may be discriminated using features of the power spectrum of the signal backscattered from the seabed.

Among the main methodologies used in swath bathymetry system / multi-narrow beam sonar that employ the variability in the echo structure to infer information on the structure of the seabed, are texture mapping, spectral estimation, echo amplitude peak probability density function (PDF) and acoustic backscatter angular dependence functions (de Moustier, 2000).

Texture mapping is used for seabed image classification and it is based on the identification of significant changes in the characteristics of echoes both within a ping and over a number of consecutive pings. It is an estimation of the 2D statistics on the acoustic backscatter amplitude image of the floor. Boundaries of like texture patterns can be identified using the gray level co-occurrence matrices, that characterize the 2D spatial interrelationships of the gray levels in the image with the texture scale ranging from fine to coarse texture (Barad *et al.* , Spring

2003), (de Moustier, 2000).Classification is based on different texture measures extracted from co-occurrence matrices such as uniformity of energy, entropy, contrast and correlation. In this approach ground truth is required to identify the bottom type properties because there are no models that correlate the physical properties to textures from gray level co-occurrence matrices.

Because amplitude of the seafloor echoes inherits the roughness of the backscattering surface (Lambert's law), the power spectrum shape might be used in classification of the bottom return signals. In order to obtain the geological information, the scattering process and the spatial distribution of the scatterers have to be considered. This method has to take into account the design of the given sonar. The stochastic behavior of the backscatter process can be described by Gaussian distributed instantaneous quadrature samples (de Moustier, 1986)-(Stanton, 1984b), with an echo amplitude distributed accordingly to a Rayleigh-Rice probability density function (Stewart *et al.* , 1994), and the phase uniformly distributed in the interval $[0, 2\pi]$. One can derive a measure of the degree of the coherence of the reverberation process from the statistics of the envelope (a coherent reflection will tend to generate a Gaussian distributed amplitude value and an incoherent scattering will generate Rayleigh distributed values) and offer a link to the surface roughness. The constant mean amplitude over a region gives information about a homogeneous seabed type and gross changes in mean amplitude imply changes in the seabed.

Existing models (de Moustier, 2000) predict angular dependence of the seafloor acoustic backscatter based on the impedance contrast of the sediment-water interface, on the statistics of the roughness of that interface and on possible contributions from volume inhomogeneities within the sediment. The backscattering strength per unit area per unit solid angle that is obtained from measurements is compared to the model predictions to estimate the generating parameters. In order to associate a measurement of backscatter amplitude to a specific grazing angle, an estimation of the reflected ray path and of the seabed slope must be employed. To interpret the

angular response in terms of seabed physical properties, one needs to refer to an appropriate scattering model. One of the most comprehensive models is that of Jackson (Jackson *et al.* , 1986). With no prior knowledge of the seafloor and with the angular response curve as an input, six parameters (ratio of the density and sound speed for seawater and sediment, the exponent and scaling factor of the power law spectral density function describing roughness of the seafloor interface, ratio of the sediment volume backscattering over acoustic attenuation in the sediment and the loss tangent factor) have to be determined and this is a very difficult inverse problem.

Artificial neural networks (ANN) are powerful tools for classification problems. An ANN can learn the classification task from a set of examples known as training set. Multi Layer Perceptron (MLP) is one of the most popular supervised learning ANN models which is frequently used for classification problems. However, when the prior knowledge about the classes in the data is limited, it is difficult to prepare a data set for training the neural network classifier (Baan & Jutten, 2000), (Duda *et al.* , 2004). Neural networks may yield important contributions to finding solutions for underwater applications. Mahale et al. (Mahale *et al.* , 2005) employ various artificial neural network architectures such as Self-Organization Feature Maps (SOFM), Multi-Layer Perceptron (MLP) and Learning Vector Quantization (LVQ) for seafloor classification. They show that in the case of SOFM, a simple moving average echo waveform pre-processing technique yields good classification results on their specific set of data. The LVQ was found to be an efficient seafloor classifier for real-time applications.

A novel statistical scheme for the classification of shallow water acoustic signals aiming at the recovery of the geoacoustical parameters is introduced by Taroudakis et al. in (Taroudakis *et al.* , 2006). The proposed method is based on a transformation of the acoustic signals via a one-dimensional wavelet decomposition and then by fitting the distribution of the subband coefficients using an appropriate function. The classification is achieved by employing a

Kullback-Leibler Divergence similarity measure between underwater acoustic signals.

In this dissertation, a pattern recognition approach with the final goal of improving seabed classification and buried target classification is introduced. The proposed feature extraction method is based on the Fractional Fourier Transform and time-frequency representations.

1.2 Target Classification

Multi-path is a complex problem in sonar data signal processing and represents the arrival of signals at the hydrophones after the first arrival. It may occur due to reflection of a signal at the sea surface, at the sea floor, or at a target, but it can also be caused by bending the acoustic rays via sound speed differences.

The acoustic detection and classification of completely or partially buried objects in the multipath environment of the coastal ocean represent challenging tasks. It is a much more difficult problem than detection and classification of objects in water, due to high backscattering noise generated by sediments and the attenuation experienced in the sediment. Acoustic noise in normal incidence-reflection generated by the volume scattering (from inhomogeneities within the sediments) and surface scattering (from roughness of the sediment) is frequently higher than amplitude of echoes reflected from the buried target of interest (Schock *et al.* , 2001). One more important physical factor which has to be considered is that compressional wave attenuation in sediment is much higher than in water. Taking this into consideration, sonar designed for this type of application will operate at lower frequencies than those used for generating images of targets in water (sidescan sonar).

An acoustic shadow can be formed in the reverberation field, when the target is large compared to the resolution (that is restricted by the acoustic wavelength). The geometry and the target shape will influence the shadow, which therefore play an important role in classification. The contrast of shadows can be improved for better performance.

Acoustic shadow regions in the sidescan sonar images if available could be used for detection

and classification purposes of targets like pipelines by applying segmentation and line fitting (Petillot *et al.* , 2002).

For sonars designed to produce images of buried targets, the acoustic shadows will,unfortunately, not be present due to the diffraction around the target, transmission through the target and relatively high acoustic noise due to backscattering from sediments surrounding the target (Schock *et al.* , 2001). One type of sonar in which the acoustic shadows are absent is the parametric sonar. The author's work is based on parametric sonar data that will be discussed in Chapter 8. Parametric sonars can transmit acoustic signals in the water with a very narrow beam and almost no sidelobes. These characteristics make the echo due to the backscattering from the seafloor surface to be separated in time from the echo due to the signal transmitted through the surface backscattered by the inhomogeneity in the seafloor sediment (Caiti *et al.* , 1999). In addition, the property of the parametric sonar that the difference-frequency wave has no sidelobes makes it attractive for shallow water measurements since it prevents interference from unwanted boundary interactions (Hines, 1999). The first work regarding parametric sonar was reported by Westervelt in (Westerwelt, 1957). Hines (Hines, 1999), Voronin and Timoshenko (Voronin & Timoshenko, 1994) and Cook et al. (Cook *et al.* , 1997) present various designs of the receiving parametric array that improve the performance of the standard parametric sonar. Using linearly frequency-modulated signals gives information about frequency dependence of volume backscattering coefficient at one pulse, and in addition increases the signal to noise ratio (Voronin *et al.* , 1994). Parametric sonars have been used in an increasing number of applications in past years, ranging from traditional seismic processing to more complex systems for object detection and classification (Woodward *et al.* , 1994a), (Woodward *et al.* , 1994b). Woodward and Lepper report in (Woodward & Lepper, 2003) a study based on an open-water trial using a parametric sonar system with the aim of detecting and classifying embedded or partially embedded

objects such as pipelines, lost cargo and mines. The main finding was that both specular reflections and resonance effects could be observed and they proposed that these could contribute to the classification of targets.

Guyonic introduced in (Guyonic, 2000) a new concept suitable for mine detection and classification in shallow and very shallow water, based on 3-D high-resolution imaging information obtained from a 2-D scanning sonar. Underwater mine and object detection and shape classification have been successfully demonstrated up to half a meter sediment burial.

In the absence of shadows the classification of buried targets such as pipes and cables is more difficult because the images do not provide information about the target shape due to the fact that scattering from oblique target surfaces is not detectable (Schock *et al.* , 2001). The geometry of the arrays of multibeam and sidescan sonars makes it barely possible to detect buried objects not oriented parallel to the ship's track. For improving the imaging of these buried objects, synthetic aperture sonars are being developed (Feranadez & Christoff, 2000), (Neudorfer *et al.* , 2000). Using this type of sonar and an energy detector algorithm, the coordinates of buried targets can be obtained (Schock *et al.* , 2001).

In recent years pattern recognition techniques have been employed for solving various underwater problems such as seabed classification discussed earlier and detection/classification of buried objects. The general procedure of these techniques consists of mapping the signal into a favorable space by one or more projection methods and then obtaining feature vectors extracted in order to perform the classification of the patterns. Sonar echo features which are useful in capturing details rich in target information such as rise time, decay time, echo shape and power spectrum are often employed. Backscatter image features such as mean, standard deviation, higher order statistics, Haralick features, histogram, fractal dimension, etc. can also be used. Among the most widely used projection techniques are short time Fourier transform, Principal Component

Analysis (PCA), fractal analysis and spectra. Regarding the final step that involves classification of the computed features, different approaches have been presented in the literature including Bayesian classifiers, nonparametric techniques (nearest neighbor), hidden Markov models and neural networks.

Shin and Kil introduced in (Shin & Kil, 1996) the classify-before-detect algorithm for detection of signals that are partially known and deeply embedded in noise. The processing strategy is based on three steps: exploitation of any microstructure present in target signature by projecting raw data onto appropriate low-dimensional projection spaces, followed by identification of "features" crucial in determining the presence of signal, and finally designing a classifier topology that best matches the underlying feature distribution to minimize modeling errors.

Boulinguez *et al*. proposed in (Boulinguez *et al.* , 1998) an adapted technology for a parametric sonar for obtaining a complete identification and localization of objects embedded in sediment. The parametric sonar is used to acquire 3D data on the subbottom area. Wavelets are employed for eliminating the noise and high order spectra are used both to improve the range resolution and for classification. Later on Boulinguez and Quinquis investigated in (Boulinguez & Quinquis, 2000) object classification using features extracted from the entropy of the Wavelet packet coefficients and from fractal analysis.

Miao *et al*. introduced in (Miao *et al.* , 1998) a new system consisting of six channels which uses principal component analysis for features extraction and then neural networks for detection and classification of targets in six different optical bands ranging from near UV to near IR. The outputs of the detector/classifier networks in all the channels were fused together in the final decision making system.

Azimi-Sadjadi *et al*. proposed in (Azimi-Sadjadi *et al.* , 1998) and (Azimi-Sadjadi *et al.* , 2000) a classification system that consists of a feature extractor using wavelet packets in conjunction

with linear predictive coding, a feature selection scheme and a backpropagation neural network classifier. A multiaspect fusion scheme was also employed for improving the classification performance.

Donghui *et al.* tested and benchmarked different classification algorithms for underwater targets in (Donghui *et al.* , 2004) not only for their performance but also to gain insight into the properties of the feature space. Results for a wideband 80 kHz acoustic backscattered data set collected for six different objects are presented in terms of the receiver operating characteristic (ROC) and robustness of the classifiers with respect to reverberation.

Trucco and Pesceto in (Trucco & Pescetto, 2000), and Trucco (Trucco, 2001) presented a pattern recognition method for the detection of buried objects. The beamformed signals are divided into partially overlapped frames and then projected in the joint time-frequency space. Features are extracted and fed into a multivariate Gaussian classifier.

Kundu *et al*. use hidden Markov model (HMM) for sonar transient classification in (Kundu *et al.* , 1994). In HMM methodology, the signal is divided into a sequence of frames, and each frame is represented by a feature vector. This sequence of feature vectors is then modeled by one HMM. Thus, the HMM methodology is highly suitable for classifying the patterns that are made of concatenated sequences of micro patterns. The sonar transient signals often display an evolutionary pattern over the time scale. Three different feature vectors based on an autoregressive (AR) model, Fourier power spectra, and wavelet transforms are considered in their work. One HMM is further developed for each class of signals. During testing, the signal to be recognized is matched against all models. The best matched model identifies the signal class. The set of features extracted is then used with a multilayer perceptron neural network (NN) classifier. A combined NN/HMM classifier is proposed, and its performance is evaluated with respect to other classifiers.

Runkle *et al*. introduced in (Runkle *et al.* , 1999) an approach for target identification, in which they fuse scattering data from multiple target-sensor orientations. The multiaspect data is processed via hidden Markov model (HMM) classifiers, based on physics-based feature extraction. That approach explicitly accounts for the fact that the target-sensor orientation is generally unknown or "hidden".

Feature orthogonalization and independence transformation with likelihood ratio testing have been used for target classification from 2D sonar images in (Aridgides *et al.* , 1996). Neural networks and clustering algorithms were employed in (Dobeck *et al.* , 1997).

A system for detection and classification of buried objects using the Buried Object Scanning Sonar (BOSS) was presented in (Schock *et al.* , 2001), (Sternlicht *et al.* , 2002) and (Sternlicht *et al.* , 2001). It consists of four modules: localization/detection of buried objects, classification based on time series echo, image feature classification, and fusion. The image classification uses a joint Gaussian Bayesian classifier, the Soft Tree Score (STS). The STS measures feature distributions, transforms these to Gaussian distributions, then computes covariances of the features, and finally classifies using a log-likelihood ratio and a threshold. Detection is performed with an energy-clustering algorithm. Scalar and volume cell distribution features are extracted and used for target classification. Features include dimensions and co-occurrence statistics. Sternlicht *et al*. are using features extracted from 3D images such as target strength, energy density, and spatial measure as classification features for buried targets (Sternlicht *et al.* , 2002). Short-time Fast Fourier Transforms (STFFT) and PCA are used on the echo time series for signal classification to provide compressed features to a back-propagation neural network (BP NN) 2-class classifier.

Dobeck presents in (Dobeck, 2005) a probabilistic score-based algorithm fusion that achieves significant false alarm reduction. Score-based algorithm fusion is the fusion of multiple detection

and classification algorithms where only the scores of the individual algorithms are used to make a final determination on whether an object is a target or not. Multiple detection and classification algorithms process the same sensor data looking for target-like objects. A positive score is assigned to each object detected and classified as target-like by a given algorithm, which indicates the degree to which the algorithm considers the object target-like. Despite the fact that only the scores are used in the fusion process, false alarm reduction has been remarkable, according to the author while still preserving a high probability of target detection and classification.

1.3 Sonar Signal Processing

In this subsection of the introduction, a review of relevant issues in sonar signal processing is presented. Underwater acoustic systems employ a limited variety of signals that are chosen based on their capability to carry information, on the underwater environment and on the applications (detection, communication, measurement, characterization). Active sonars use controlled signals, whose characteristics are imposed during the transmission phase (duration, frequency content, level) and whose reception involves suited filtering of these characteristics. On the other hand, passive sonars do not have the capability to control the characteristics of the signals that need to be analyzed. The data processing is based on the *a priori* assumptions of the signal received (broadband, narrowband, pulse) (Lurton, 2002).

In the case of active sonars, the selection of the transmitted signal characteristics is made to minimize the effects of the channel, or medium (i.e. surface, bottom and volume scatters). The effects of the channel, namely time dispersion, frequency dispersion and angle dispersion, are largely discussed in the literature (Urick, 1975), (Burdic, 1984), (Nielsen, 1991). The spread of the pulse in time is a result of the presence of different propagation paths, whereas frequency dispersion depends on the scatterer movements with respect to the transmitter (Nielsen, 1991). The most common sonar signal design parameters used are frequency spectrum, time and space resolution of the signal, correlation function, time and frequency resolution.

One of the frequently used signals in underwater acoustics is a narrowband pulse (continuous wave (CW) pulse or a "burst"). A CW pulse consists of a constant amplitude sine wave of a specific frequency f_o, for a limited time. The frequency spectrum is a sinc function. Generally, the frequency range is from 12 kHz to 200 kHz for corresponding pulse durations of 10 ms to 0.1 ms (bandwidth of 0.1 kHz -10 kHz) (Lurton, 2002). The ratio $\frac{\delta f}{f_0}$ is very small for this type of signal and it is considered as a narrowband pulse. One advantage of using CW pulses is the simplicity of their transmission and processing. Processing employs bandpass filtering and envelope detection of the filtered signal. Their narrow frequency band makes them well matched with narrowband transducers that are easy to design, cheap and efficient (Lurton, 2002). Their poor spectral content, however, has led to a decrease in interest in using them in advanced processing for target characterization.

Another commonly used signal in underwater acoustics is the linear frequency modulated (LFM) pulse or linear chirp. The instantaneous frequency of the chirp signal is given by the time derivative of the phase and the frequency spectrum of the chirp signal can be roughly approximated by a rectangle centered at the central frequency. A time correlation procedure followed by an envelope detection is the coherent processing for frequency-modulation signals (Lurton, 2002). Chirp signals (processed by correlator) achive high PG processing gain ($PG = 10\log(BT)$, where T is the duration of the chirp and B is the bandwidth of the chirp) by increasing independently T and B. For this reason, chirp signals are more attractive than narrowband pulses. In this case a good time resolution at the receiver is maintained. The chirp processing is more complex than that of the CW pulse but it is necessary when high SNR is needed such as in miltary applications for accurate long range detection, sediment and buried target classification.

Sonar signal processing includes conventional and adaptive beamforming, broadband

processing, matched field processing or passive and active signal processing.

Although adaptive beamforming can provide significant gains in performance in some environments and for some tactical situations, matched field methods can provide additional gains or information. Matched field processing couples signal processing with a thorough understanding of the acoustic environment. Environmental models are used to define signal representations used in the signal processing algorithms. This requires advanced simulation modeling capability. The signal representations are then used in specially designed signal processing algorithms to extract information on the contacts of interest (Baggeroer *et al.* , 1993).

Passive sonar signal processing with military applications has a primary objective to develop signal processing algorithms that detect, classify and locate modern submarines at tactically useful ranges in shallow water environments. The interest in active sonar signal processing has increased in the last decade. Military applications in this field include surveillance and defense. The research is focused on improving the effectiveness of operating active sonar systems in acoustically complex shallow water environments.

Active sonar processing chain is a series of operations that has to be performed to go from the raw acoustic data reception to the final output (detection or classification). The data from the sensor array are beamformed to assess the directionality of the arrival echoes (Baldacci & Haralabus, 2006). The standard chain procedure consists in applying a matched filter in order to improve the signal to noise ratio and then to normalize the obtained output in order to remove the background interference. The matched filter correlates the receiver echo with a real or synthetic replica of the transmitted signal. Synthetic replicas are easy to use but may vary severely from the actual transmitted signal due to source and environmental conditions. The final algorithm for sonar signal processing will depend on the application such as detection or classification.

One of the most frequently used tools in signal processing is Fourier analysis. In the last

couple of decades, the interest in the time-frequency representations of the signal has increased (Mecklenbrauker & F.Hlawatsch, 1997)-(Lin *et al.* , 2004). Different types of joint time-frequency distributions are often employed in signal processing in order to extract the characteristic behavior of signals. Major research directions include time-frequency analysis for target and pattern recognition, noise reduction, beam forming, and optical processing. One of the important tools for time-varying signal analysis is the Fractional Fourier transform (FrFT), that is a generalization of the classical Fourier transform. Time-varying signal analysis uses a time-frequency plane, with two orthogonal axes, time and frequency (Hlawatsch & Bourdeaux-Bartels, 1992). Besides being a generalization of the Fourier transform, the FrFT has been proven to be related to other time-vaying signals tools, such as Wigner distribution, short Fourier transform (Hlawatsch & Bourdeaux-Bartels, 1992), wavelet transform, and so on. The relationship between time-frequency distributions and the fractional operations, and some of their applications (such as filter design, pattern recognition, beam shaping) are presented by Pei and Ding in (Pei & Ding, 2001). Traditionally, FrFT has been used as a modeling tool in quantum mechanics (Namias, 1980) and in optics systems (Ozaktas *et al.* , 1994). Recent applications of the FrFt include signal characterization (Coetmellec *et al.* , 2001)-(Capus *et al.* , 2000), signal recovery and restoration (Kutay *et al.* , 1995)-(Erden *et al.* , 1999), beamforming (Yetik & Nehorai, 2003), detection and parameter estimation (Lin *et al.* , 2004).

Signal compression is another application (Yetik *et al.* , 2001) where one or more Fractional Fourier Transforms are computed and filtered to obtain simpler representations of the signal. FrFT has played an important role in digital image processing (i.e., image encryption, digital watermarking) as well as (Hennelly & Sheridan, 2003a)-(Djurovic *et al.* , 2001).

The traditional Fourier transform decomposes signals by sinusoids whereas Fractional Fourier transform corresponds to expressing the signal in terms of an orthonormal basis formed by chirps,

and therefore more suitable for radar and sonar signal processing.

Akay proposed in (Akay, 2002) a possible application of fractional cross-correlation for signal detection in radar or active sonar systems. Fractional cross-correlation was computed between the transmitted signal and the return signal. The results showed that the fractional cross-correlation might perform better in noisy environments than the conventional cross-corelation. Thus a good resolution in terms of detecting closely spaced targets could be achieved. In general, a conventional radar can not directly resolve the targets flying in a group in both range and azimuth.

The FrFT has also been considered in underwater applications. In order to achieve the maximum detection range for active sonars, various sonar arrays and sonar signal processing algorithms have been proposed in the literature. A method for prediction of the radiation characteristics of the array using the Fractional Fourier transform algorithm was introduced by Musha et al. in (Musha *et al.* , 2002).

Modern methods for acoustic underwater channel characterization employ the passive tomography concept. Quinquis et al. used the FrFT in (Quinquis *et al.* , 2003) for expressing the received signal for an ideal acoustic channel as a sum of sinusoids. Their frequencies are directly related to the time delays of the arrivals. In order to distinguish the arrivals which are close together in time, a high resolution spectral estimation method was applied, providing their time delays. Thus the characteristics of the acoustic channel could be estimated.

A method of anti-reverberation based on the FrFT was introduced by Bin et al. in (Bing *et al.* , 2003) which could be interpreted as a swept-frequency filter. A narrow-band filter in the Fractional Fourier domain was used to remove the reverberation and then the filtered signal was reverted back by applying the inverse Fractional Fourier transform.

Levonen shows through empirical studies on sonar data in (Levenon & McLaughlin, 2002) that short time Fractional Fourier Transform (STFrFT) has significant advantages over the

traditional short time Fourier Transform. STFrFT has a great potential in sonar signal processing applications, given the known parameters of the transmitted pulse.

In this Ph. D. dissertation the author develops a feature extraction method based on the FrFT and time-frequency representations that improve the performance of the acoustic seabed and buried target classification.

Chapter 2 System Description

In this dissertation, the author uses data collected by the Volume Search Sonar (VSS) for sediment classification and parametric sonar synthetic data for target classification. For buried target classification only the simulated data are analyzed. All generated simulations correspond to a parametric sonar. Relevant characteristics and specification of each used systems are summarized in this chapter.

Multibeam sonars use a fan of elementary beams that rapidly sweeps a large swathe of the seabed and measures its relief. Interpretation of the acquired data leads to a better understanding of seabed features and processes. If the angular aperture is large enough acoustic images can be obtained like those produced by sidescan sonars.

2.1 Volume Search Sonar (VSS)

Raytheon's AN/AQS 20 system (Raytheon, 1999) incorporates a towed body that is towed using a fiber optic tow cable by an MH 53 or MH 63 helicopter . The towed body has a length of 10.6 ft and a width of 15.5 in and it consists of the five sonars and various sensors. One of the five sonars is the Volume Search Sonar that is a multibeam sonar. It can operate in two modes: volume mode and single pass deep mode, but in this thesis only the former is considered (Raytheon, 1999).

The acoustic energy received by the hydrophone array is preamplified and then conditioned. Signal conditioning consists in the following: dynamic range compensation using time varying gain (TVG), bandshifting to a common intermediate frequency of 750 KHz and bandpass filtering. Next, the data is A/D converted and undersampled at a rate of 200 KHz (Raytheon, 1999).

A beamforming function forms all beams and then quadrature demodulates the beam data to baseband. The beamforming is a hybrid time delay-phase shift function. The beam output are

produced by shading (weighted sum) of array element data, delayed to compensate for cylindrical array geometry.

VSS presents two separate arrays: the projector array and the receive array and they are presented in the following subsections.

2.1.1 Receive Array

The VSS receive cylindrical array consists of 54 beams in total, 27 beams fore and 27 beams aft. The configuration of the of the fore-aft beam pair depends on the mode as well as on the range used. In the Volume mode the pairs are normal to the tow body with one beam squinted slightly forward and one beam slightly aft. The beamwidth is narrow at long ranges and broad at short ranges.

The cylinder has a diameter of 15.5 in and the receive aperture is 12.6 in. The cylinder is partially populated with horizontal staves. There are 40 staves, each consisting of 9 receive elements. The staves are spaced at 7.16° thus covering 286.4° of the cylinder (there are nine receive elements on each stave, each element is 1.26 in long and 0.89 in wide). Radially, the central beams are formed using 16 adjacent staves and the outer beams are formed using 14 staves. Nine elements are used for long ranges (narrow beam), and five elements are used for short range (wide beam) (Raytheon, 1999).

2.1.2 Projector Array

The projector array has five rings of ceramic elements on the same cylinder as, and just forward of, the receive array. There are either 2 or 3 elements on two adjacent staves, each element dimension being 0.84 in $\times$ 1.27 in. Hence for 40 staves there are 100 transmit elements. The five rings are driven in phase for the Volume mode (Raytheon, 1999).

The VSS transmitted waveform is a chirp with a duration of 4.32 ms. It can be described as a 10.4 KHz wide stepped frequency modulated (FM) signal consisting of 12 sub-pulses, each 360 microsecond long. The signal is a stepped approximation to a linear FM waveform (Kaminsky,

2002) and the separation between each subpulse is 867 Hz. A synthesized VSS transmited IQ pair is shown in Figure 2.2. The duration and the corresponding bandwidth of the source transmitted signal is illustrated in Figure 2.3.

2.2 Parametric Sonar

2.2.1 Standard Parametric Sonar

Parametric sonars have been developed for more than 30 years. Their performance has increased and they are now widely used in sub-bottom profiling as well as in detecting and discriminating buried objects (Foote & Francis, 2005). The principle governing the behavior of the parametric sonar consists of simultaneously generating of two collinear acoustic waves at different high frequencies. The intrinsic nonlinearity of the medium causes the two waves to interact, forming new, secondary waves at the sum and difference frequencies (Foote & Francis, 2005). If the primary waves are close in frequency, then the difference-frequency will be quite low, but the corresponding beam will preserve the basic directionality of the primary source without sidelobes. As a result of differential absorption, the primary and the sum-frequency waves are more rapidly absorbed compared to the difference-frequency wave, that can propagate to relatively large distances with little absorption.

The interest in parametric acoustic arrays derives from their great directivity, narrow beamwidth and absence of side lobes in the radiation patterns. The narrow beam is a result of the shape of the zone of modulation (Muir, 1974) (the longer the zone, the smaller the bandwidth). The attributes of the parametric sonar can be used to achieve significant reduction in the volume and surface scattering strength in the reverberation, especially in shallow water where a multipath interference occurs for the conventional linear sonar. Slight changes in, or modulation of one or both of the primary frequencies can generate a relatively broad, low frequency band. Recent systems can operate with various signal waveforms for optimum performance. Ricker pulses are generally used for very high resolution work, chirp pulses are used for deep water and high penetration

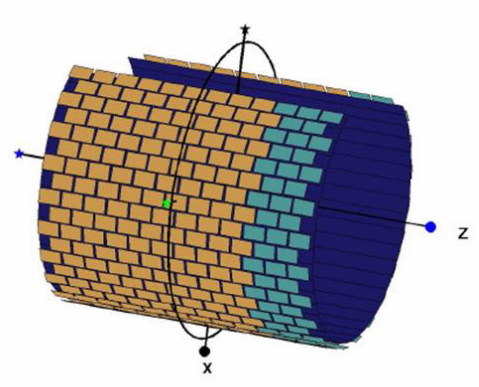

Figure 2.1: VSS Array Geometry

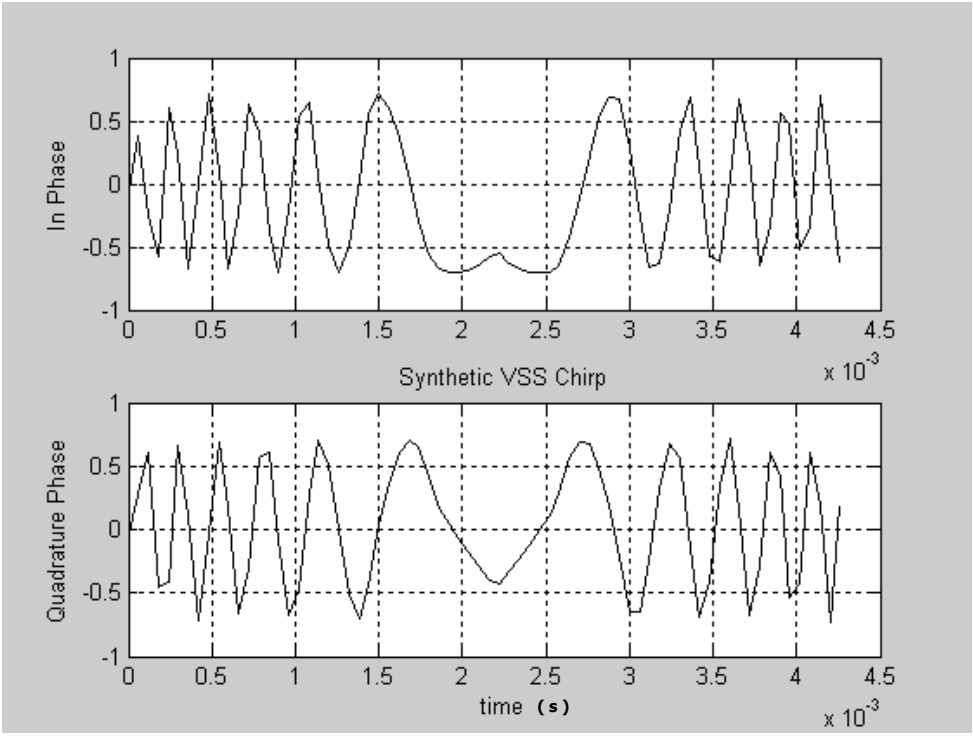

Figure 2.2: VSS transmitted pulse

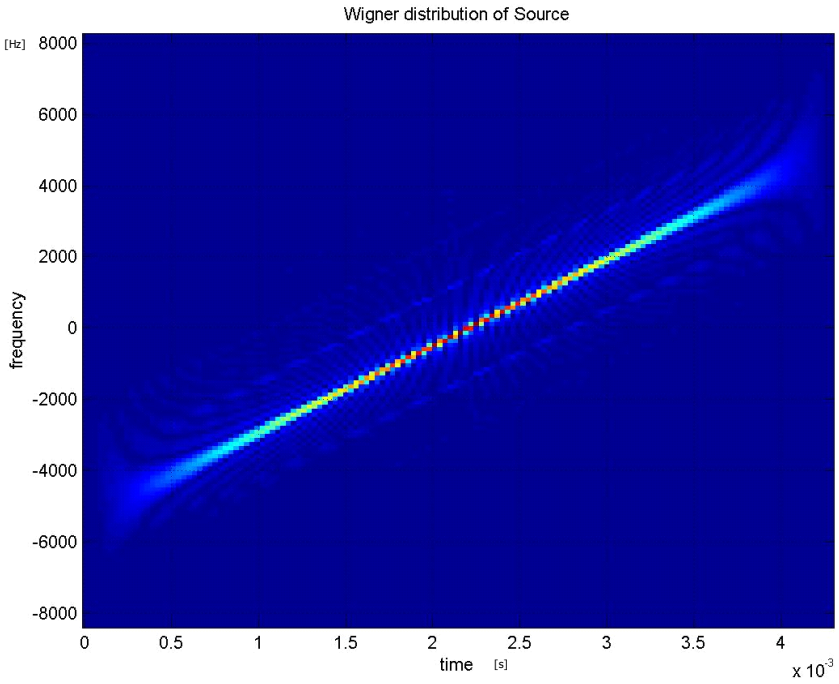

Figure 2.3: Wigner distribution of VSS transmitted pulse

applications, and continous wave (CW) pulses are used for narrow band, frequency sensitive work (Dybedal, 1993).

These advantages determine high relative spatial and temporal resolution, that are useful in applications such as object detection and classification.

Chapter 3 Sonar Signal Enhancement using Fractional Fourier Transform

Madalina Barbu, Edit J. Kaminsky, Russell E. Trahan*

Department of Electrical Engineering, *College of Engineering,

University of New Orleans, 2000 Lakeshore Dr., New Orleans, LA, 70148

Abstract

In this paper we present an approach for signal enhancement of sonar signals. Work reported is based on sonar data collected by the Volume Search Sonar (VSS), as well as VSS synthetic data. The Volume Search Sonar is a beamformed multibeam sonar system with 27 fore and 27 aft beams, covering almost the entire water volume (from above horizontal, through vertical, back to above horizontal). The processing of a data set of measurement in shallow water is performed using the Fractional Fourier Transform algorithm. The proposed technique will allow efficient determination of seafloor bottom characteristics and bottom type using the reverberation signal. A study is carried out to compare the performance of the presented method with conventional methods. Results are shown and future work and recommendations are presented.

Keywords: Fractional Fourier transform, impulse response, sonar signal processing, Wigner distribution, volume search sonar.

3.1 Introduction

The reported data herein is based on sonar data collected by the Volume Search Sonar (VSS), one if the five sonar System in the AN/AQS-20. The AQS-20 system is an underwater towed body containing a high resolution, side-looking, multibeam sonar system used for minehunting along the ocean bottom, as well as a forward looking sonar, and the volume search sonar. The system is illustrated in Figure 3.1. The VSS consists of two separate arrays: the transmit array and the receive array. The VSS is a beamformed multibeam sonar system with 54 beams arranged as 27

Figure 3.1: AQS – 20 mine hunting sonar

fore–aft beam pairs, covering almost the entire water volume (from above horizontal, through vertical, back to above horizontal) (Raytheon, 1999).The VSS can be used in two modes: volume mode and Single Pass Deep (SDP) mode. The acoustic energy received by the VSS hydrophone array is pre-amplified and conditioned. Conditioning includes dynamic range compensation using time varying gain (TVG), bandshifting to IF (750 KHz), and band pass filtering. After conditioning, analog to digital (A/D) conversion is performed and signals are undersampled at 200 KHz. The beamforming function forms all beams and then quadrature demodulates the beam data to baseband (only the image centered at 50 KHz is retained and basebanded). A hybrid time delay phase shift function is used to beamform by using a Hilbert transform after the element delays. The beam outputs are produced by shading (weighted sum) of array element data, delayed to compensate for cylindrical array geometry. Data from this sonar may be used for bathymetry computation, bottom classification, target detection, and water volume investigations (Raytheon, 1999), (Kaminsky, 2002).

Our investigation is focused on the bottom-return signals since we are interested in determination the impulse response of the ocean bottom floor. The bottom-return signal is the convolution between the impulse response of the bottom floor and the transmitted sonar chirp

signal. The method developed here is based on Fractional Fourier Transform, a fundamental tool for optical information processing and signal processing. In recent years, interest in and use of time-frequency tools has increased and become more suitable for sonar and radar applications (Levenon & McLaughlin, 2002), (Akay, 2002), (Yetik & Nehorai, 2003). Major research directions include the use of time-frequency analysis for target and pattern recognition, noise reduction, beamforming, and optical processing. In this paper we begin by presenting the essential concepts and definitions related to Fractional Fourier transform. The overview is followed by a description of the implementation of the Fractional Fourier transform and the methods proposed for evaluating the impulse response of the ocean bottom. The Fractional Fourier transform requires finding the optimum order of the transform based on the properties of the chirp signal. The bottom impulse response is given by the magnitude of the Fractional Fourier transform applied to the bottom return signal. The technique introduced in this work has been tested both on the synthetic data and real sonar data. A study is carried out to compare the performance of the presented method to conventional methods. Results are shown and future work and recommendations are presented.

3.2 Fractional Fourier Transform Overview

The Fractional Fourier transform (FrFT) is a generalization of the identity transform and the conventional Fourier transform (FT) into fractional domains. The traditional Fourier transform decomposes signal by sinusoids whereas Fractional Fourier transform corresponds to expressing the signal in terms of an orthonormal basis formed by chirps. The Fractional Fourier transform can be understood as a Fourier transform to the a^{th} power where a is not required to be an integer. There are several ways to define the FrFT; the most direct and formal one is given by (Ozaktas *et al.* , 2001):

$$f_\alpha(u) = \int_{-\infty}^{\infty} K_a(u, u') f(u') du' \tag{3.1}$$

where

$$\alpha = \frac{a\pi}{2}$$

$$K_\alpha(u, u') = A_\alpha \exp[i\pi(\cot\alpha \cdot u^2 - 2\csc\alpha \cdot u \cdot u' + \cot\alpha \cdot u'^2)]$$

$$A_\alpha = \sqrt{1 - i\cot\alpha}$$

when $a \neq 2k$,

$$K_\alpha(u, u') = \delta(u - u')$$

when $a = 4k$, and

$$K_\alpha(u, u') = \delta(u + u')$$

when $a = 4k + 2$, where k is a integer and A_α is a constant term and the square root is defined such that the argument of the result lies in the interval $(-\frac{\pi}{2}, \frac{\pi}{2}]$.The order of the transform is a. If we set $a = 1$, that corresponds to $\alpha = \frac{\pi}{2}$ and $A_\alpha = 1$ such that the FrFT becomes the ordinary Fourier transform of $f(u)$:

$$f(u) = \int_{-\infty}^{\infty} e^{-i2\pi uu'} f(u') du' \tag{3.2}$$

Due to periodic properties, the range of a , the order of the transform can be restricted to $(-2, 2]$or $[0, 4)$, respectively $\alpha \in (-\pi, \pi]$ or $\alpha \in [0, 2\pi)$. The Fractional Fourier transform operator, F^a, satisfies important properties such as linearity, index additivity $F^{a_1}F^{a_2} = F^{a_1+a_2}$, commutativity$F^{a_1}F^{a_2} = F^{a_2}F^{a_1}$, and associativity$(F^{a_1}F^{a_2})F^{a_3} = F^{a_1}(F^{a_2}F^{a_3})$. In the operator

notation, these identities follow: $F^0 = I$; $F^1 = F$; $F^2 = P$; $F^3 = FP = PF$;$F^4 = F^0 = I$; and $F^{4k+a} = F^{4k\prime+a}$, where I is an identity operator, P is a parity operator, and k and $k\prime$ are arbitrary integers. According to the above definition 3.1 the zero-order transform of a function is the same as the function itself $f(u)$, the first order transform is the Fourier transform of $f(u)$, and the $\pm 2^{nd}$ order transform is equal to $f(-u)$.

One of the most important properties of the FrFT states that the Wigner distribution of the FrFT of a function is a rotated version of the Wigner distribution of the original function (Ozaktas *et al.* , 2001):

$$W_{f_a}(u,\mu) = W_f(u\cos\alpha - \mu\sin\alpha, u\cos\alpha + \mu\sin\alpha) \tag{3.3}$$

The Wigner distribution of a signal f is defined as:

$$W_f(u,\mu) = \int f^*(u - u'/2) f(u + u'/2) e^{-j2\pi\mu u'} du' \tag{3.4}$$

and can be interpreted as a function that indicates the distribution of the signal energy over the time-frequency space.

The most significant properties of the Wigner distribution are stated in the following equations:

a.

$$\int W_f(u,\mu) d\mu = |f(u)|^2 \tag{3.5}$$

b.

$$\int W_f(u,\mu) du = |F(\mu)|^2 \tag{3.6}$$

c.

$$\iint W_f(u,\mu) du d\mu = E[f] \tag{3.7}$$

d. If

$$g(u) = h(u) * f(u)$$

then,

$$W_g(u,\mu) = \int W_h(u-u',\mu) W_g(u',\mu) du' \tag{3.8}$$

e. If

$$g(u) = h(u) f(u)$$

then,

$$W_g(u,\mu) = \int W_h(u,\mu-\mu') W_g(u,\mu') d\mu' \tag{3.9}$$

g. Wigner distribution of the Fourier transform is the Wigner Distribution of the original function rotated clockwise by the right angle.

The Wigner distribution is completely symmetric with respect to time-frequency domains, it is everywhere real but not always positive. The Wigner distribution exhibits advantages over the spectrogram (short-time Fourier transform): the conditional averages are exactly the instantaneous frequency and the group delay, whereas the spectrogram fails to achieve this result, no matter what window is chosen. The Wigner distribution is not a linear transformation, a fact that complicates the use of the Wigner distribution for time-frequency filtering.

The ambiguity function has a correlative interpretation and it is defined as (Ozaktas *et al.* , 2001):

$$A_f(\overline{u},\overline{\mu}) = \int f^*(u'-\overline{u}/2) f(u'+\overline{u}/2) e^{-j2\pi\overline{\mu}u'} du' \tag{3.10}$$

This ambiguity function is related to the Wigner distribution as a two-dimensional Fourier transform:

$$A_f(\overline{u},\overline{\mu}) = \iint W_f(u,\mu) e^{-j2\pi(\overline{\mu}u-\overline{u}\mu)} du d\mu \tag{3.11}$$

Another relationship between the Wigner distribution and the Fractional Fourier transform is

given by the Radon transform operation, RDN_α, which maps a two-dimensional function to its integral projection onto an axis making angle $\alpha$with the u axis (Ozaktas *et al.* , 2001):

$$\int W_{fa}(u,\mu)d\mu = RDN_\alpha[W_f(u,\mu)] \tag{3.12}$$

Using equation 3.12 equations 3.7 and 3.8 can be generalized and expressed in terms of the Radon transform as:

$$RDN_\alpha[W_f(u,\mu)] = |f_a(u)|^2 \tag{3.13}$$

Equation 3.13 is a powerful relation that can be applied to determine the relationship between the magnitude of the a order of the Fractional Fourier transform and the Wigner distribution .

3.3 Application of the Fractional Fourier Transform

In order to evaluate Fractional Fourier transform techniques, several methods have been proposed (Ozaktas & Arikan, 1996). Fast computation of the Fractional Fourier transform implies different decompositions that lead to different algorithms. Successive steps of simple operations such as chirp multiplication followed by chirp convolution followed by another chirp multiplication yield the fast convolution algorithm(Ozaktas & Arikan, 1996). Optimization of the main interval of the fractional order increases calculation accuracy (Yang *et al.* , 2004).

In this paper we use a Fractional Fourier transform Matlab routine available from the Mathworks website. First, a chirp with the specific parameters characterizing the system in questions —such as a bandwidth of 10400 Hz and a chirp duration of 4.32 ms for VSS— are generated. In order to corroborate our techniques we generate a synthetic impulse response of the seafloor, a Green function is utilized. The synthetic sonar return signal is generated by the convolution between the Green function and the transmitted VSS chirp. This synthetic data were used for testing both methods: classical frequency-domain deconvolution and our proposed deconvolution using Fractional Fourier transform.

The classical method applies the inverse Fourier transform to equation 3.14 to obtain the impulse response

$$H(\varpi) = H_I(\varpi) + H_Q(\varpi) \tag{3.14}$$

where $H(\varpi)$ is the Fourier transform of the impulse response and it has a real (in-phase) part and imaginary (quadrature-phase) part given by:

$$H_I(\varpi) = \frac{R_I(\varpi)P_I(\varpi) + R_Q(\varpi)P_Q(\varpi)}{P_I^2(\varpi) + P_Q^2(\varpi)} \tag{3.15}$$

$$H_Q(\varpi) = \frac{-R_I(\varpi)P_Q(\varpi) + R_Q(\varpi)P_I(\varpi)}{P_I^2(\varpi) + P_Q^2(\varpi)} \tag{3.16}$$

In equations 3.14 and 3.15 , $R(\varpi)$ and $P(\varpi)$ are the Fourier transforms of complex baseband received signal and of transmitted pulse, respectively. The subscripts I and Q denote, respectively, the real (in-phase) and imaginary (quadrature-phase).

The second method consists of using the Fractional Fourier transform that is applied to the sonar return data. The order of the transform is determined by the chirp properties: the rate of change λ , sampling rate fs and the length of the data segment N (Levenon & McLaughlin, 2002):

$$\alpha = \frac{2}{\pi}\tan^{-1}(fs^2/2\lambda N) \tag{3.17}$$

Wigner distribution has been used to visually determine the correct order of the transform. The optimum transfer order is achieved when the representation of the chirp in the Wigner distribution is a delta function. If the properties of the chirp are not known, a can be optimized visually. The impulse response is given by the absolute value of the correct order of the Fractional Fourier transform of the function that represents the return data:

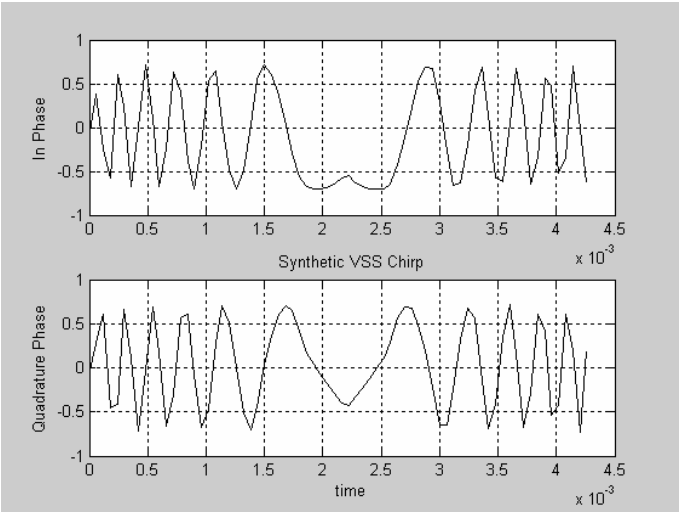

Figure 3.2: In-phase and Quadrature-phase components of the synthetic VSS pulse vs. time

$$|f_a(u)| \approx |h| \tag{3.18}$$

3.4 Experimental Results

In this section we present the experimental results for synthetic data as well as for real sonar data. The synthetic transmitted chirp pulse presented in Figure 3.2 consists of a synthesized version of the actual VSS transmitted pulse. The synthetic Green function has been simulated using an exponential function and three impulses. The synthetic data has been generated by convolving a chirp signal with the previously mentioned characteristics and a Green function as illustrated in Figures 3.3 and 3.4. The impulse response of the seafloor can be obtained in two different ways. The first method uses the classical deconvolution between the return data and the chirp signal producing the results presented in Figure 3.4 b.

Given the deconvolved signal (Figure 3.4 (b)) it is simple to find the time (or sample number) of the returns. The return signal location in time is found to be equal to the original location in the Green function. The impulses in the original Green's function occur at sample numbers 600, 1100, and 1500. The peaks of the deconvolved return (once shifted by the length of the source), also occur at 600, 1100, and 1500.

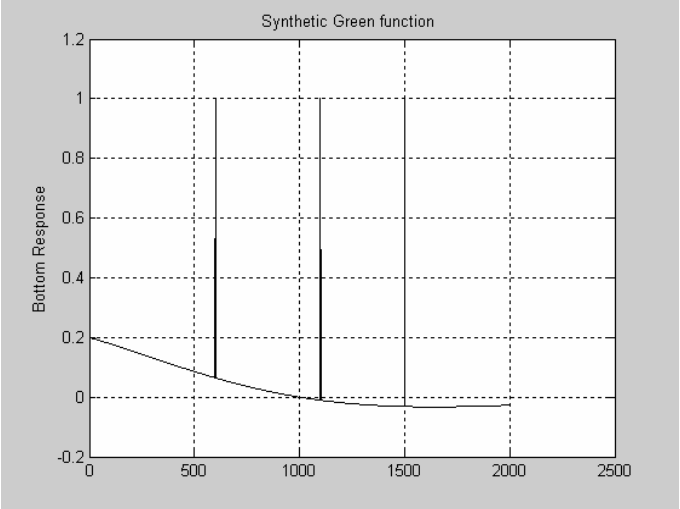

Figure 3.3: Synthetic Green function

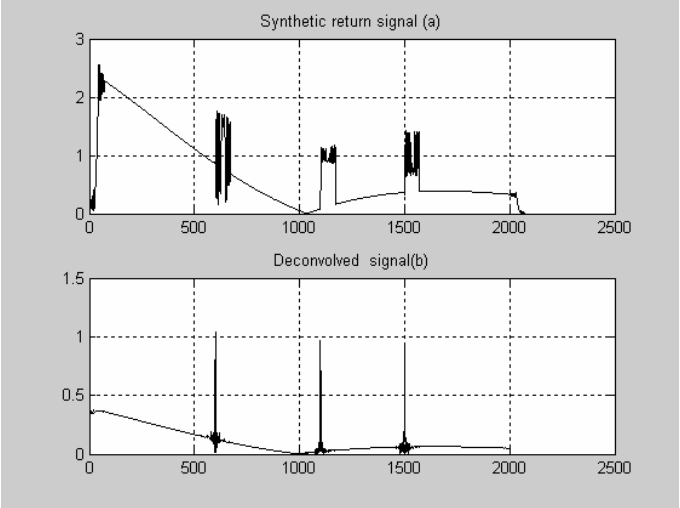

Figure 3.4: (a) Synthetic return signal (convolution of VSS Synthetic Source with the simulated Green function (b) Deconvolved signal (using classical method from ref 2)

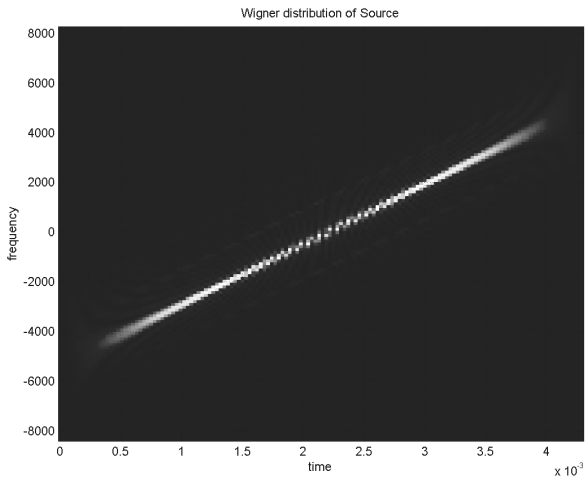

Figure 3.5: Wigner Distribution of the source with BW=10400 Hz

The second method investigated in this paper employs Fractional Fourier Transform applied to the return data.

In order to determine the order of the transform we used equation 3.17 and we validated its value by examination of the chirp's Wigner distribution as shown in Figures 3.5 and 3.6. In general the Wigner distribution of the chirp function is found to be concentrated along the line giving the instantaneous frequency of the chirp (Ozaktas *et al.* , 2001). The Wigner Distribution of the synthetic return data corresponds to the convolution of the Wigner distribution of the chirp signal with the Wigner distribution of the Green function.

After choosing the optimum order (0.035) the Fractional Fourier transform was applied to the bottom synthetic data return. The Wigner distribution of the chirp's Fractional Fourier transform at optimum order is a delta function as illustrated in Figure 3.6.The synthetic bottom impulse response (synthetic Green function) was obtained by taking the magnitude of the Fractional Fourier transform of the bottom synthetic data return as shown in Figure 3.7. Although a slight shift occurred in determining the bottom impulse response, a good match between it and the original Green function has been achieved. The Fractional Fourier transform is represented as a function of sample number, hence the x-axis is a-dimensional.

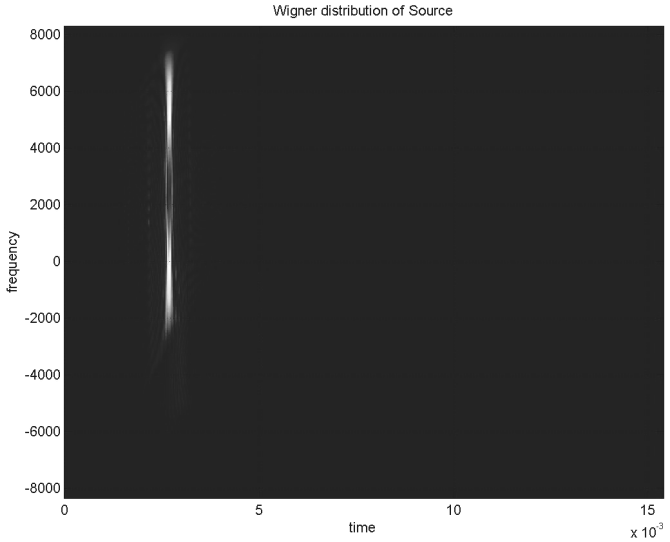

Figure 3.6: Wigner Distribution of the source a=0.035

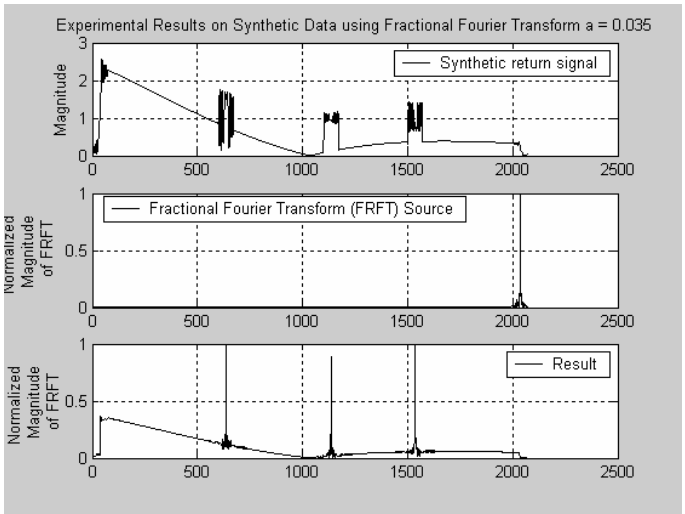

Figure 3.7: Experimental Results on Synthetic Data using Fractional Fourier transform

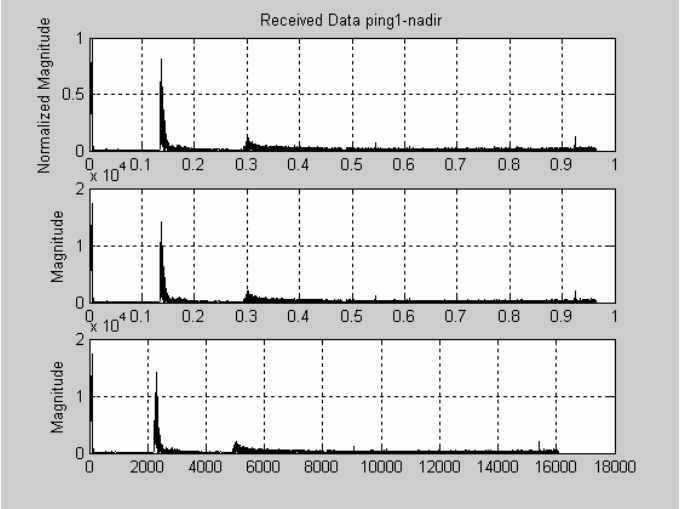

Figure 3.8: Received Ping data

We applied the same techniques to actual VSS sonar data and the results are shown in Figures 3.8 thru 3.11. The data available consist of a small number of pings. A typical nadir beam amplitude return in its raw received form is illustrated in Figure 3.8. The "transmitted pulse" (as seen by the receiver array) and the main return are clear on this plot, where the bottom return occurs at 0.132 seconds from transmission. The total length of the signal is 0.9648 seconds. As expected the nadir beam raw data shows a clear bottom return with high amplitude and little spreading. The received signal shown is normalized to a maximum amplitude of 1.

The deconvolution method in (Kaminsky, 2002) and the Fractional Fourier transform method presented here have been applied to the same beams and pings and their respective results are presented in Figures 3.9 and 3.10.. We used the same window of 256 samples for both methods. The optimum order of the Fractional Fourier transform corresponds to the highest pulse compression and it was found to be 0.269 for this specific chirp. The amplitude of the Fractional Fourier transform applied to the bottom return data for the optimum order represents the bottom impulse response (Figure 3.9).

Figure 3.11 illustrates the bottom impulse response using both methods discussed in this paper. The plots are shifted so that they can be compared easily by visual inspection.

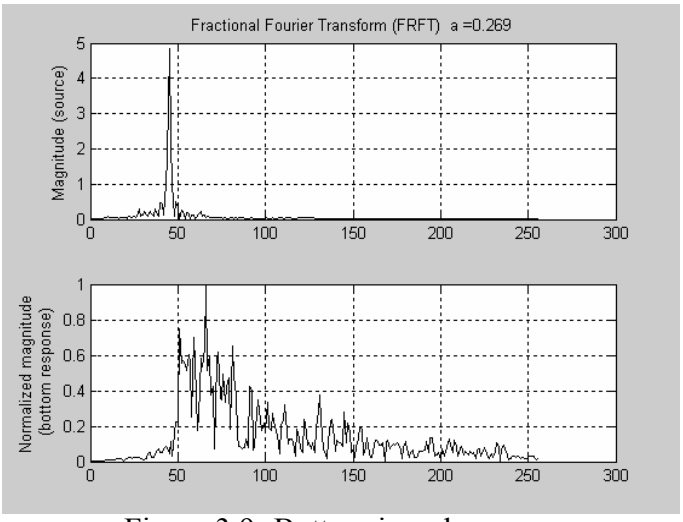

Figure 3.9: Bottom impulse response

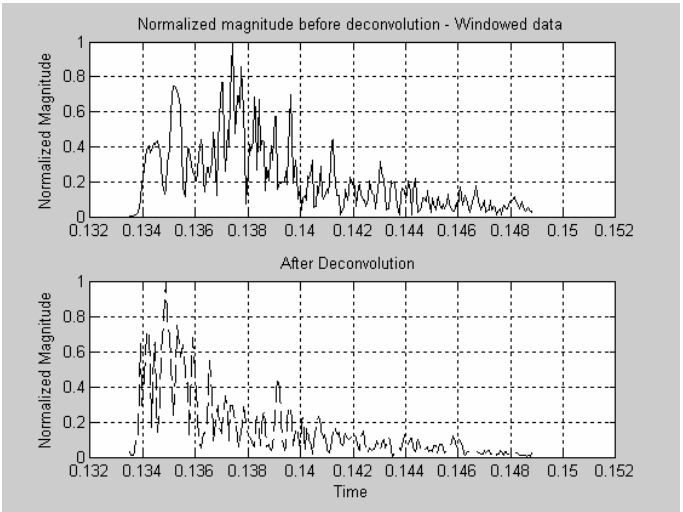

Figure 3.10: Normalized Magnitude of the windowed data before and after deconvolution

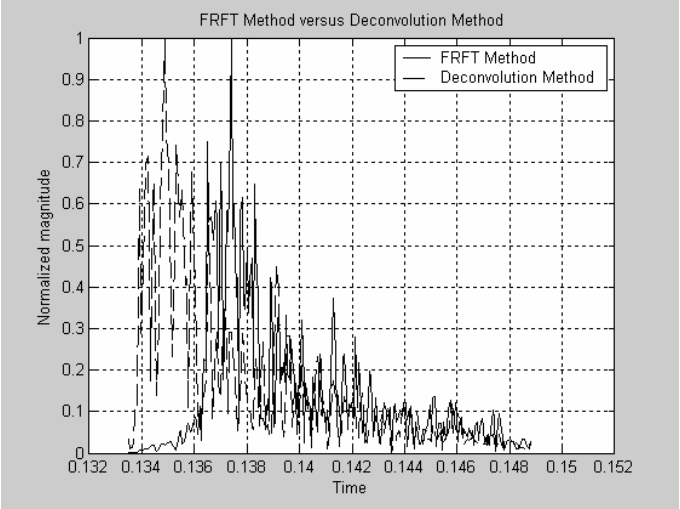

Figure 3.11: Comparison between Fractional Fourier Transform method (solid line) and Deconvolution method (dash line)

Table 3.1: Comparison between FrFT method and deconvolution method

	Mean	Standard Deviation	Energy
FrFT method	0.2681	0.2025	10.1385
Deconvolution	0.3039	0.2316	12.66
Percent Difference [%]	11.7	12.56	12.92

The energy levels, mean and standard deviation of the bottom impulse response for 100 samples corresponding to a range 10 % - 90 % have been computed for both methods and they are presented in Table 3.1.

3.5 Conclusions

In this paper we proposed a technique for determining the bottom impulse response by using the Fractional Fourier transform that has great potential in sonar signal processing. We also presented a classical method for determining the bottom impulse response based on frequency domain deconvolution. The two methods have been tested and compared on synthetic as well as on real sonar data. The experimental results shown demonstrate a good agreement between the two methods. Future work includes a complete statistical analysis of the obtained impulse responses for further sediment classification.

3.6 Acknowledgements

The authors acknowledge Dr. Dale Bibee with the Geoscience Division at Naval Research Laboratory, Stennis Space Center, for his cooperation.

Chapter 4 Fractional Fourier Transform for Sonar Signal Processing

Madalina Barbu, Edit J. Kaminsky, Russell E. Trahan*

Department of Electrical Engineering, *College of Engineering,

University of New Orleans, 2000 Lakeshore Dr., New Orleans, LA, 70148

Abstract

In this paper we present an approach for processing of sonar signals with the ultimate goal of ocean bottom sediment classification. Work reported is based on sonar data collected by the Volume Search Sonar (VSS) in the Golf of Mexico, as well as on VSS synthetic data. The Volume Search Sonar is a beamformed multibeam sonar system with 27 fore and 27 aft beams, covering almost the entire water volume (from above horizontal, through vertical, back to above horizontal). Our investigation is focused on the bottom-return signals since we are interested in determination of the impulse response of the ocean bottom floor. The bottom-return signal is the convolution between the impulse response of the bottom floor and the transmitted sonar chirp signal. The method developed here is based on Fractional Fourier transform, a fundamental tool for signal processing and optical information processing. Fractional Fourier transform is a generalization of the classical Fourier transform. The traditional Fourier transform decomposes signal by sinusoids whereas Fractional Fourier transform corresponds to expressing the signal in terms of an orthonormal basis formed by chirps. In recent years, interest in and use of time-frequency tools have increased and become more suitable for sonar applications. The Fractional Fourier transform requires finding the optimum order of the transform that can be estimated based on the properties of the chirp signal. The bottom impulse response is given by the magnitude of the Fractional Fourier transform applied to the bottom return signal. The technique used in this work has been tested both on synthetic data and real sonar data collected by the VSS. The synthetic sonar return

signal has been generated by the convolution between the Green function, which has been utilized to simulate the impulse response of the seafloor and the transmitted VSS chirp. A study is carried out to compare the performance of our method to a conventional method based on deconvolution in the frequency domain (using standard Fourier transform). The amplitude and shape of an acoustic signal reflected from the sea floor is determined mainly by the seabottom roughness, the density difference between water and the sea floor, and reverberation within the substrate. Since the distribution of seafloor types is a very important tool in different applications, a sediment classification has been implemented based on a statistical analysis of the obtained impulse response. In order to perform a robust analysis of the signal, a joint time-frequency analysis is necessary. In this paper the analysis has been evaluated using the Wigner distribution, which can be thought of as a signal energy distribution in joint time-frequency domain. Singular value decomposition of the Wigner distribution has been used in order to perform the seafloor sediment classification. A comparative analysis of the experimental results for classical deconvolution and Fractional Fourier method is presented. Results are shown and suggestions for future work are provided.

4.1 Introduction

In this paper we present an approach for processing of sonar signals with the ultimate goal of ocean bottom sediment classification.

The reported data herein is based on sonar data collected in the Golf of Mexico by the Volume Search Sonar (VSS), one of the five sonar systems in the AN/AQS-20. The AQS-20 system is an underwater towed body containing a high resolution, side-looking, multibeam sonar system used for mine-hunting along the ocean bottom, a forward-looking sonar, and a Volume Search Sonar as illustrated in Figure 4.1. The VSS consists of two separate arrays: the transmit array and the receive array. The VSS is a beamformed multibeam sonar system with 54 beams arranged as 27 fore–aft beam pairs, covering almost the entire water volume (from above horizontal, through

vertical, back to above horizontal) (Raytheon, 1999). The VSS can be used in two modes: volume modeand Single Pass Deep (SDP) mode. The acoustic energy received by the VSS hydrophone array is pre-amplified and conditioned. Conditioning includes dynamic range compensation using time varying gain (TVG), band-shifting to IF and band pass filtering. After conditioning, analog to digital (A/D) conversion is performed and signals are undersampled. The beamforming function forms all beams and then quadrature demodulates the beam data to baseband . A hybrid time delay phase shift function is used to beamform by using a Hilbert transform after the element delays. The beam outputs are produced by shading (weighted sum) of array element data, delayed to compensate for cylindrical array geometry. Data from this sonar may be used for bathymetry computation, bottom classification, target detection, and water volume investigations (Raytheon, 1999), (Kaminsky, 2002).

Our investigation is focused on the bottom-return signals because we are interested in ocean bottom sediment classification. The bottom-return signal is the convolution between the impulse response of the bottom floor and the transmitted sonar chirp signal. The objective of this paper is to investigate sediment classification based on singular value decomposition of the Wigner distribution applied to the impulse response of the seafloor. The impulse response has been obtained using two methods. The first one is based on the deconvolution method whereas the second method is based on the Fractional Fourier Transform, a fundamental tool for optical information processing and signal processing. In recent years, interest in and use of time-frequency tools has increased and become more suitable for sonar and radar applications (Levenon & McLaughlin, 2002), (Akay, 2002), (Yetik & Nehorai, 2003) .

In this paper we begin by presenting the essential concepts and definitions related to the Fractional Fourier transform, Wigner distribution and singular value decomposition. The overview is followed by a description of the applications of the Fractional Fourier transform and Wigner

Figure 4.1: AQS – 20 mine hunting sonar

distribution with emphasis on sediment classification using sonar data. The experimental results are shown and an evaluation of them is carried out to present the performance of the singular values decomposition method for the classical deconvolution and Fractional Fourier transform methods. The last section of the paper gives a summary of the presented work,conclusions, future work, and recommendations.

4.2 Theoretical Aspects

4.2.1 Fractional Fourier Transform

The Fractional Fourier transform (FrFT) is a generalization of the identity transform and the conventional Fourier transform (FT) into fractional domains. The traditional Fourier transform decomposes signal by sinusoids whereas Fractional Fourier transform corresponds to expressing the signal in terms of an orthonormal basis formed by chirps. The Fractional Fourier transform can be understood as a Fourier transform to the ath power where a is not required to be an integer. There are several ways to define the FrFT; the most direct and formal one is given by (Ozaktas *et al.* , 2001):

$$f_\alpha(u) = \int_{-\infty}^{\infty} K_a(u, u') f(u') du' \tag{4.1}$$

where

$$\alpha = \frac{a\pi}{2}$$

$$K_\alpha(u, u') = A_\alpha \exp[i\pi(\cot\alpha \cdot u^2 - 2\csc\alpha \cdot u \cdot u' + \cot\alpha \cdot u'^2)]$$

$$A_\alpha = \sqrt{1 - i\cot\alpha}$$

when $a \neq 2k$,

$$K_\alpha(u, u') = \delta(u - u')$$

when $a = 4k$, and

$$K_\alpha(u, u') = \delta(u + u')$$

when $a = 4k + 2$, where k is a integer and A_α is a constant term and the square root is defined such that the argument of the result lies in the interval $(-\frac{\pi}{2}, \frac{\pi}{2}]$.The order of the transform is a. If we set $a = 1$, that corresponds to $\alpha = \frac{\pi}{2}$ and $A_\alpha = 1$ such that the FrFT becomes the ordinary Fourier transform of $f(u)$:

$$f(u) = \int_{-\infty}^{\infty} e^{-i2\pi uu'} f(u')du' \tag{4.2}$$

Due to periodic properties, the range of a , the order of the transform can be restricted to $(-2, 2]$or $[0, 4)$, respectively $\alpha \in (-\pi, \pi]$ or $\alpha \in [0, 2\pi)$. The Fractional Fourier transform operator, F^a, satisfies important properties such as linearity, index additivity $F^{a_1}F^{a_2} = F^{a_1+a_2}$, commutativity$F^{a_1}F^{a_2} = F^{a_2}F^{a_1}$, and associativity$(F^{a_1}F^{a_2})F^{a_3} = F^{a_1}(F^{a_2}F^{a_3})$. In the operator notation, these identities follow: $F^0 = I$; $F^1 = F$; $F^2 = P$; $F^3 = FP = PF$;$F^4 = F^0 = I$; and $F^{4k+a} = F^{4k\prime+a}$, where I is an identity operator, P is a parity operator, and k and $k\prime$ are arbitrary

integers. According to the above definition 3.1 the zero-order transform of a function is the same as the function itself $f(u)$, the first order transform is the Fourier transform of $f(u)$, and the $\pm 2^{nd}$ order transform is equal to $f(-u)$.

4.2.2 Wigner Distribution

The Wigner distribution function is a powerful time-frequency analysis tool and it can be used to illustrate the time-frequency properties of a signal. The Wigner distribution of a function f(t) is defined as (Cohen, 1995):

$$W_f(t,\nu) = \int f^*(t-\tau/2) f(t+\tau/2) e^{-j2\pi\nu\tau} d\tau \tag{4.3}$$

and it can be interpreted as a function that indicates the distribution of the signal energy over the time-frequency space. The most significant properties of the Wigner distribution and the relationships between Wigner distribution and FrFT are stated in the following equations:

1.

$$\int W_f(t,\nu) d\nu = |f(t)|^2 \tag{4.4}$$

2.

$$\int W_f(t,\nu) dt = |F(\nu)|^2 \tag{4.5}$$

3

$$\int W_f(t,\nu) dt d\nu = E[f] \tag{4.6}$$

4. If

$$g(t) = h(t) * f(t)$$

then,

$$W_g(t,\nu) = \int W_h(t-\tau,\nu) W_g(\tau,\nu) d\tau \tag{4.7}$$

5. If

$$g(t) = h(t)f(t)$$

then,

$$W_g(t,\nu) = \int W_h(t,\nu-\nu')W_g(t,\nu')d\nu' \tag{4.8}$$

6.Wigner distribution of the Fourier transform is the Wigner Distribution of the original function rotated clockwise by a right angle. One of the most important properties of the FrFT states that the Wigner distribution of the FrFT of a function is a rotated version of the Wigner distribution of the original function:

$$W_{f_a}(t,\nu) = W_f(t\cos\alpha - \nu\sin\alpha, t\cos\alpha + \nu\sin\alpha) \tag{4.9}$$

The Wigner distribution is completely symmetric with respect to the time-frequency domains, it is always real but not always positive. The Wigner distribution exhibits advantages over the spectrogram (short-time Fourier transform): the conditional averages are exactly the instantaneous frequency and the group delay, whereas the spectrogram fails to achieve this result, no matter what window is chosen. The Wigner distribution is not a linear transformation, a fact that complicates the use of the Wigner distribution for time-frequency filtering.

4.2.3 Singular Value Decomposition

A decomposition of joint time-frequency signal representation using the techniques of linear algebra, called singular value decomposition determines a qualitative signal analysis tool. The concept of decomposing a Wigner distribution in this manner was first presented by Marinovich and Eichman (Marinovich & Eichmann, 1985). One motivation for such decomposition is noise reduction because when keeping only the first few terms most of the noise is lost; the other motivation for this decomposition is for the purpose of classification (Cohen, 1995). The basic idea in the latter case is that singular values contain unique characterization of the time-frequency

structure of a distribution and may be used for classification. The set of representations of singular values is called singular value spectrum of the signal. The singular value decomposition (SVD) of the discrete Wigner distribution is given by (Mecklenbrauker & F.Hlawatsch, 1997) :

$$A = UDV^T = \sum_{i=1}^{N} \sigma_i u_i v_i^T,$$

$$\|A\|_F^2 = \sum_{i=1}^{N} \sigma_i^2 \tag{4.10}$$

where T denotes transpose, $D = diag(\sigma_{1,}\sigma_{2,}, \sigma_{3,}, \ldots . \sigma_N)$ with singular values $\sigma_1 \geq \sigma_2 \geq \ldots . \geq \sigma_N$, U and V are matrices that contain singular vectors and $\|W\|_F$ is the Frobenius norm matrix. The properties of the Wigner distribution lead us to the conclusion that the volume under the surface that corresponds to a particular expansion term is equal to the signal energy contained in that term. Permutations of the rows (columns) or unitary transformation of W lead to similarity transformations of WW^T and W^TW. The singular values are invariant under this transformation and also invariant to time and/or frequency shifts in the signal. The number of non-zero spectrum coefficients equals the time-bandwidth product of the signal. Because singular values of the Wigner distribution encode certain invariant features of the signal, the set of singular values can be considered as the feature vectors that describe the signal.

4.3 Application of the Fractional Fourier Transform for Sediment Classification

The current authors have developed singular value decomposition of the Wigner distribution of the bottom impulse response for seafloor sediment classification. The proposed technique will allow efficient determination of seafloor bottom characteristics and bottom type using the reverberation signal. The impulse response of the seafloor can be determined using the classical deconvolution method or using FrFT. We have tested the techniques employed in this work for impulse response determination both on synthetic data and actual sonar data collected by the VSS (Barbu *et al.* , 2005b). The synthetic sonar return signal is generated by the convolution between

the transmitted VSS chirp, with the specific parameters characterizing the system in question — such as a bandwidth of 10400 Hz, chirp duration of 4.32 ms (Barbu *et al.* , 2005b) and the Green function that has been utilized to simulate the synthetic impulse response of the seafloor. Applying a classical deconvolution method to the return signal allows us to determine the bottom impulse response by taking the inverse Fourier transform of 4.11 :

$$H(\varpi) = H_I(\varpi) + H_Q(\varpi) \tag{4.11}$$

where $H(\varpi)$ is the Fourier transform of the impulse response and it has a real (in-phase) part and imaginary (quadrature-phase) part given by:

$$H_I(\varpi) = \frac{R_I(\varpi)P_I(\varpi) + R_Q(\varpi)P_Q(\varpi)}{P_I^2(\varpi) + P_Q^2(\varpi)} \tag{4.12}$$

$$H_Q(\varpi) = \frac{-R_I(\varpi)P_Q(\varpi) + R_Q(\varpi)P_I(\varpi)}{P_I^2(\varpi) + P_Q^2(\varpi)} \tag{4.13}$$

In equations 4.12 and 4.13, $R(\varpi)$ and $P(\varpi)$ are the Fourier transforms of complex baseband received signal and of transmitted pulse, respectively. The subscripts I and Q denote, respectively, the real (in-phase) and imaginary (quadrature-phase).

The Fractional Fourier transform requires finding the optimum order of the transform that can be estimated based on the properties of the chirp signal: the rate of change λ,sampling rate fs, and the length of the data segment N (Levenon & McLaughlin, 2002):

$$\alpha = \frac{2}{\pi}\tan^{-1}(fs^2/2\lambda N) \tag{4.14}$$

The bottom impulse response is given by the magnitude of the Fractional Fourier transform for optimal order applied to the bottom return signal (Barbu *et al.* , 2005b).

Our evaluation is based on actual data acquired by the VSS sonar. Two types of sediments

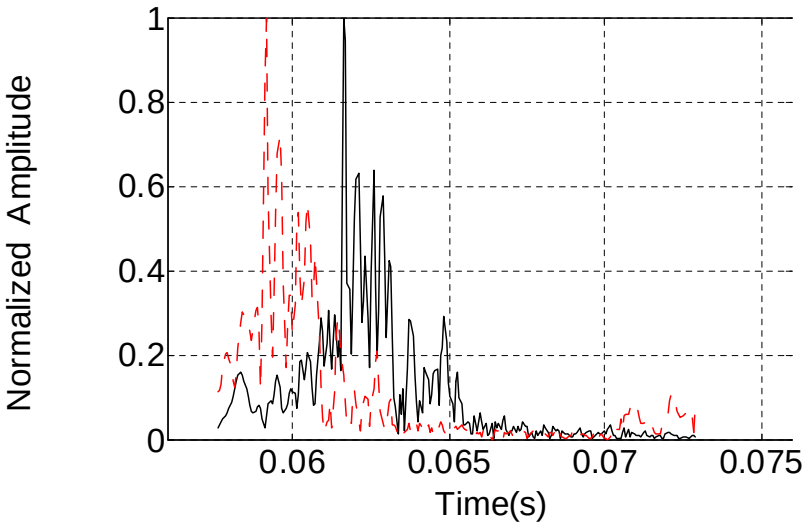

Figure 4.2: Normalized amplitude Impulse response of sand using Deconvolution (red,dashed) and FrFT (black, solid) methods on the nadir beam.

are present in the area surveyed: sand and mud. The deconvolution method and the Fractional Fourier transform method presented here have been applied to the same beams and pings. We used the same window of 256 samples for both methods. The optimum order of the Fractional Fourier transform corresponds to the highest pulse compression and it was found to be 0.269 for this specific VSS chirp. In order to determine the order of the transform we used eq. 4.14 and we validated its value by examination of the chirp's Wigner distribution. In general, the Wigner distribution of the chirp function is found to be concentrated along the line giving the instantaneous frequency of the chirp. For the optimal order the Wigner distribution of the chirp becomes the delta function.

The amplitude of the Fractional Fourier transform applied to the bottom return data for the optimum order represents the amplitude of the bottom's impulse response. Figure 4.2 presents the normalized amplitude impulse response of sand corresponding to the nadir beam using the two methods.

The amplitude and the shape of an acoustic signal reflected from the seafloor are determined

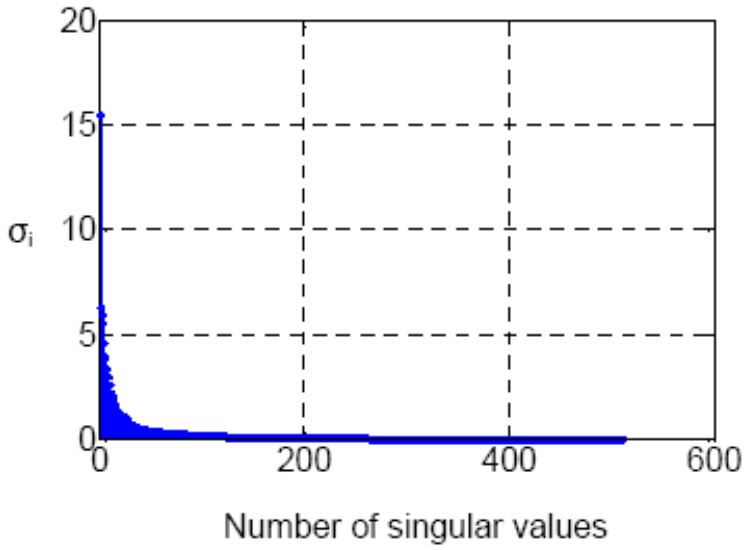

Figure 4.3: SV of Wigner distribution of the impulse response obtained by using deconvolution

mainly by the seabottom roughness, by the density difference between water and the seafloor, and by the reverberation within the substrate. Since the distribution of the seafloor types is a very important tool in different applications, a sediment classification has been implemented based on the singular value decomposition of the Wigner distribution of the obtained impulse response. Joint time-frequency representation of the signal offers the possibility to determine the time-frequency configuration of the signal as its characteristic features for classification purposes.

After computing the Wigner distribution for each amplitude impulse response corresponding to each beam, a normalization is performed. The next step is to compute the singular values for each beam and each sediment class.

Figures 4.3 and 4.4 represent, respectively, the singular value (S.V.) spectrum corresponding to the nadir beam for sand using the two mentioned methods. The set of the singular values represent the desired feature vectors that describe the properties of the signal. This set can be called as singular value descriptors. It can be observed from the plots that the first two singular values are the most significant. Because feature analysis involves dimensionality reduction, we

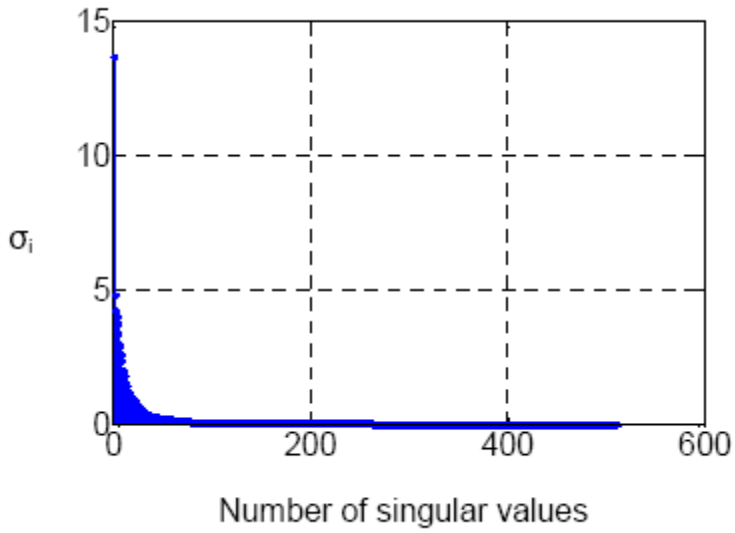

Figure 4.4: SV of Wigner distribution of the impulse response obtained by using FrFT

consider the first two terms from the S.V. spectrum. A representation of the two singular values in two dimensional space will lead to an unsupervised classification. Initially we use 10 beams per sediment class while performing the unsupervised sediment classification.

The representation of the largest S.V. descriptors for each beam and each class are shown in Figure 4.5 and Figure 4.6. One can notice the clustering and separability provided by the S.V. descriptors. Although only the two largest singular values descriptors have been used, clear separation has been achieved. The small number of S.V. descriptors used demonstrates the high data compression property of the descriptors. The sediment classification is performed using 10 beams. These beams correspond to the central five beams from the fore and aft fans. Beam 27 (B27) and beam 28 (B28) correspond to nadir. Figure 4.5 has been obtained applying the deconvolution method. Figure 4.6 has been achieved applying FrFT method for the same data and the same window.

One can observe an improvement by approximately 50% for class separation from a margin width of 0.7 to 1.1. In Figures 4.5. and 4.6., respectively, the standard deviation of the sand class

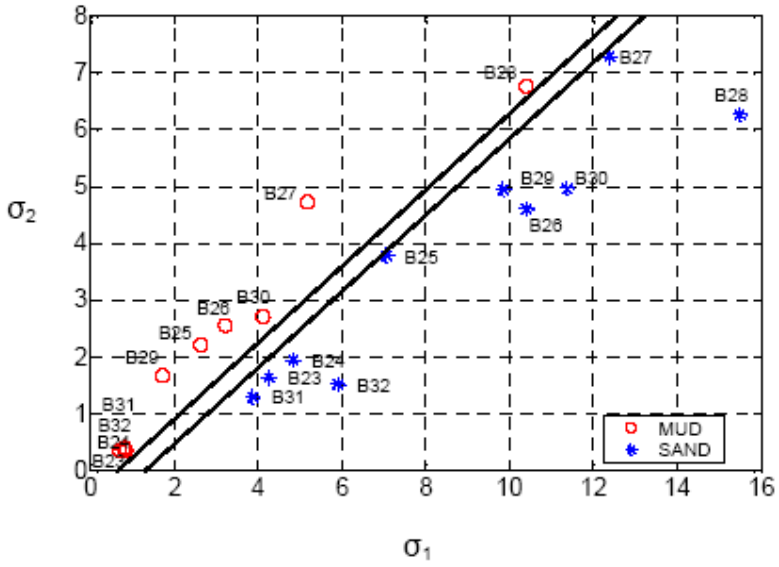

Figure 4.5: SV for Wigner distribution of impulse response using deconvolution method on 10 beams

points using the deconvolution method was found to be larger (4.48) than using FrFT (4.045). The standard deviation of the mud class points, was found again larger (4.48) using the deconvolution method comparing to the FrFT that gives a standard deviation of 4.23. This improvement can be explained by the fact that part of undesired signal components - such as noise - was eliminated when the impulse response was obtained using FrFT.

The next step in our evaluation was performed using 14 beams, seven fore and seven aft. In this case, the return signal presents components due to the side lobes of the main return. These components negatively influence our classification. In the deconvolution method the two classes are linearly inseparable. The outer beams B21, B22, B31, B34 for sand and mud induce difficulties in separation. The mud class got a large undesired spread that requires a more complex evaluation. Using our FrFT method the two classes are barely linearly separable, but this methods provides much better results compared to the deconvolution method.The standard deviation of the sand as well as for mud class points, were found again larger (4.94 respectively 4.9) using the deconvolution method compared to the FrFT that gives a standard deviation for corresponding

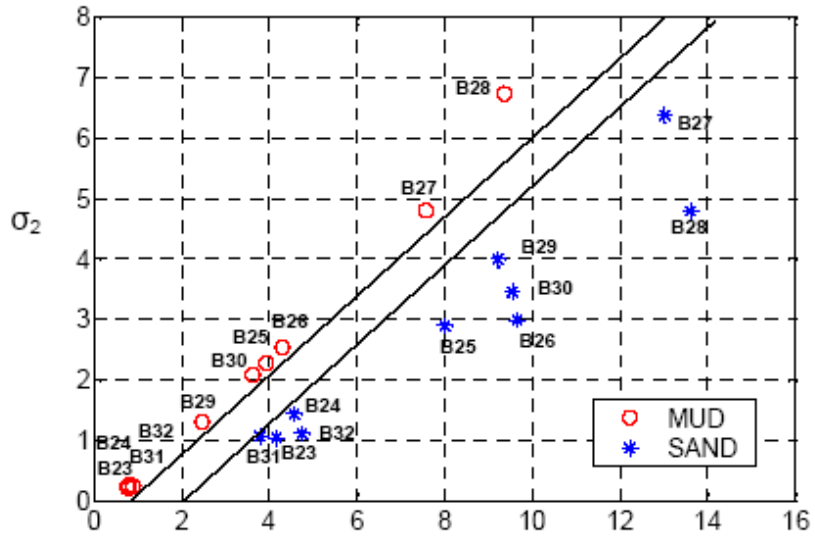

Figure 4.6: SV for Wigner distribution of impulse response using FrFT method on 10 beams

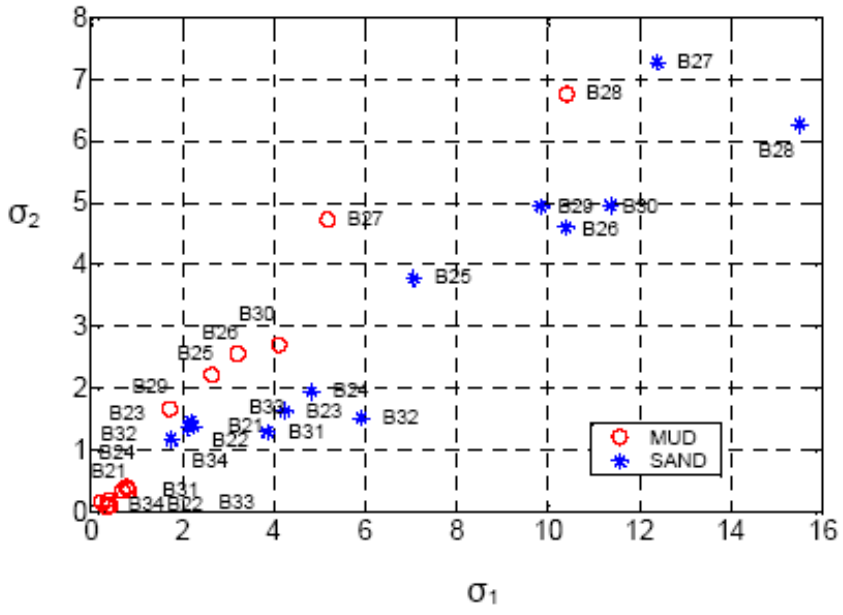

Figure 4.7: SV of Wigner Distribution corresponding to the impulse response using the deconvolution method on 14 beams

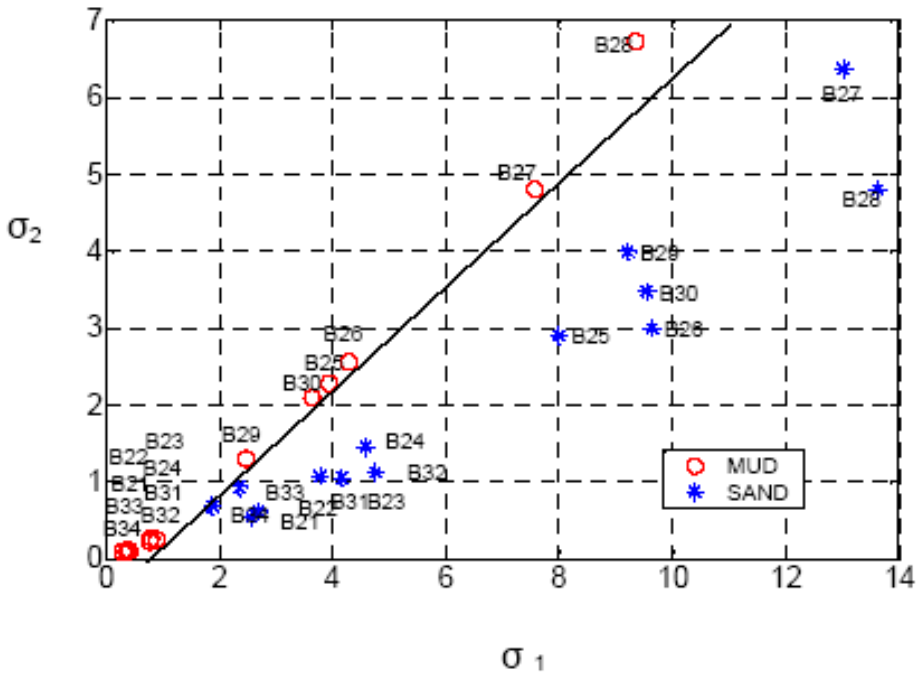

Figure 4.8: SV of Wigner Distribution corresponding to the impulse response using the FrFT method on 14 beams

classes of 4.41 and 4.51.

4.4 Conclusions

In this paper we present an approach for processing of sonar signals with the ultimate goal of ocean bottom sediment classification. The approach is based on Fractional Fourier Transform (FrFT), a newly developed time-frequency analysis tool which has become attractive in signal processing. The final classification is based on singular value decomposition of the Wigner distribution applied to the impulse response obtained using two different methods: FrFT and classical deconvolution method. The evaluation has been performed on data collected by the AQS-20 sonar system. The classification has proved to be very effective when only the central beams, near nadir, are used. The separation between the two classes, sand and mud, using our FrFT method is approximately 50 % better than when classical deconvolution is used. When outer beams were considered, the classification performance decreased due to the fact that the return signals presented unwanted reflection due to the side lobes, and no effort was made to

window the significant signal return. Also, the signals returned by mud are very weak. When the deconvolution method was employed the sediment classes were not linearly separable and the standard deviation of the class points was greater by approximately 10% compared to the case when FrFT was used.

In order to obtain better classification performance, signal windowing and filtering in the time-frequency domain are recommended. Thus the Wigner distribution will eventually suppress unwanted artifacts and a noise elimination will be performed. More features from the Wigner distribution (e.g. first, second moments) can also be considered and a classification based on neural networks can be implemented in order to achieve a better seafloor sediment classification.

4.5 Acknowledgments

The authors would like to thank Dr. Dale Bibee with the Geoscience Division at Naval Research Laboratory, Stennis Space Center, for his cooperation, support, and for providing data.

Chapter 5 Acoustic Seabed Classification using Fractional Fourier Transform

Madalina Barbu, Edit J. Kaminsky, Russell E. Trahan*

Department of Electrical Engineering, *College of Engineering,

University of New Orleans, 2000 Lakeshore Dr., New Orleans, LA, 70148

Abstract

In this paper we present a time-frequency approach for acoustic seabed classification. Work reported is based on sonar data collected by the Volume Search Sonar (VSS), one of the five sonar systems in the AN/AQS-20. The Volume Search Sonar is a beamformed multibeam sonar system with 27 fore and 27 aft beams, covering almost the entire water volume (from above horizontal, through vertical, back to above horizontal). The processing of a data set of measurement in shallow water is performed using the Fractional Fourier Transform algorithm in order to determine the impulse response of the sediment. The Fractional Fourier transform requires finding the optimum order of the transform that can be estimated based on the properties of the transmitted signal. Singular Value Decomposition and statistical properties of the Wigner and Choi-Williams distributions of the bottom impulse response are employed as features which are, in turn, used for classification. The Wigner distribution can be thought of as a signal energy distribution in joint time-frequency domain. Results of our study show that the proposed technique allows for accurate sediment classification of seafloor bottom data. Experimental results are shown and suggestions for future work are provided.

Keywords: Fractional Fourier transform, impulse response, seabed classification, time-frequency distributions, volume search sonar.

5.1 Introduction

In this paper we present a time-frequency approach for acoustic seabed classification. Work

reported is based on sonar data collected by the Volume Search Sonar (VSS), one of the five sonar systems in the AN/AQS-20. The collection of data was performed in the Gulf of Mexico. The AQS-20 system is an underwater towed body containing a high resolution, side-looking, multibeam sonar system used for minehunting along the ocean bottom, as well as a forward looking sonar, and the volume search sonar which provided the data we use for our work. The system is illustrated in Figure 5.1.

The VSS consists of two separate arrays: the transmit array and the receive array. The VSS is a beamformed multibeam sonar system with 54 beams arranged as 27 fore–aft beam pairs, covering almost the entire water volume (from above horizontal, through vertical, back to above horizontal) (Raytheon, 1999). The VSS can be used in two modes: volume mode and Single Pass Deep (SPD) mode. The acoustic energy received by the VSS hydrophone array is pre-amplified and conditioned. Conditioning includes dynamic range compensation using time varying gain (TVG), bandshifting to IF, and band pass filtering. After conditioning, analog to digital (A/D) conversion is performed and signals are undersampled at 200 KHz. The beamforming function forms all beams and then quadrature demodulates the beam data to baseband. A hybrid time delay phase shift function is used to beamform by using a Hilbert transform after the element delays. The beam outputs are produced by shading (weighted sum) of array element data, delayed to compensate for cylindrical array geometry. Data from this sonar may be used for bathymetry computation, bottom classification, target detection, and water volume investigations (Kaminsky, 2002).

The analysis presented here focuses on the bottom-return signals because we are interested in determining the impulse response of the ocean floor. The bottom-return signal is the convolution between the impulse response of the bottom floor and the transmitted sonar chirp signal. The objective of this paper is to investigate sediment classification based on singular value

Figure 5.1: AQS – 20 mine hunting sonar

decomposition (SVD) of different time-frequency distributions applied to the impulse response of the seafloor. The time frequency distributions used in this paper are the Wigner distribution and the Choi Williams distribution. The impulse response has been obtained using two methods. The first method is standard deconvolution, whereas the second method is based on the Fractional Fourier Transform (FrFT), a fundamental tool for optical information processing and signal processing. In recent years, interest in and use of time-frequency tools has increased and become more suitable for sonar and radar applications (Levenon & McLaughlin, 2002),(Akay, 2002),(Yetik & Nehorai, 2003) . Both methods are presented in order to show that the proposed technique based on the Fractional Fourier Transform (FrFT) allows efficient sediment classification of seafloor bottom data compared to the conventional method based on deconvolution.

This paper starts with a presentation of the essential concepts and definitions related to the Fractional Fourier transform, time frequency distributions, and singular value decomposition. It then proceeds with the description of the proposed technique that improves the performance of unsupervised sediment classification. The conventional and the proposed methods are tested on real sonar data. The experimental results are shown and an their evaluation is carried out. The last section of the paper gives a summary of the presented work, conclusions, proposals for future

work, and recommendations; references follow at the end.

5.2 Theoretical Aspects

5.2.1 Fractional Fourier Transform

The Fractional Fourier transform (FrFT) is a generalization of the identity transform and the conventional Fourier transform (FT) into fractional domains. The traditional Fourier transform decomposes signal by sinusoids whereas Fractional Fourier transform corresponds to expressing the signal in terms of an orthonormal basis formed by chirps. The Fractional Fourier transform can be understood as a Fourier transform to the a^{th} power where a is not required to be an integer. There are several ways to define the FrFT; the most direct and formal one is given by (Ozaktas *et al.* , 2001):

$$f_\alpha(u) = \int_{-\infty}^{\infty} K_a(u, u') f(u') du' \tag{5.1}$$

where

$$\alpha = \frac{a\pi}{2}$$

$$K_\alpha(u, u') = A_\alpha \exp[i\pi(\cot\alpha \cdot u^2 - 2\csc\alpha \cdot u \cdot u' + \cot\alpha \cdot u'^2)]$$

$$A_\alpha = \sqrt{1 - i\cot\alpha}$$

when $a \neq 2k$,

$$K_\alpha(u, u') = \delta(u - u')$$

when $a = 4k$, and

$$K_\alpha(u, u') = \delta(u + u')$$

when $a = 4k + 2$, where k is a integer and A_α is a constant term and the square root is defined such that the argument of the result lies in the interval $(-\frac{\pi}{2}, \frac{\pi}{2}]$.The order of the transform is a. If we set $a = 1$, that corresponds to $\alpha = \frac{\pi}{2}$ and $A_\alpha = 1$ such that the FrFT becomes the ordinary Fourier transform of $f(u)$:

$$f(u) = \int_{-\infty}^{\infty} e^{-i2\pi uu'} f(u')du' \tag{5.2}$$

Due to periodic properties, the range of a , the order of the transform can be restricted to $(-2, 2]$or $[0, 4)$, respectively $\alpha \in (-\pi, \pi]$ or $\alpha \in [0, 2\pi)$. The Fractional Fourier transform operator, F^a, satisfies important properties such as linearity, index additivity $F^{a_1}F^{a_2} = F^{a_1+a_2}$, commutativity$F^{a_1}F^{a_2} = F^{a_2}F^{a_1}$, and associativity$(F^{a_1}F^{a_2})F^{a_3} = F^{a_1}(F^{a_2}F^{a_3})$. In the operator notation, these identities follow: $F^0 = I$; $F^1 = F$; $F^2 = P$; $F^3 = FP = PF$;$F^4 = F^0 = I$; and $F^{4k+a} = F^{4k\prime+a}$, where I is an identity operator, P is a parity operator, and k and $k\prime$ are arbitrary integers. According to the above definition 5.1 the zero-order transform of a function is the same as the function itself $f(u)$, the first order transform is the Fourier transform of $f(u)$, and the $\pm 2^{nd}$ order transform is equal to $f(-u)$.

5.2.2 Time-Frequency Analysis

The generalized time-frequency representation can be expressed in term of the kernel, $\varphi(\theta, \tau)$, a two dimensional function (Cohen, 1995):

$$C(t, \varpi) = \frac{1}{4\pi^2} \int\int\int f^*(u - \tau/2) f(u + \tau/2) \varphi(\theta, \tau) e^{-j\theta t - j\tau\varpi + ju\theta} du d\tau d\theta \tag{5.3}$$

The kernel determines the properties of the distribution. Here are some distributions that can be obtained based on the value of the kernel :

1. Wigner distribution can be derived from the generalized time-frequency representation for $\varphi(\theta, \tau) = 1$

$$W(t,\varpi) = \frac{1}{2\pi}\int f^*(t-\tau/2)f(t+\tau/2)e^{-j\tau\varpi}d\tau \tag{5.4}$$

2. Choi-Williams distributionis obtained for $\varphi(\theta,\tau) = e^{-\theta^2\tau^2/\sigma}$:

$$C(t,\varpi) = \frac{1}{4\pi^{3/2}}\int\int \frac{1}{\sqrt{\tau^2/\sigma}} f^*(u-\tau/2)f(u+\tau/2)e^{-\sigma(u-t)^2/\tau^2 - j\tau\varpi}dud\tau \tag{5.5}$$

3. Spectrogram is obtained for $\varphi(\theta,\tau) = \int h^*(u-\tau/2)e^{-ju\theta}h^*(u+\tau/2)du$

$$C(t,\varpi) = \left|\frac{1}{\sqrt{2\pi}}\int f(\tau)h(\tau-t)e^{-j\varpi\tau}d\tau\right|^2 \tag{5.6}$$

The Wigner distribution function is a time-frequency analysis tool and it can be used to illustrate the time-frequency properties of a signal; it can be interpreted as a function that indicates the distribution of the signal energy over the time-frequency space. The most significant properties of the Wigner distribution and the relationships between Wigner distribution and FrFT are stated in the following equations:

a.

$$\int W(t,\varpi)d\varpi = |f(t)|^2 \tag{5.7}$$

b.

$$\int W(t,\varpi)dt = |F(\varpi)|^2 \tag{5.8}$$

c.

$$\int W(t,\varpi)dtd\varpi = E[f] \tag{5.9}$$

d. If

$$g(t) = h(t) * f(t)$$

then,

$$W_g(t,\varpi) = \int W_h(t-\tau,\varpi) W_g(\tau,\varpi) d\tau \tag{5.10}$$

e. If

$$g(t) = h(t) f(t)$$

then,

$$W_g(t,\varpi) = \int W_h(t,\varpi-\varpi') W_g(t,\varpi') d\varpi' \tag{5.11}$$

The Wigner distribution of the Fourier transform is the Wigner Distribution of the original function rotated clockwise by a right angle. The Wigner distribution is completely symmetric with respect to the time-frequency domain, it is always real but not always positive. The Wigner distribution exhibits advantages over the spectrogram (short-time Fourier transform): the conditional averages are exactly the instantaneous frequency and the group delay, whereas the spectrogram fails to achieve this result, no matter what window is chosen. The Wigner distribution is not a linear transformation, a fact that complicates the use of the Wigner distribution for time-frequency filtering. One disadvantage of the Wigner distribution is that sometimes it indicates intensity in regions where one would expect zero values. These effects are due to cross terms but are minimized by choosing a different kernel. The kernel of the form $\varphi(\theta,\tau) = e^{-\theta^2\tau^2/\sigma}$, yields the Choi William distribution which, by appropriately choosing the parameter σ minimizes the cross terms. When the Choi-Williams kernel is used, the marginals are satisfied and the distribution is real. In addition, if the σ parameter has a large value, the Choi-Williams distribution approaches the Wigner distribution, because the kernel approaches one. For small σ values it satisfies the reduced interference criterion.

5.2.3 Singular Value Decomposition

A decomposition of joint time-frequency signal representation using the techniques of linear algebra, called singular value decomposition yields a qualitative signal analysis tool. The concept of decomposing a Wigner distribution in this manner was first presented by Marinovich and

Eichman (Marinovich & Eichmann, 1985). One motivation for such decomposition is noise reduction because when keeping only the first few terms most of the noise is lost; the other motivation for this decomposition is for the purpose of classification (Cohen, 1995). The basic idea in the latter case is that singular values contain unique characterization of the time-frequency structure of a distribution and may be used for classification. The set of representations of singular values is called the singular value spectrum of the signal. For the discrete Wigner distribution, the singular value decomposition (SVD) is given by (Mecklenbrauker & F.Hlawatsch, 1997) :

$$A = UDV^T = \sum_{i=1}^{N} \sigma_i u_i v_i^T,$$

$$\|A\|_F^2 = \sum_{i=1}^{N} \sigma_i^2 \tag{5.12}$$

where T denotes transpose, $D = diag(\sigma_{1,}\sigma_{2,}, \sigma_{3,}, \ldots . \sigma_N)$with singular values $\sigma_1 \geq \sigma_2 \geq \ldots . \geq \sigma_N$, $U$and V are matrices that contain singular vectors and$\|W\|_F$ is the Frobenius norm matrix. The properties of the Wigner distribution lead us to the conclusion that the volume under the surface that corresponds to a particular expansion term is equal to the signal energy contained in that term. Permutations of the rows (columns) or unitary transformation of W lead to similarity transformations of WW^T and W^TW. The singular values are invariant under this transformation and also invariant to time and/or frequency shifts in the signal (Mecklenbrauker & F.Hlawatsch, 1997). The number of non-zero spectrum coefficients equals the time-bandwidth product of the signal. Because singular values of the Wigner distribution encode certain invariant features of the signal, the set of singular values can be considered as the feature vectors that describe the signal and therefore be used in classification.

5.3 Approach

The proposed seafloor sediment classification method is based on singular value decomposition

of the time-frequency distributions of the bottom impulse response. Our technique accurately determines the seafloor bottom characteristics and bottom type using the reverberation signal as the starting point. The impulse response of the seafloor can be determined using the classical deconvolution method or using FrFT (Barbu *et al.* , 2005b). We have previously tested the techniques employed in this work for impulse response determination both on synthetic data and actual sonar data collected by the VSS (Barbu *et al.* , 2005b), (Barbu *et al.* , 2005a). The synthetic sonar return signal is generated by the convolution between the transmitted VSS chirp, with the specific parameters characterizing the system in question —such as a bandwidth of 10400 Hz, chirp duration of 4.32 ms (Kaminsky, 2002), (Barbu *et al.* , 2005b) — and the Green function that has been utilized to simulate the synthetic impulse response of the seafloor. Applying a classical deconvolution method to the return signal allows us to determine the bottom impulse response by taking the inverse Fourier transform of 5.13:

$$H(\varpi) = H_I(\varpi) + H_Q(\varpi) \tag{5.13}$$

where $H(\varpi)$ is the Fourier transform of the impulse response and it has a real (in-phase) part and imaginary (quadrature-phase) part given by:

$$H_I(\varpi) = \frac{R_I(\varpi)P_I(\varpi) + R_Q(\varpi)P_Q(\varpi)}{P_I^2(\varpi) + P_Q^2(\varpi)} \tag{5.14}$$

$$H_Q(\varpi) = \frac{-R_I(\varpi)P_Q(\varpi) + R_Q(\varpi)P_I(\varpi)}{P_I^2(\varpi) + P_Q^2(\varpi)} \tag{5.15}$$

In equations 5.14 and 5.15 , $R(\varpi)$ and $P(\varpi)$ are the Fourier transforms of complex baseband received signal and of transmitted pulse, respectively. The subscripts I and Q denote, respectively, the real (in-phase) and imaginary (quadrature-phase).

The Fractional Fourier transform requires finding the optimum order of the transform; the

order be estimated based on the properties of the chirp signal: the rate of change λ,sampling rate fs, and the length of the data segment N (Levenon & McLaughlin, 2002):

$$\alpha = \frac{2}{\pi} \tan^{-1}(fs^2/2\lambda N) \tag{5.16}$$

The bottom impulse response is given by the magnitude of the Fractional Fourier transform for optimal order applied to the bottom return signal (Barbu *et al.* , 2005b).

The amplitude and the shape of an acoustic signal reflected from the seafloor are determined mainly by the seabottom roughness, by the density difference between water and the seafloor, and by the reverberation within the substrate. Because accurate characterization of the distribution of the seafloor types is a very important tool in many commercial and military applications, we developed and implemented a sediment classification procedure which is based on the singular value decomposition of the Wigner and Choi Williams distributions of the obtained impulse response corresponding to each beam and each sediment class. Joint time-frequency representation of the signal offers the possibility of determining the time-frequency configuration of the signal as characteristic features for classification purposes. The sets of the singular values represent the desired feature vectors that describe the properties of the deconvolved signal and, therefore, the sediment. Because feature analysis involves dimensionality reduction, we consider the first two terms from the S.V. spectrum. A representation of the two singular values in two dimensional space will lead to unsupervised classification.

5.4 Experimental Results

Our evaluation is based on actual data acquired by the VSS sonar. Two types of sediments are present in the area surveyed: sand and mud. The deconvolution method and the fractional Fourier transform method presented here have been applied to the same beams and pings before (Barbu *et al.* , 2005a). We used the same window of 256 samples for both methods. The optimum order of the fractional Fourier transform corresponds to the highest pulse compression and it was

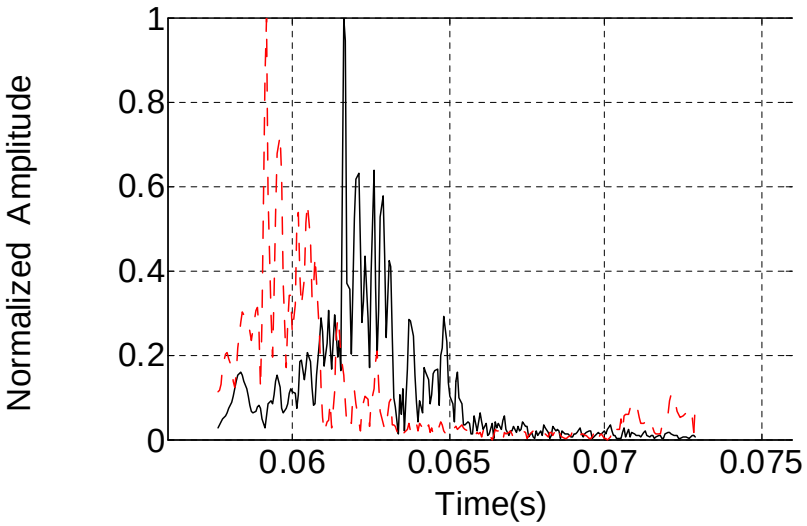

Figure 5.2: Normalized amplitude Impulse response of sand using Deconvolution (red,dashed) and FrFT (black, solid) methods on the nadir beam.

found to be 0.269 for this specific VSS chirp. To determine the order of the transform we used eq. 5.16 and we validated its value by examination of the chirp's Wigner distribution. In general, the Wigner distribution of the chirp function is found to be concentrated along the line giving the instantaneous frequency of the chirp. For the optimal order the Wigner distribution of the chirp becomes the delta function. The amplitude of the fractional Fourier transform applied to the bottom return data for the optimum order represents the amplitude of the bottom's impulse response. Figure 5.2 presents the normalized amplitude impulse response of sand corresponding to the nadir beam using the two methods.

The Wigner distribution is computed for each amplitude impulse response obtained via each method (standard deconvolution and fractional Fourier transform-based deconvolution) corresponding to each beam. Normalization is further performed and the singular values for each beam and each sediment class are computed as shown in our previous work (Barbu *et al.* , 2005a). The representation of the largest S.V. descriptors for each beam and each class has been obtained. A representation of the two singular values in two-dimensional space will lead to an unsupervised

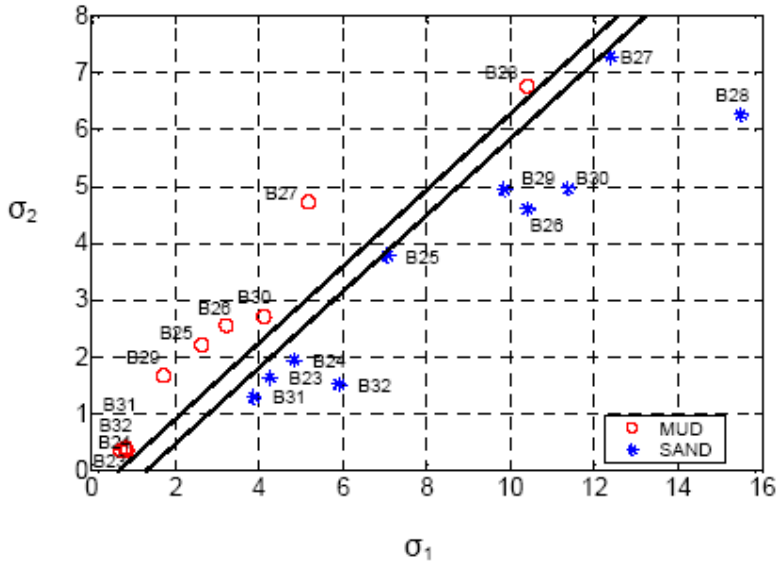

Figure 5.3: SV for Wigner distribution of impulse response using deconvolution method on 10 beams

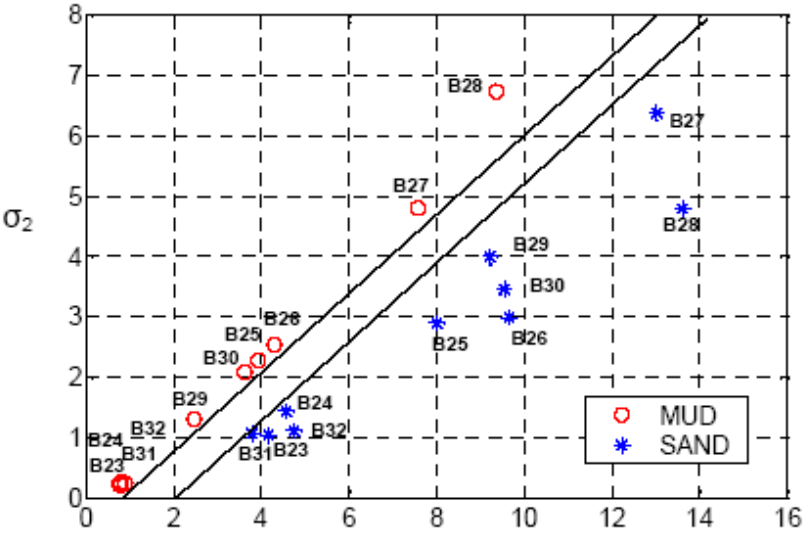

Figure 5.4: SV for Wigner distribution of impulse response using FrFT method on 10 beams

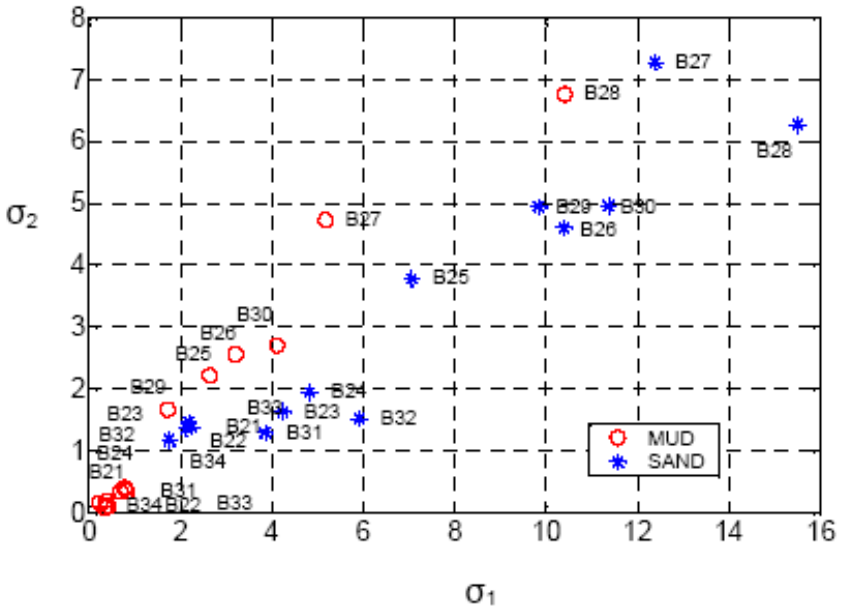

Figure 5.5: SV of Wigner Distribution corresponding to the impulse response using the deconvolution method on 14 beams

classification. The sediment classification is performed first using only 10 beams (corresponding to the central five beams from the fore and aft fans) and then 14 beams (the central seven beams from the fore and aft fans). Beam 27 (B27) and beam 28 (B28) correspond to nadir. The results are illustrated in Figure 5.3 through 5.6. Figure 5.3 has been obtained applying the deconvolution method. Figure 5.4 shows the results obtained when applying the FrFT method for the same data and the same window, for the 10 beams. Figure 5.5 uses the standard deconvolution method while Figure 5.3 has been achieved applying the FrFT method for the same data and the same window, but for the 14 central beams.

An improvement by approximately 50% can be observed for class separation from a margin width of 0.9 to 1.4 from Figure 5.3 to 5.4, respectively. This improvement can be explained by the fact that parts of undesired signal components - such as noise - were eliminated when the impulse response was obtained using FrFT.

When 14 beams were analyzed, the return signal presented significant components due to

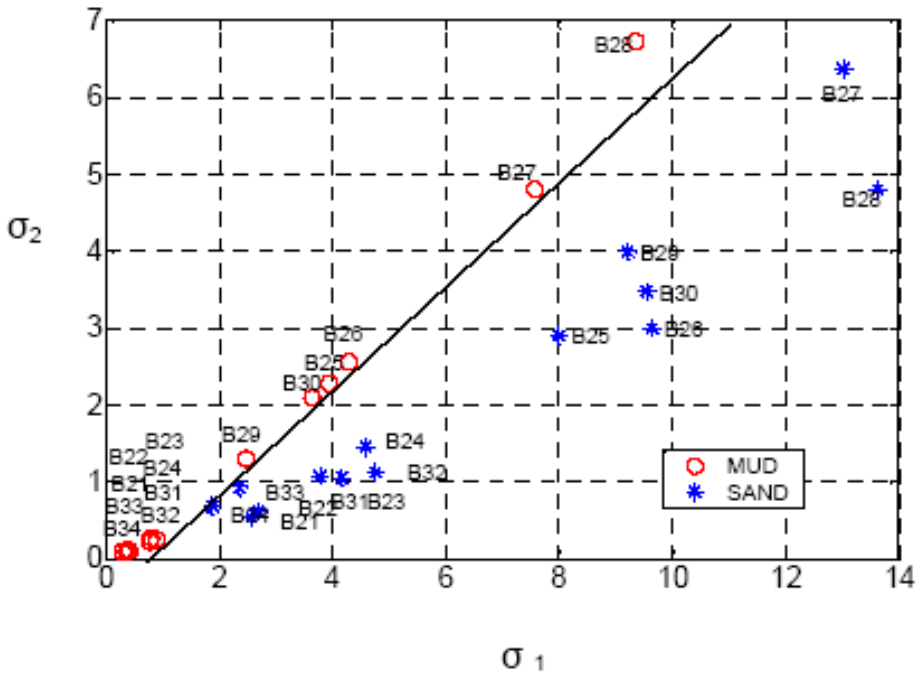

Figure 5.6: SV of Wigner Distribution corresponding to the impulse response using the FrFT method on 14 beams

the side lobes of the main return. These components negatively influence our classification. In the standard deconvolution method the two classes are linearly inseparable. The outer beams B21, B22, B31, B34 for sand and mud induce difficulties in separation. The mud class got a large undesired spread that requires a more complex evaluation. Using our FrFT method the two classes are barely linearly separable, but this method provides much better results compared to the standard deconvolution method. In order to improve the classification performance, the Choi-Williams distribution was employed. These results are presented in Figure 5.7 through 5.10 . One can observe an increase of the classification margin width for the 10 central beams when the Choi Williams distribution was applied to both the standard and the FrFT-based deconvolution methods as compard to the Wigner distribution. In the case of the 14 beams the two classes, Mud and Sand, became linearly separable with a larger margin width for both the standard deconvolution and the FrFT methods. This better classification performance is determined by the reduction of the cross interference terms when the Choi-Williams distribution is applied.

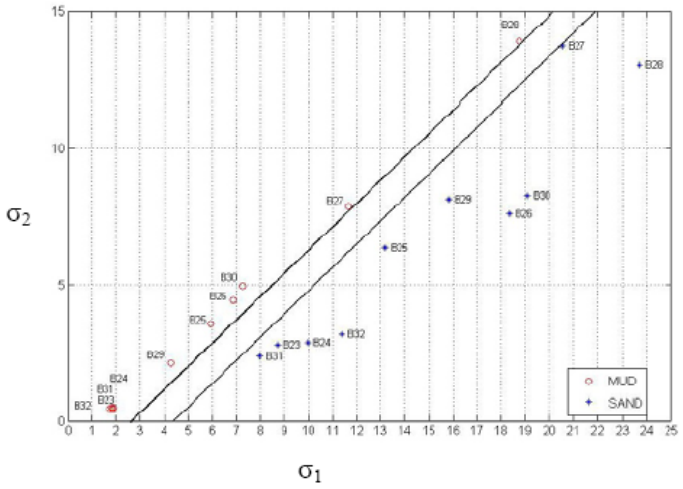

Figure 5.7: SV for Choi-Williams distribution of impulse response using standard deconvolution on 10 beams

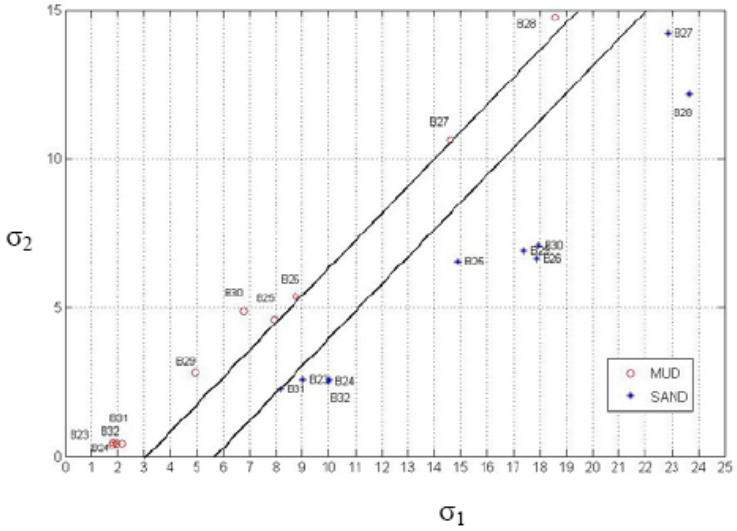

Figure 5.8: SV for Choi-Williams distribution of impulse response using FrFT on 10 beams

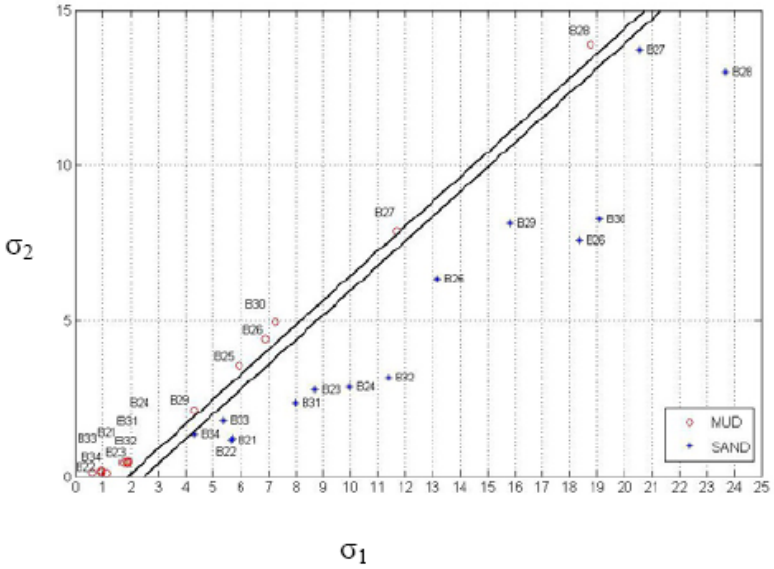

Figure 5.9: SV for Choi-Williams distribution of impulse response using standard deconvolution on 14 beams

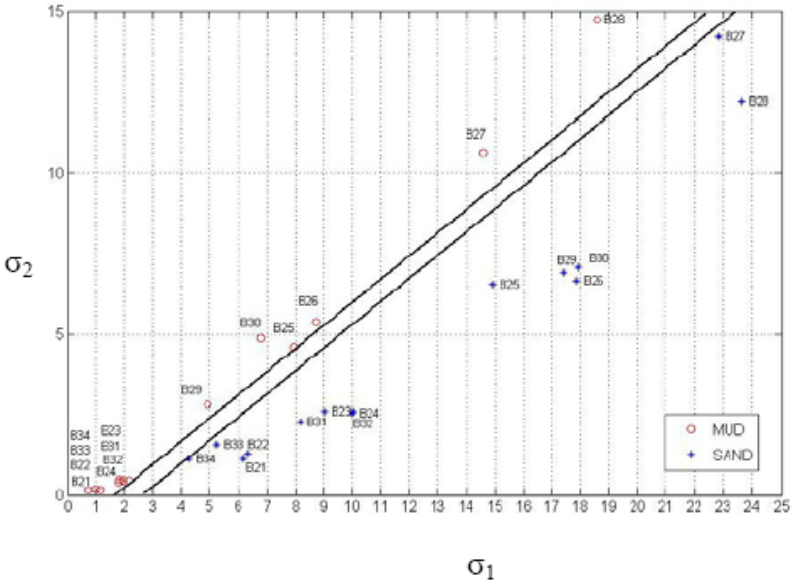

Figure 5.10: SV for Choi-Williams distribution of impulse response using FrFt on 14 beams

Table 5.1: Margin width between classes for the techniques used

Number of beams used	Impuse response method	Margin width	
		Wigner distribution	Choi -Williams distribution
10	Standard deconvolution	0.9	1.9
10	FrFT method	1.4	2.8
14	Standard deconvolution	Not linearly separable	0.5
14	FrFT method	Barely lineraly separable	0.95

Table 5.1 illustrates the significant improvement of class separation that is achieved when the Choi-Williams distribution is used instead of the more popular Wigner distribution. Moreover, the best classification performance is achieved when fractional Fourier yransform and Choi-Williams distribution are employed together.

5.5 Conclusions

In this paper we presented an approach for processing of sonar signals with the ultimate goal of ocean bottom sediment classification. The approach is based on fractional Fourier transform (FrFT), a newly developed time-frequency analysis tool which has become attractive in signal processing. The best results on the final classification are achieved when singular value decomposition of the Choi-Williams distribution is applied to the impulse response obtained using deconvolution based on FrFT. Using Choi-Williams instead of Wigner improves both the classical deconvolution results and the Fr-FT-based results. The performance evaluation of our methods have been performed on data collected by the volume sonar system of the AQS-20 sonar system suite. The classification has proved to be very effective not only when the central beams, near nadir, were used, but also for a larger number of beams. The separation between the two classes, sand and mud, using our FrFT method together with the Choi-William distribution is approximately 60 % better than when classical deconvolution is used. FrFT method with Choi Williams distribution showed a better classification performance than competing techniques due to its property of cross-terms interference reduction. Future work includes multi-class seabed classification using more features obtained from Choi Williams distribution applied to impulse

response using FrFT.

Chapter 6 Acoustic Seabed Classification using Fractional Fourier Transform and Time-Frequency Transform Techniques

Madalina Barbu, Edit J. Kaminsky, Russell E. Trahan*

Department of Electrical Engineering, *College of Engineering,

University of New Orleans, 2000 Lakeshore Dr., New Orleans, LA, 70148

Abstract

In this paper we present an approach for processing sonar signals with the ultimate goal of ocean bottom sediment classification. Work reported is based on sonar data collected by the Volume Search Sonar (VSS), one of the five sonar systems in the AN/AQS-20. Our technique is based on the Fractional Fourier Transform (FrFT), a time-frequency analysis tool which has become attractive in signal processing. Because FrFT uses linear chirps as basis functions, this approach is better suited for sonar applications. The magnitude of the bottom impulse response is given by the magnitude of the Fractional Fourier transform for optimal order applied to the bottom return signal. Joint time-frequency representations of the signal offer the possibility to determine the time-frequency configuration of the signal as its characteristic features for classification purposes. The classification is based on singular value decomposition of the Choi William distribution applied to the impulse response obtained using Fractional Fourier transform. The set of the singular values represents the desired feature vectors that describe the properties of the signal. The singular value spectrum has a high data reduction potential. It encodes the following signal features: time-bandwidth product, frequency versus time dependence, number of signal components and their spacing. The spectrum is invariant to shifts of the signal in time and frequency and is well suited for pattern recognition and classification tasks. The most relevant features (singular values) have been mapped in a reduced dimension space where an unsupervised

classification has been employed for acoustic seabed sediment classification. The theoretical method is addressed and then tested on field sonar data. In our classification we used the central beams. Good agreement between the experimental results and the ground truth is shown. A performance comparison of our method to a k–means based technique is also given. Results and recommendations for future work are presented.

6.1 Introduction

In the last several years, novel techniques have been implemented and exploited for several underwater tasks like classification of the seafloor, detection and classification of buried objects and classification of fish and vegetation, among others. The procedures depend on the type of signals, the nature of the system (sonar), and the final objective. Some of the proposed seafloor classification methods (Sternlicht & de Moustier, 2003b) involve estimating the physical properties and acoustical properties of the superficial ocean sediments from the normal incidence reflection data acquired by a chirp sonar (Schock, 2004); others are applying projection techniques such as Fast Fourier Transform and wavelet transform (Roitblat *et al.* , 1995), (Pace & Gao, 1988). Pattern recognition approaches based on neural networks have been also exploited (Trucco, 2001). Neural networks may yield important contributions to finding solutions for underwater applications (Roitblat *et al.* , 1995), (Baan & Jutten, 2000).

In recent years interest in time-frequency tools in sonar and radar applications has increased (Mecklenbrauker & F.Hlawatsch, 1997)-(Lin *et al.* , 2004). Major research directions include the use of time-frequency analysis for pattern recognition, noise reduction, beam forming, and optical processing. A recent method based on the Fractional Fourier transform has been evaluated for analyzing sonar data (Lenon & McLaughlin, 2002). The Fractional Fourier transform is a generalization of the classical Fourier transform. The traditional Fourier transform decomposes signals by sinusoids whereas Fractional Fourier transform corresponds to expressing the signal in terms of an orthonormal basis formed by chirps, and therefore more suitable for underwater signal

processing. In order to compute the impulse response of the sediment using the Fractional Fourier Transform, an optimal order is required. The optimal order depends on the characteristic of the transmitted sonar signal (length, sampling frequency, chirp rate).

In this paper we present an approach for acoustic seabed classification continuing the work presented in (Barbu *et al.* , 2005a). Work reported is based on sonar data collected by the Volume Search Sonar (VSS), one of the five sonar systems in the AN/AQS-20. The AQS-20 system is an underwater towed body containing a high resolution, side-looking, multibeam sonar system used for minehunting along the ocean bottom, as well as a forward looking sonar, and the volume search sonar. The VSS consists of two separate arrays: the transmit array and the receive array. The VSS is a beamformed multibeam sonar system with fifty-four beams arranged as twenty-seven fore–aft beam pairs, covering almost the entire water volume (from above horizontal, through vertical, back to above horizontal). The VSS can be used in two modes: volume mode and single pass deep (SPD) mode. Data from this sonar may be used for bathymetry computation, bottom classification, target detection, and water volume investigations (Raytheon, 1999).

The proposed technique for sediment classification is based on projection techniques using the Fractional Fourier Transform in order to determine the impulse response of the sediment (Barbu *et al.* , 2005a). The signals that need to be classified are first represented in an appropriate time frequency space, and then projected into a favorable space that allows feature extraction for unsupervised classification. In unsupervised classification the acoustic data are divided into classes based on their characteristics and determine their "own class". Labels such as sand, mud, rock, may be attached to classes after unsupervised classification. The data used in this paper represent returns from two classes found in the Gulf of Mexico: mud and sand.

This paper starts with a presentation of the essential concepts and definitions related to the Fractional Fourier transform, time frequency distributions and singular value decomposition.

It then proceeds with the description of the proposed technique that is shown to improve the performance of unsupervised sediment classification. Our method is presented and compared to a k-means-based technique where wavelets were used for feature extraction. The last section of the paper gives a summary of the presented work, conclusions, future work, and recommendations.

6.2 Theoretical Aspects

6.2.1 Fractional Fourier Transform

The Fractional Fourier Transform (FrFT) is a generalization of the Fourier Transform and provides an important tool in time-frequency domain theory for the analysis and synthesis of linear chirp signals. The traditional Fourier transform decomposes a signal by sinusoids whereas the Fractional Fourier transform corresponds to expressing the signal in terms of an orthonormal basis formed by chirps. Since the FrFT uses linear chirps as the basis function, this approach is better suited for chirp sonar applications.

There are several ways to define the FrFT; the most direct and formal one is given (Ozaktas *et al.* , 2001):

$$f_\alpha(u) = \int_{-\infty}^{\infty} K_a(u, u') f(u') du' \tag{6.1}$$

where

$$\alpha = \frac{a\pi}{2} \tag{6.2}$$

$$K_\alpha(u, u') = A_\alpha \exp[i\pi(\cot\alpha \cdot u^2 - 2\csc\alpha \cdot u \cdot u' + \cot\alpha \cdot u'^2)] \tag{6.3}$$

$$A_\alpha = \sqrt{1 - i\cot\alpha} \tag{6.4}$$

when $a \neq 2k$,

$$K_\alpha(u, u') = \delta(u - u') \tag{6.5}$$

when $a = 4k$, and

$$K_\alpha(u, u') = \delta(u + u') \tag{6.6}$$

when $a = 4k + 2$, where k is a integer and A_α is a constant term and the square root is defined such that the argument of the result lies in the interval $(-\frac{\pi}{2}, \frac{\pi}{2}]$.

Due to periodic properties, the a range can be restricted to $(-2, 2]$ or $[0, 4)$. The Fractional Fourier transform operator, Fa, satisfies important properties such as linearity, index additivity, commutativity, and associativity. In the operator notation, these identities follow (Ozaktas *et al.* , 2001): $F^0 = I; F^1 = F; F^2 = P; F^3 = FP = PF; F^4 = F^o = I$; and $F^{4k+a} = F^{4k'+a}$, where I is an identity operator, P is a parity operator, and k and k' are arbitrary integers. According to the above definition, the zero-order transform of a function is the same as the function itself $f(u)$, the first order transform is the Fourier transform of $f(u)$, and the 2^{nd} order transform is equal to $f(-u)$.

The definition can be understood as a multiplication by a chirp, followed by the Fourier transformation, followed by another chirp multiplication and finally a complex scaling.

Numerical calculation of the FrFT is of fundamental importance for the applications described here. There exist different algorithms that can improve the calculation accuracy (Yang *et al.* , 2004).

6.2.2 Time-Frequency Analysis

Time-frequency methods are powerful tools for studying variations in spectral components. The spectrum's time dependency of the return signal could be a strong indicator of the seafloor's acoustic signature.

The generalized time-frequency representation can be expressed in term of the kernel $\varphi(\theta, \tau)$, which determines the properties of the distribution (Mecklenbrauker & F.Hlawatsch, 1997):

$$C(t,\varpi) = \frac{1}{4\pi^2}\int\int\int f^*(u-\tau/2)f(u+\tau/2)\varphi(\theta,\tau)e^{-j\theta t - j\tau\varpi + ju\theta}dud\tau d\theta \tag{6.7}$$

The Wigner distribution can be derived from the generalized time-frequency representation for the value of the kernel $\varphi(\theta,\tau) = 1$:

$$W(t,\varpi) = \frac{1}{2\pi}\int f^*(t-\tau/2)f(t+\tau/2)e^{-j\tau\varpi}d\tau \tag{6.8}$$

The Wigner distribution function is a time-frequency analysis tool that can be used to illustrate the time-frequency properties of a signal, and it can be interpreted as a function that indicates the distribution of the signal energy over the time-frequency space. The Wigner distribution is symmetric with respect to the time-frequency domains, it is always real but not always positive. The Wigner distribution exhibits advantages over the spectrogram (short-time Fourier transform): the conditional averages are exactly the instantaneous frequency and the group delay, whereas the spectrogram fails to achieve this result, no matter what window is chosen. The Wigner distribution is not a linear transformation, a fact that complicates its use for time-frequency filtering.

One disadvantage of the Wigner distribution is that it sometimes indicates intensity in the regions where one would expect zero values. These effects are due to cross terms and can be minimized by choosing a kernel that has the form $\varphi(\theta,\tau) = e^{-\theta^2\tau^2/\sigma}$, and in this case the distribution becomes the Choi-Williams distribution:

$$C(t,\varpi) = \frac{1}{4\pi^{3/2}}\int\int\frac{1}{\sqrt{\tau^2/\sigma}}f^*(u-\tau/2)f(u+\tau/2)e^{-\sigma(u-t)^2/\tau^2 - j\tau\varpi}dud\tau \tag{6.9}$$

Choosing this kernel, the marginals are satisfied and the distribution is real. In addition, if the σ parameter has a large value, the Choi-Williams distribution approaches the Wigner distribution, since the kernel approaches one. For small σ values, it satisfies the reduced interference criterion.

6.2.3 Singular Value Decomposition

A decomposition of joint time-frequency signal representation using the techniques of linear algebra, called singular value decomposition determines a qualitative signal analysis tool. Singular value decomposition (SVD) is an important factorization of a rectangular matrix with several applications in signal processing and statistics. Singular value decomposition provides an acceptable approximation with a minimum number of expansion terms. The set of representations of singular values is called singular value spectrum of the signal, which has a high data reduction potential. It encodes the following signal features: time-bandwidth product, frequency versus time dependence, number of signal components and their spacing. The SVD spectrum is invariant to shifts of the signal in time and frequency and is well suited for pattern recognition and signal detection classification tasks (Mecklenbrauker & F.Hlawatsch, 1997).

The concept of decomposing a Wigner distribution in this manner was first presented by Marinovich and Eichman (Marinovich & Eichmann, 1985). One motivation for such decomposition is noise reduction because when keeping only the first few terms most of the noise is lost; the other motivation for this decomposition is for the purpose of classification (Cohen, 1995). The basic idea in the latter case is that singular values contain a unique characterization of the time-frequency structure of a distribution and may be used for classification.

The singular value decomposition of a matrix A is given by (**?**):

$$A = UDV^T = \sum_{i=1}^{N} \sigma_i u_i v_i^T, \tag{6.10}$$

$$\|A\|_F^2 = \sum_{i=1}^{N} \sigma_i^2 \tag{6.11}$$

where superscript T denotes transpose, $D = diag(\sigma_1, \sigma_2, ..., \sigma_N)$ with singular values $\sigma_1 \geq \sigma_2 \geq \ldots \geq \sigma_N$, U and V are matrices that contain singular vectors, and $\|A\|_F$ is the

Frobenius norm matrix.

Permutations of the rows (columns) or unitary transformation of A lead to similarity transformations of AA^T and A^TA. The singular values are invariant under this transformation and also invariant to time and/or frequency shifts in the signal. The number of non-zero spectrum coefficients equals the time-bandwidth product of the signal. Because singular values of the time-frequency distribution encode certain invariant features of the signal, the set of singular values can be considered as the feature vectors that describe the signal, and used for classification purposes.

6.3 Technique for Sediment Classification

Our proposed technique for sediment classification is based on the Fractional Fourier Transform in order to determine the impulse response of the sediment. The signals that need to be classified are represented in time frequency space and then projected into a favorable space that allows feature extraction for unsupervised classification. The acoustic data are discriminated into classes via an unsupervised classification, based on their most relevant features. Class labels such as sand, mud, rock are assigned after unsupervised classification. Our technique efficiently classifies sediment types using the reverberation bottom return signal.

The following steps are performed in the proposed technique:

1) Compute the impulse response using the FrFT for each beam

2) Determine the Choi-Williams distribution of the impulse response (for each beam)

3) Compute the SVD of the time-frequency distribution

4) Capture the first few SV's (for each beam) as features and use them as a new reduced dimensional space where unsupervised classification is performed.

The FrFt which produces the most compact support for a given linear chirp is defined as the optimal fractional Fourier transform of that signal (Capus & Brown, 2003).

The optimum order of the transform can be estimated based on the properties of the chirp

signal: the rate of change, sampling rate f_s, and the length of the data segment N (Capus *et al.* , 2000):

$$a = \frac{2}{\pi} \tan^{-1} \left(\frac{f_s^2/N}{2\lambda} \right) \tag{6.12}$$

The bottom impulse response is given by the magnitude of the Fractional Fourier transform for optimal order applied to the bottom return signal (Barbu *et al.* , 2005b):

$$|h(t)| \approx |fa| \tag{6.13}$$

The sediment classification procedure has been implemented based on the singular value decomposition of the Choi-Williams distribution of the obtained impulse response corresponding to each beam and each sediment class. Because feature analysis involves dimensionality reduction, we consider the first two terms from the SVD spectrum. A representation of the two singular values in two dimensional space will lead to unsupervised classification.

6.4 Experimental Results

Our evaluation uses data acquired by the VSS sonar in the Gulf of Mexico. Two types of sediments are present in the area surveyed: sand and mud. Standard deconvolution and the Fractional Fourier transform method (Barbu *et al.* , 2005a) have been applied to the same beams and pings. We used the same window of 256 samples for both methods. The optimum order of the Fractional Fourier transform corresponds to the highest pulse compression and was found to be 0.269 for this specific VSS chirp, that has a bandwidth of 10,400 Hz and chirp duration of 4.32 ms.

In order to evaluate the performance of the proposed sediment classification technique, an alternative method for unsupervised classification has been employed. The impulse response was computed using both a standard deconvolution method (Kaminsky, 2002) and a Fractional Fourier transform method of (Barbu *et al.* , 2005a). We applied 1D wavelet decomposition at level 3 using

Table 6.1: Experimental results using K-means and wavelets

Number of beams used	Impulse response method	Accuracy
20	Standard Deconvolution	65%
20	FrFT	70%
28	Standard Deconvolution	61%
28	FrFT	65%

Daubechies wavelets to each beam's impulse response signal for feature extraction. The next step was to use K-means algorithm for clustering the features (wavelet coefficients) extracted into two classes: mud and sand. We initially used ten beams (corresponding to the central five beams from the fore and aft fans) and then fourteen beams (the central seven beams from the fore and aft fans) for each sediment type. Beam 27 (B27) and beam 28 (B28) correspond to nadir.

The summary of the experimental results for the K-means based technique for the number of beams used is presented in Table 6.1.

Experimental results using K-means and wavelets have shown that the best classification accuracy has been obtained when the impulse response has been computed via the FrFT. When the FrFT was used a higher classification accuracy was achieved if twenty central beams were considered. These results are based on a very small data set, but we expect them to be representative of the system's performance.

In our proposed technique, the Choi-Williams distribution is computed for the amplitude of the impulse response obtained via each method (standard deconvolution and Fractional Fourier Transform) corresponding to each beam. Normalization of the Choi-Williams distributions for all beams to unity maximum is further performed and then the singular values for each beam are computed. The Choi-Williams distribution was preferred to the Wigner distribution because an improved classification performance is achieved due to the reduction of the cross interference terms. The representation of the largest SV descriptors for each beam and each class has been obtained. A representation of the two largest singular values of all beams in a two dimensional

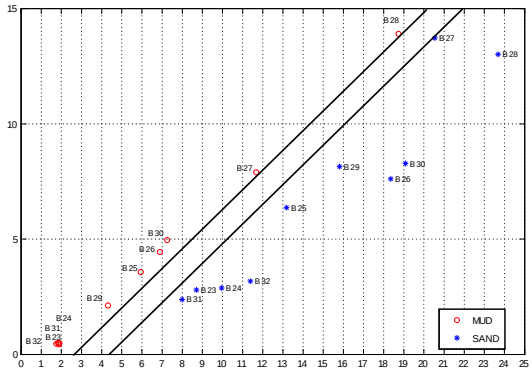

Figure 6.1: SV for Choi-Williams distribution of impulse response using standard deconvolution method on 20 beams (X axis represents σ_1, Y axis represents σ_2)

space will lead to an unsupervised classification. The class labels are data driven; the only *a priori* knowledge is that there are two classes.

The results are illustrated in Figures 6.1 through 6.4. Figure 6.1 has been obtained applying the standard deconvolution method. Figure 6.2 shows results achieved applying the FrFT method for the same data and the same window, for twenty beams. Figure 6.3 shows results obtained by applying the deconvolution method, while Figure 6.4 has been achieved applying FrFT method for the same data and the same window, for the twenty-eight central beams. The two lines shown in the figures below represent the maximal margin of separation between classes achievable using parallel straight lines determined by the most extremes points of each class. Hence, the optimum straight line of separation between classes would be the median line of the margin. The two classes are linearly separable when they are mapped by SVD in the reduced dimensional space. The summary of the experimental results for the proposed technique is presented in Table 6.2. The margin width values are also presented in Table 6.2. Notice the large increases of 47% and 90% for twenty and twenty-eight respectively, of the margin when the FrFT is used.

Using SVD of the Choi-Williams distribution of the impulse response and mapping the data in a reduced dimensional space, linearly separable classes were achieved, and a boosted

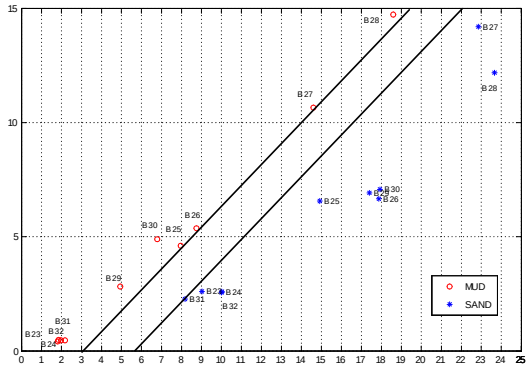

Figure 6.2: SV for Choi-Williams distribution of impulse response using FrFT method on 20 beams (X axis represents σ_1, Y axis represents σ_2)

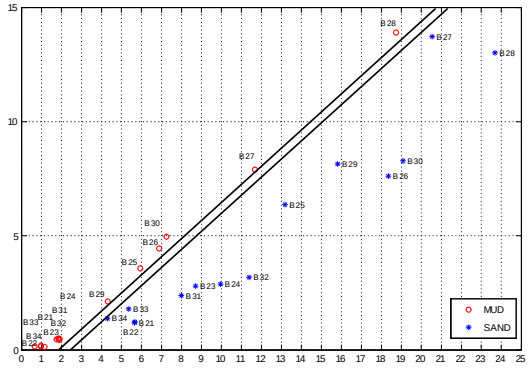

Figure 6.3: SV for Choi-Williams distribution of impulse response using standard deconvolution method on 28 beams (X axis represents σ_1, Y axis represents σ_2)

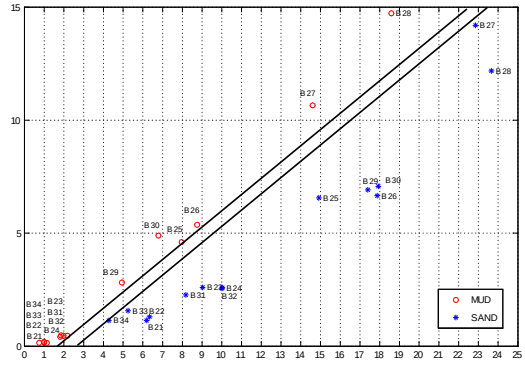

Figure 6.4: SV for Choi-Williams distribution of impulse response using FrFT on 28 beams (X axis represents σ_1, Y axis represents σ_2)

Table 6.2: Experimental results using the SVD of the Choi-Williams distribution

Number of beams used	Impulse response method	Margin width in % of scale	Accuracy
20	Standard Deconvolution	7.6	100%
20	FrFT	11.2	100%
28	Standard Deconvolution	2	100%
28	FrFT	3.8	100%

classification accuracy was obtained. We expect this large improvement in classification accuracy to be representative of results obtained with a larger data set.

6.5 Conclusions

In this paper we presented an approach for processing of sonar signals with the ultimate goal of ocean bottom sediment classification. The technique is based on the Fractional Fourier Transform (FrFT) of the optimum order of the bottom impulse response. The final classification, as currently devised, is based on singular value decomposition of the Choi-Williams distribution applied to the impulse response obtained using the Fractional Fourier Transform. The set of the singular values represents the desired feature vectors that describe the properties of the signal. The most relevant features (singular values) have been mapped in a reduced dimensionality space where an unsupervised classification has been employed for acoustic seabed classification. We used the central beams for the sediment classification. Perfect agreement between the experimental results and the ground truth is shown for our proposed technique on the small data set available. A comparison of the presented method with a k-means-based technique where wavelets were used for feature extraction was also given. The performance of the sediment classification when k-means was used is better by approximately 5% when the impulse response was determined via the FrFT rather than via a classical deconvolution method. Our classification technique has proved to be very effective not only when the central beams, near nadir, were used, but also for a larger number of beams (twenty-eight beams). The separation between the two classes, sand and mud,

using our FrFT method together with Choi-Williams distribution is approximately 50 % better than when classical deconvolution is used. The proposed classification technique outperforms the k-means competing technique.

Future work includes multi-class seabed classification using more features obtained from the Choi-Williams distribution applied to impulse response using FrFT and to determine the optimum discriminant function. We also hope to obtain larger data sets of data to corroborate the very promising results presented here.

Chapter 7 Experimental Results for Sediment Classification using Techniques on Sonar Data

7.1 Introduction

In this chapter, the author presents experimental results using sonar data collected in a field trial, and processed using the technique introduced in Chapters 3 through 6. In those chapters a small data set was used for a proof of concept. In addition, in this chapter, a brief presentation of the discriminant functions used for classification is made. Larger size real data sets have been recently released by the Naval Research Laboratory for testing the proposed classification algorithm. The data were acquired by Volume Search Sonar (VSS) during a mission in the Gulf of Mexico. Two sediment types were present and therefore considered for classification: mud and sand. The data set sizes are presented in Table 7.1. The first four data sets include data extracted from the response of the seabottom sediments corresponding to nadir beams only, and the last three data sets contain data from ten central beams per ping, five beams fore and five beams aft. In all data sets equal size subsets of mud and sand data are considered. In addition, the testing data sets are chosen from slightly different geographical locations than the training data sets. Two methods are employed to compute the impulse response of the sediment: the standard deconvolution method, implemented in the frequency domain and the author's Fractional Fourier Transform method described in Chapter 3. The impulse response is then represented in the time-frequency domain using the Wigner distribution and the Choi-Williams distribution. The singular value decomposition of these distributions are computed next. In this way, important discriminant features for classification are obtained because the singular value spectrum encodes the characteristic features of the signal. The features thus obtained are mapped in a reduced dimensional space (2D space and 3D space, respectively), by discarding all except the first, second, or the third singular values. Three classification approaches (linear classifier,

Table 7.1: Data sets size

Data sets	Training set	Testing set
Set 1	60 nadir beams	22 nadir beams
Set 2	60 nadir beams	30 nadir beams
Set 3	60 nadir beams	40 nadir beams
Set 4	40 nadir beams	40 nadir beams
Set 5	300 central beams	200 central beams
Set 6	260 central beams	102 central beams
Set 7	260 central beams	142 central beams

quadratic classifier and Mahalanobis classifier) are then applied to the resulting features, and their performances compared.

7.2 Discriminant Functions Overview

In pattern recognition, a classifier is a mapping from a feature space X to a discrete set of labels Y (Duda *et al.* , 2004). One way to represent pattern classifiers is in terms of the discriminant function.

The classifiers for which the discriminant functions have well defined mathematical functional forms are called parametric classifiers. Nonparametric classifiers are those for which there is no assumed function form for the discriminants and they are solely driven by the data. A linear classifier is a classifier that uses a linear function of its inputs to base its decision upon. For a two-class classification problem, one can visualize the operation of a linear classifier as splitting a high-dimensional input space with a hyperplane: all points on one side of the hyperplane belong to one class, while the others belong to the second. A linear classifier is often used in situations where the speed of classification is an issue, because it is often the fastest classifier. A quadratic classifier separates measurements of two or more classes of objects or events by a quadratic surfaces. In pattern classification applications, the choice of the discriminant function is not unique (Duda *et al.* , 2004).

7.2.1 Quadratic and Mahalanobis Discriminant Functions

A feature vector x is assigned to class ω_i by a classifier if $g_i(x) > g_j(x)$ for all $j \neq i$,

$i = 1, ..., c$,where c is the total number of classes. It is more common to define a single discriminant function by $g(x) \equiv g_i(x) - g_j(x)$, (Duda *et al.* , 2004). In this case the vector x is assigned to class ω_i if $g(x) > 0$. The decision boundary between the classes ω_i and ω_j is obtained when $g(x) = 0$.

In particular, for minimum-error-rate classification, when the maximum discriminant function corresponds to the maximum posterior probability, the discriminant function g_i is given by:

$$g_i(x) = \ln p(x|\omega_i) + \ln P(\omega_i) \tag{7.1}$$

where $p(x|\omega_i)$ represent the conditional densities and $P(\omega_i)$ are the prior probabilities for each class. Assuming the densities $p(x|\omega_i)$ are multivariate normal, $p(x|\omega_i) \tilde{} N(\mu_i, \Sigma_i)$ the discriminant function becomes (Duda *et al.* , 2004):

$$g_i(x) = -\frac{1}{2}(x - \mu_i)^T \Sigma_i^{-1}(x - \mu_i) - \frac{d}{2}\ln(2\pi) - \frac{1}{2}\ln(\Sigma_i) + \ln P(\omega_i) \tag{7.2}$$

where x is a d-dimensional column vector; for each class ω_i, μ_i is a d-dimensional mean vector, Σ_i is a $d \times d$ covariance matrix and Σ_i^{-1} is its inverse. The distance

$$D_i = \sqrt{\frac{1}{2}(x - \mu_i)^T \Sigma_i^{-1}(x - \mu_i)} \tag{7.3}$$

is called the Mahalanobis distance between the vector x and the mean vector μ_i for the data in class ω_i (Duda *et al.* , 2004).

The discriminant function for a number of special cases are discussed below:

Case 1: $\Sigma_i = \sigma^2 I$

In this case the features are statistically independent and each feature has the same variance σ^2. Geometrically, this corresponds to the situation in which the sample falls in equal size hyperspherical clusters, the clusters for the i-th class being centered about the mean vector μ_i. The

discriminant function is given by g_i (Duda *et al.* , 2004):

$$g_i(x) = -\frac{\|x - \mu_i\|^2}{2\sigma^2} + \ln P(\omega_i) \tag{7.4}$$

where $\|\cdot\|$ denotes the Euclidian norm, that is $\|x - \mu_i\|^2 = (x - \mu_i)^T(x - \mu_i)$

The classifier is called minimum distance classifier. The single discriminant function for this case, $g(x) = g_i(x) - g_j(x)$ becomes a linear function, because the quadratic term is the same for all classes, assuming the same prior probability.

Case 2: $\Sigma_i = \Sigma$

In this case the covariance matrices for all classes are identical but otherwise arbitrary. Geometrically, this corresponds to the situation where the samples fall in hyperellipsoidal clusters of equal size and shape; the cluster for the i^{th} class being centered about the mean vector μ_i. This leads to the discriminant function g_i (Duda *et al.* , 2004):

$$g_i(x) = -\frac{1}{2}(x - \mu_i)^T\Sigma^{-1}(x - \mu_i) + \ln P(\omega_i) \tag{7.5}$$

The last term in the above equation can be ignored if the prior probabilities for all classes are the same. The discriminant function expansion results in a sum involving a quadratic term $x^T\Sigma^{-1}x$ which here is independent of i. The resulting discriminant function, $g(x)$ is again linear. If the covariance matrix Σ is not diagonal, then the classifier becomes a minimum (Mahalanobis) distance classifier.

Case 3: $\Sigma_i \neq \Sigma_j$, $i \neq j$

In the general multivariate normal case, the covariance matrices are different for each class. The discriminant function for this case is (Duda *et al.* , 2004):

$$g_i(x) = -\frac{1}{2}(x - \mu_i)^T\Sigma_i^{-1}(x - \mu_i) - \frac{d}{2}\ln(2\pi) - \frac{1}{2}\ln(\Sigma_i) + \ln P(\omega_i) \tag{7.6}$$

In the binary classification case, the decision surfaces are hyperquadrics, and they can assume any of the general forms: hyperplanes, pairs of hyperplanes, hyperspheres, hyperellipsoids, hyperparaboloids (Duda *et al.* , 2004).

7.2.2 Fisher's Linear Discriminant Function

One of the popular discriminant functions is Fisher's linear discriminant, that is used in statistics to find the linear combination of features which best separates two or more classes of objects or events. The resulting combinations may be used as a linear classifier. The concept is based on projecting data from d-dimensions onto a line. An arbitrary projection will usually produce a confusion mixture of the samples determining a poor recognition performance. However, one can find an orientation of the line for which the projected samples are well separated (Duda *et al.* , 2004).

Let's assume a set of n d-dimensional samples, $x_{1,...,}x_n$, n_1 is labeled ω_1 and n_2 is labeled ω_2, where $n = n_1 + n_2$.The linear combination of the components of x is given by the scalar inner product

$$y = \mathbf{w}^T x \tag{7.7}$$

A set of n samples (projections of the corresponding x_i onto a line in direction w) are obtained, $y_1, ..., y_n$ divided into the subsets Y_1 and Y_2.

The Fisher linear discriminant entails finding an optimal $\mathbf{w}$ (direction vector) that maximizes the Fisher criterion (Duda *et al.* , 2004):

$$J(w) = \frac{\mathbf{w}^T S_B \mathbf{w}}{\mathbf{w}^T S_W \mathbf{w}} \tag{7.8}$$

where the between-class scatter matrix is $S_B = (\mu_1 - \mu_2)(\mu_1 - \mu_2)^T$ and the within-class scatter matrix $S_W = S_1 + S_2$ with $S_i = \sum_{x \in D_i} (x - \mu_i)(x - \mu_i)^T$. It can be shown that the maximum

separation between the classes occurs when :

$$\mathbf{w} = S_W^{-1}(\mu_1 - \mu_2) \tag{7.9}$$

7.3 Experimental Results

In the experiments the author discusses in this chapter, three types of classifiers are employed, namely, Fisher's linear discriminant, quadratic and Mahalanobis discriminant functions. The training and testing sets shown in Table 7.1 have been used for evaluation of the classification performance. Sets 1 through 4 employ nadir beams only and there are 2 nadir beams for each ping (one fore and one aft). Sets 5 through 7 use 5 fore beams and 5 aft beams from each ping (10 central beams per ping).

Figure 7.1 and Figure 7.2 show the intensity of the seabottom return of a sample of nadir for the sand and mud sediment classes, respectively, with stacked pings.Notice the much higher intensities as well as a large ping-to-ping variability for sand.

Experimental results for the seven data sets are presented in the following order: Tables 7.2 through 7.22 and Figures 7.3 through 7.9 correspond to the two dimensional case, when the two largest singular values extracted by the technique proposed in chapters 3 through 6 are used; Tables 7.23 through 7.43 and Figures 7.10 through 7.16 correspond to the three dimensional case, when the largest three singular values are employed.

Accuracy is used as a statistical measure of how well a binary classification test (into mud and sand classes) correctly classify the testing data. The accuracy presented for all the experimental results has been computed as:

$$Accuracy = \frac{Number\ of\ testing\ points\ (from\ both\ classes)\ correctly\ classified}{Total\ number\ of\ testing\ points\ (from\ both\ classes)} \tag{7.10}$$

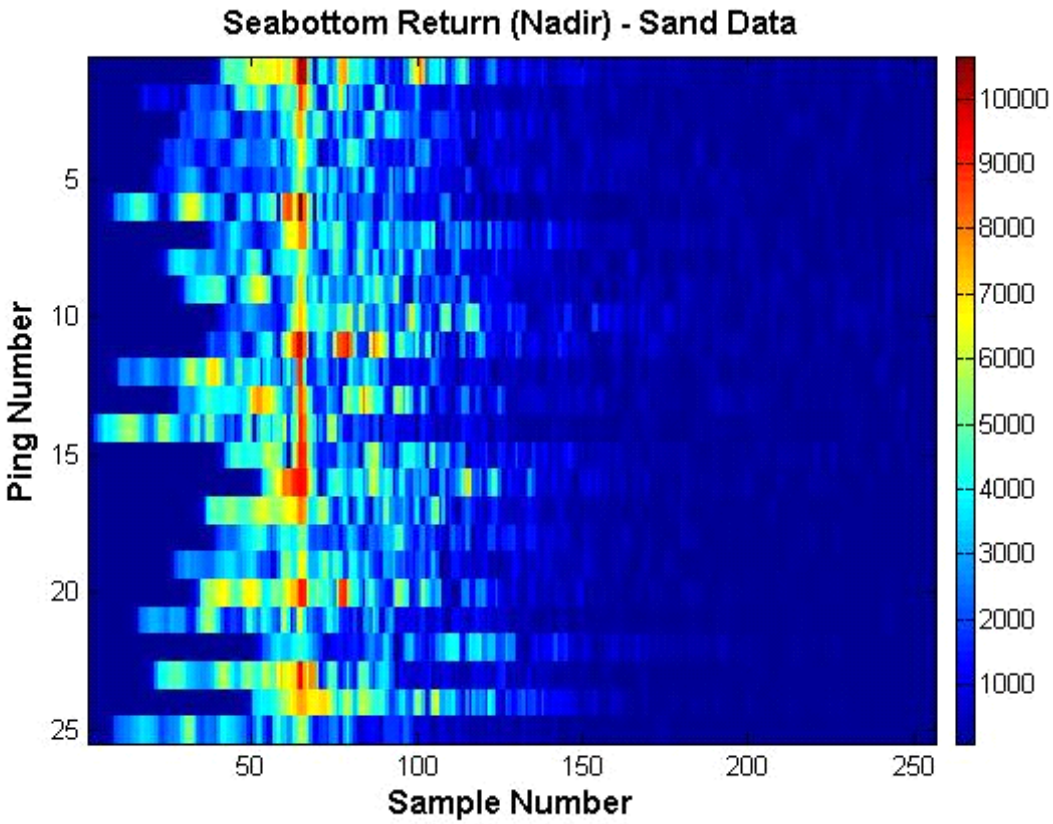

Figure 7.1: Seabottom return (nadir) for sand

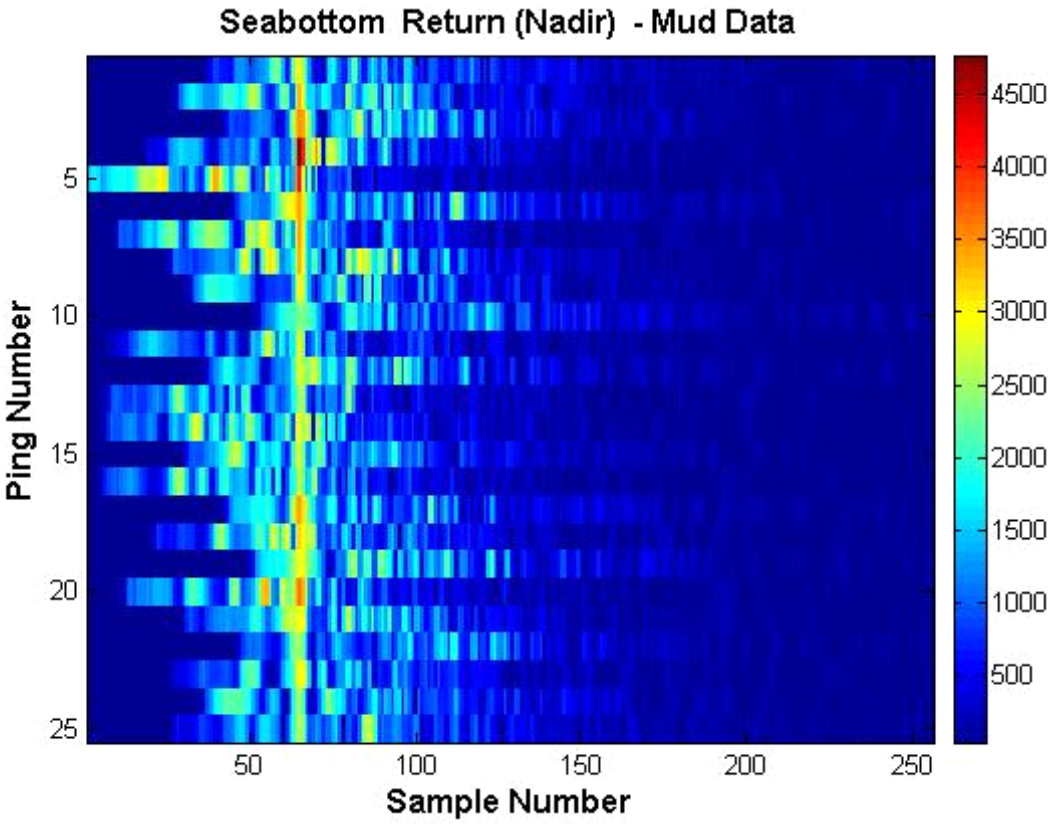

Figure 7.2: Seabottom return (nadir) for mud

7.3.1 Results using only the Two Largest Singular Values of the Time-Frequency Distributions

In this section, the author discusses first the results obtained only for nadir sets (sets 1 through 4) and then for central beam sets (sets 5 through 7). The results are consistent for nadir sets and for central beam sets, respectively, and can be summarized as follows.

In sets 1 through 4, only nadir beams (fore and aft) are used. Applying the linear discriminant function, the standard deconvolution performs better than the FrFT (by almost 5%) when the Wigner distribution is employed as shown in Tables 7.2, 7.5, 7.8 and 7.11. When the Choi-Williams distribution is used, both methods (standard deconvolution and FrFT) achieve on average, almost the same accuracy for linear discriminants. Further, when the quadratic discriminant function is used for classification based on the Wigner distribution, the FrFT method gives a better accuracy than the standard deconvolution method by about 7% as illustrated in Tables 7.2, 7.5, 7.8 and 7.11, The highest classification accuracy of 86%, reported in Table 7.2. Using the Choi-Williams distribution, the standard deconvolution method performed the best for quadratic discriminants, with the highest accuracy of 90%, also shown in Table 7.2. When the Mahalanobis discriminant function is used, the FrFT method leads if the Wigner distribution is used, as illustrated in Tables 7.2, 7.5, 7.8 and 7.11, and gives the best overall performance of 100% accuracy (Table 7.2). For the last discriminant function discussed, the FrFT method gives similar (as shown in Table 7.2) or better classification results (Tables 7.5, 7.8 and 7.11) than the standard deconvolution method when the Choi-Williams distribution is employed. For a better visualization, classification results are illustrated as bar plots in Figures 7.3 through 7.6. The confusion matrices presented in Tables 7.3, 7.4, 7.6, 7.7, 7.9, 7.10, 7.12 and 7.13 show that the mud sediment is easier to classify than sand.These results can be explained based on the fact that some seafloor regions supposed to correspond to the sand class included a mixture of sand and mud sediments.

Table 7.2: Testing results for data set 1 - (two dimensional case)

Discriminant Function	Accuracy			
	Standard deconvolution method		FrFT method	
	Wigner	Choi-Williams	Wigner	Choi-Williams
Linear	**86%**	**86%**	81%	**86%**
Quadratic	77%	**90%**	86 %	86 %
Mahalanobis	86%	95%	**100 %**	95%

Table 7.3: Confusion matrix for the classes mud and sand, for data set 1 (two dimensional case) using deconvolution method

Discriminant Function		Wigner		Choi-Williams	
		True sand	True mud	True sand	True mud
Linear	Predicted sand	8	0	8	0
	Predicted mud	3	11	3	11
Quadratic	Predicted sand	6	0	9	0
	Predicted mud	5	11	2	11
Mahalanobis	Predicted sand	8	0	10	0
	Predicted mud	3	11	1	11

Table 7.4: Confusion matrix for the classes mud and sand, for data set 1 (two dimensional case) using FrFT method

Discriminant Function		Wigner		Choi-Williams	
		True sand	True mud	True sand	True mud
Linear	Predicted sand	7	0	8	0
	Predicted mud	4	11	3	11
Quadratic	Predicted sand	8	0	8	0
	Predicted mud	3	11	3	11
Mahalanobis	Predicted sand	11	0	10	0
	Predicted mud	0	11	1	11

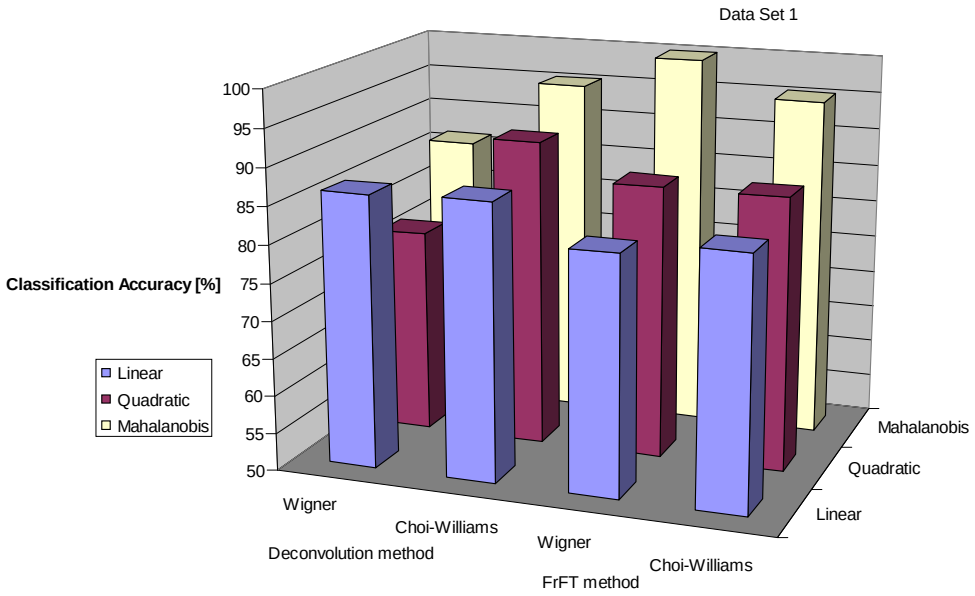

Figure 7.3: Classification accuracy data set 1 (two dimensional case)

Table 7.5: Testing results for data set 2 (two dimensional case)

Discriminant Function	Accuracy			
	Standard deconvolution method		FrFT method	
	Wigner	Choi-Williams	Wigner	Choi-Williams
Linear	**83%**	**83%**	80 %	**83 %**
Quadratic	76%	**86 %**	83 %	83 %
Mahalanobis	80%	86 %	**93%**	90%

Table 7.6: Confusion matrix for the classes mud and sand, for data set 2 (two dimensional case) using deconvolution method

Discriminant Function		Wigner		Choi-Williams	
		True sand	True mud	True sand	True mud
Linear	Predicted sand	10	0	10	0
	Predicted mud	5	15	5	15
Quadratic	Predicted sand	8	0	11	0
	Predicted mud	7	15	4	15
Mahalanobis	Predicted sand	10	1	12	1
	Predicted mud	5	14	3	14

Table 7.7: Confusion matrix for the classes mud and sand, for data set 2 (two dimensional case) using FrFT method

Discriminant Function		Wigner		Choi-Williams	
		True sand	True mud	True sand	True mud
Linear	Predicted sand	9	0	10	0
	Predicted mud	6	15	5	15
Quadratic	Predicted sand	10	0	10	0
	Predicted mud	5	15	5	15
Mahalanobis	Predicted sand	13	0	12	0
	Predicted mud	2	15	3	15

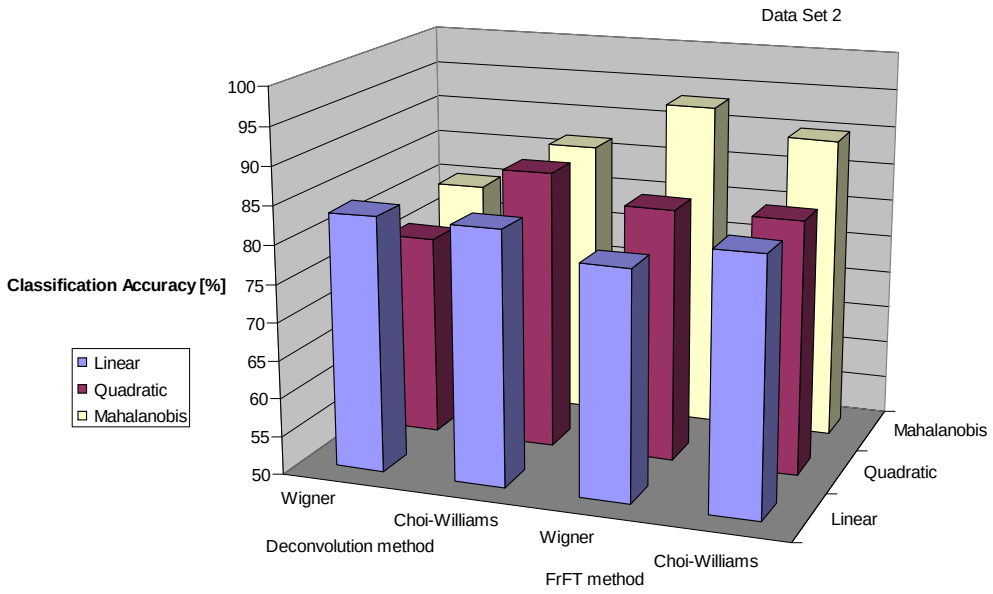

Figure 7.4: Classification accuracy data set 2 (two dimensional case)

Table 7.8: Testing results for data set 3 (two dimensional case)

Discriminant Function	Accuracy			
	Standard deconvolution method		FrFT method	
	Wigner	Choi-Williams	Wigner	Choi-Williams
Linear	**82%**	**82%**	77%	**82%**
Quadratic	75%	**85%**	82%	**85%**
Mahalanobis	80%	90%	**95%**	92 %

Table 7.9: Confusion matrix for the classes mud and sand, for data set 3 (two dimensional case) using deconvolution method

Discriminant Function		Wigner		Choi-Williams	
		True sand	True mud	True sand	True mud
Linear	Predicted sand	13	0	13	0
	Predicted mud	7	20	7	20
Quadratic	Predicted sand	10	0	14	0
	Predicted mud	10	20	6	20
Mahalanobis	Predicted sand	13	1	17	1
	Predicted mud	7	19	3	19

Table 7.10: Confusion matrix for the classes mud and sand, for data set 3 (two dimensional case) using FrFT method

Discriminant Function		Wigner		Choi-Williams	
		True sand	True mud	True sand	True mud
Linear	Predicted sand	11	0	13	0
	Predicted mud	9	20	7	20
Quadratic	Predicted sand	13	0	14	0
	Predicted mud	7	20	6	20
Mahalanobis	Predicted sand	18	0	17	0
	Predicted mud	2	20	3	20

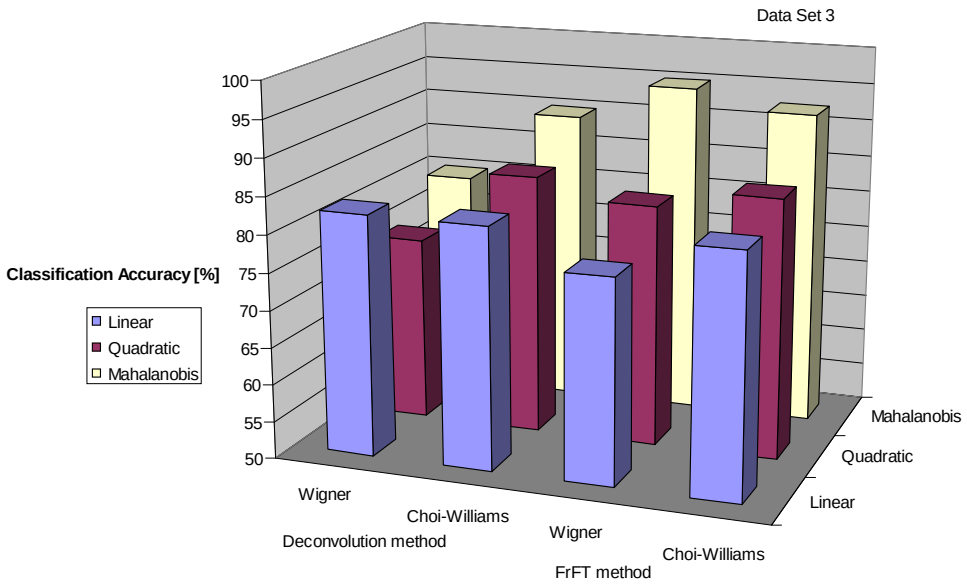

Figure 7.5: Classification accuracy data set 3 (two dimensional case)

Table 7.11: Testing results for data set 4 (two dimensional case)

Discriminant Function	Accuracy			
	Standard deconvolution method		FrFT method	
	Wigner	Choi-Williams	Wigner	Choi-Williams
Linear	**82%**	72 %	77%	**82%**
Quadratic	75%	**85%**	82%	82%
Mahalanobis	82%	87%	**95%**	92 %

Table 7.12: Confusion matrix for the classes mud and sand, for data set 4 (two dimensional case) using deconvolution method

Discriminant Function		Wigner		Choi-Williams	
		True sand	True mud	True sand	True mud
Linear	Predicted sand	13	0	9	0
	Predicted mud	7	20	11	20
Quadratic	Predicted sand	11	1	14	0
	Predicted mud	9	19	6	20
Mahalanobis	Predicted sand	15	2	15	0
	Predicted mud	5	18	5	20

Table 7.13: Confusion matrix for the classes mud and sand, for data set 4 (two dimensional case) using FrFT method

Discriminant Function		Wigner		Choi-Williams	
		True sand	True mud	True sand	True mud
Linear	Predicted sand	11	0	13	0
	Predicted mud	9	20	7	20
Quadratic	Predicted sand	13	0	13	0
	Predicted mud	7	20	7	20
Mahalanobis	Predicted sand	18	0	17	0
	Predicted mud	2	20	3	20

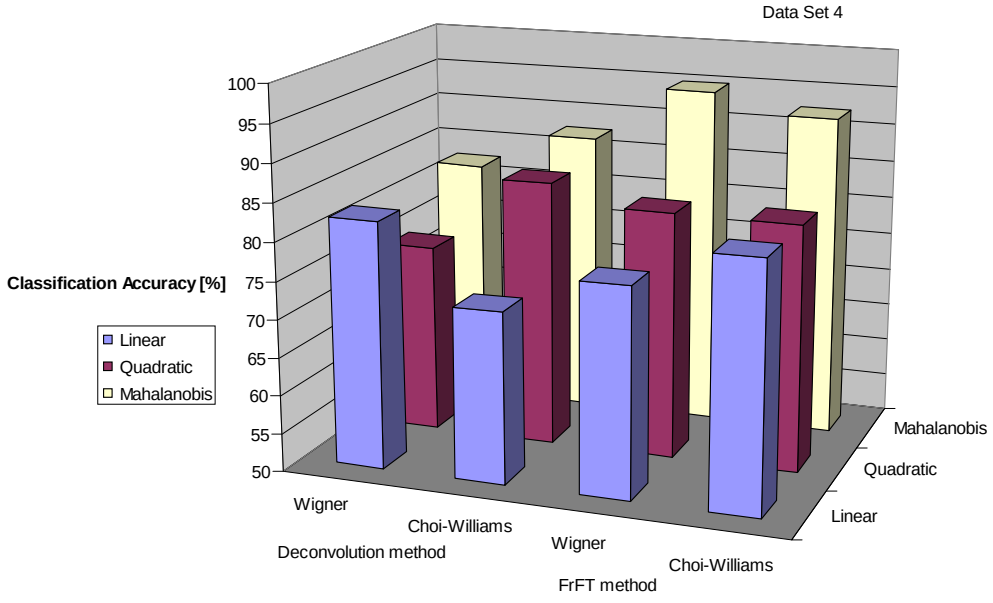

Figure 7.6: Classification accuracy data set 4 (two dimensional case)

The best combination, that gives the highest accuracy, for nadir data, using only two singular values is the FrFT/ Wigner/ Mahalanobis.

The data sets 5 through 7 consist of 10 central beams per ping. The training and testing data set sizes are shown in Table 7.1. The standard deconvolution method performs better than the FrFT method (for both Wigner and Choi Williams distributions) for the linear discriminant function as illustrated in Tables 7.14, 7.17 and 7.20. The highest accuracy achieved is 70%, on average 4% higher than that obtained with the FrFT method (Table 7.17). When using the quadratic discriminant function, the FrFT provides the best accuracy for both cases (Wigner and Choi-Williams) as presented in Tables 7.14,7.17 and 7.20. The FrFT method shows the best performance when the Mahalanobis discriminant function is employed for classification based on the Wigner and the Choi-Williams distributions (Tables 7.14,7.17 and 7.20). The highest accuracy of 81% is obtained for data set 6, when the FrFT, the Wigner distribution and Mahalanobis discriminant functions are used. For a better visualization, classification results are illustrated as bar plots in Figures 7.7 through 7.9.

The confusion matrices presented in Tables 7.15, 7.16, 7.18, 7.19, 7.21 and 7.22 show that the mud sediment is best classified compared to the sand sediment.

The author recommendation for sediment classification when using two singular values is a combination of the FrFT/Wigner/ Mahalanobis, when central beams are used.

Table 7.14: Testing results for data set 5 (two dimensional case)

Discriminant Function	Accuracy			
	Standard deconvolution method		FrFT method	
	Wigner	Choi-Williams	Wigner	Choi-Williams
Linear	**70%**	69%	68%	66%
Quadratic	68%	73%	72%	**75%**
Mahalanobis	76%	74%	**79%**	**79%**

Table 7.15: Confusion matrix for the classes mud and sand, for data set 5 (two dimensional case) using deconvolution method

Discriminant Function		Wigner		Choi-Williams	
		True sand	True mud	True sand	True mud
Linear	Predicted sand	42	2	41	2
	Predicted mud	58	98	59	98
Quadratic	Predicted sand	39	3	49	2
	Predicted mud	61	97	51	98
Mahalanobis	Predicted sand	64	12	62	14
	Predicted mud	36	88	38	86

Table 7.16: Confusion matrix for the classes mud and sand, for data set 5 (two dimensional case) using FrFT method

Discriminant Function		Wigner		Choi-Williams	
		True sand	True mud	True sand	True mud
Linear	Predicted sand	36	0	33	0
	Predicted mud	64	100	67	100
Quadratic	Predicted sand	46	1	51	0
	Predicted mud	54	99	49	100
Mahalanobis	Predicted sand	70	11	70	11
	Predicted mud	30	89	30	89

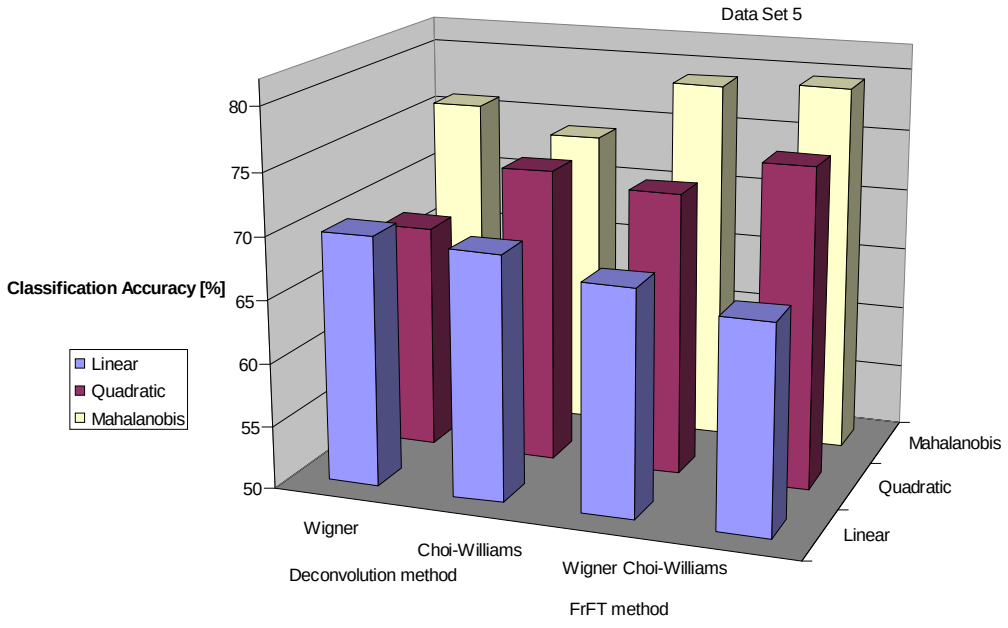

Figure 7.7: Classification accuracy data set 5 (two dimensional case)

Table 7.17: Testing results for data set 6 (two dimensional case)

Discriminant Function	Accuracy			
	Standard deconvolution method		FrFT method	
	Wigner	Choi-Williams	Wigner	Choi-Williams
Linear	**70 %**	**70%**	68%	66%
Quadratic	68%	73%	74%	**76%**
Mahalanobis	75%	76%	**81%**	79%

Table 7.18: Confusion matrix for the classes mud and sand, for data set 6 (two dimensional case) using deconvolution method

Discriminant Function		Wigner		Choi-Williams	
		True sand	True mud	True sand	True mud
Linear	Predicted sand	22	1	22	1
	Predicted mud	29	50	29	50
Quadratic	Predicted sand	21	2	25	1
	Predicted mud	30	49	26	50
Mahalanobis	Predicted sand	32	6	35	8
	Predicted mud	19	45	16	43

Table 7.19: Confusion matrix for the classes mud and sand, for data set 6 (two dimensional case) using FrFT method

Discriminant Function		Wigner		Choi-Williams	
		True sand	True mud	True sand	True mud
Linear	Predicted sand	19	0	17	0
	Predicted mud	32	51	34	51
Quadratic	Predicted sand	25	0	27	0
	Predicted mud	26	51	24	51
Mahalanobis	Predicted sand	37	5	38	8
	Predicted mud	14	46	13	43

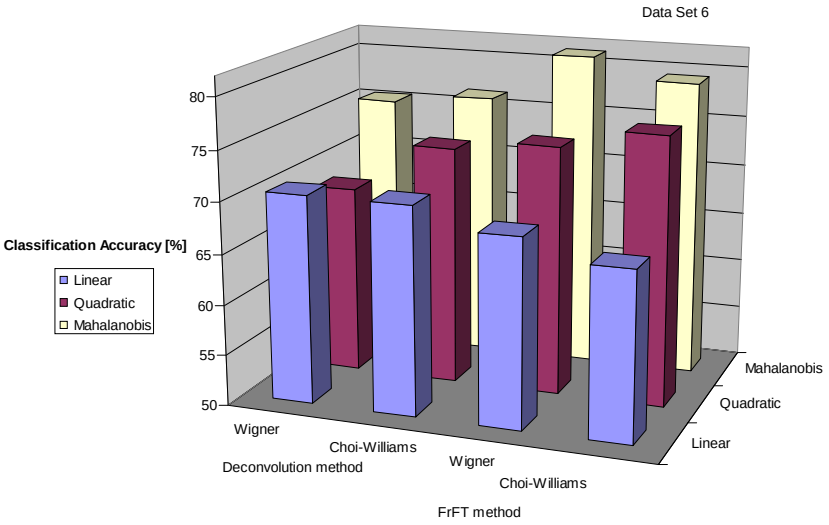

Figure 7.8: Classification accuracy data set 6 (two dimensional case)

Table 7.20: Testing results for data set 7 (two dimensional case)

Discriminant Function	Accuracy			
	Standard deconvolution method		FrFT method	
	Wigner	Choi-Williams	Wigner	Choi-Williams
Linear	**68%**	**68%**	66%	64%
Quadratic	66%	71%	71%	**73%**
Mahalanobis	74%	75%	**78%**	76%

Table 7.21: Confusion matrix for the classes mud and sand, for data set 7 (two dimensional case) using deconvolution method

Discriminant Function		Wigner		Choi-Williams	
		True sand	True mud	True sand	True mud
Linear	Predicted sand	27	1	27	1
	Predicted mud	44	70	44	70
Quadratic	Predicted sand	25	2	32	1
	Predicted mud	46	69	39	70
Mahalanobis	Predicted sand	41	6	44	8
	Predicted mud	30	65	27	63

Table 7.22: Confusion matrix for the classes mud and sand, for data set 7 (two dimensional case) using FrFT method

Discriminant Function		Wigner		Choi-Williams	
		True sand	True mud	True sand	True mud
Linear	Predicted sand	23	0	20	0
	Predicted mud	48	71	51	71
Quadratic	Predicted sand	31	0	34	0
	Predicted mud	40	71	37	71
Mahalanobis	Predicted sand	46	5	46	8
	Predicted mud	25	66	25	63

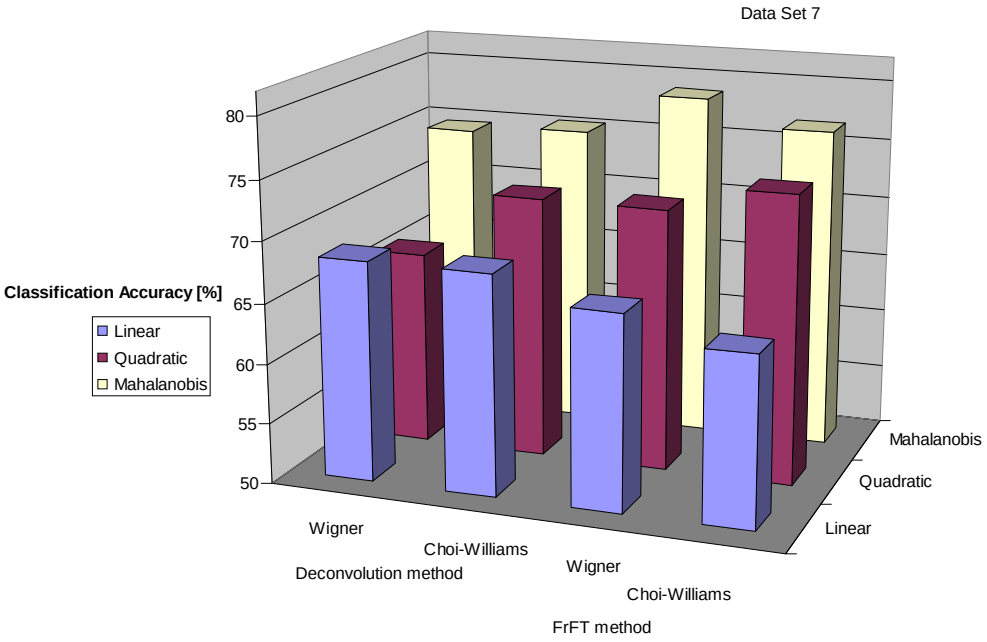

Figure 7.9: Classification accuracy data set 7 (two dimensional case)

7.3.2 Results using the Three Largest Singular Values of the Time-Frequency Distributions

As in the two dimensional case, in this section the author discusses first the results obtained only for the nadir sets and then for the central beam sets. Three dimensional case results for the data sets corresponding to nadir beams only are shown in Tables 7.23 through 7.34 and the results for the central beams sets are presented in Tables 7.35 through 7.43.

In Tables 7.23, 7.26, 7.29 and 7.32 for the linear discriminant function and the Wigner distribution, the standard deconvolution method gives the same or better accuracy than the FrFT method. When the Choi-Williams distribution is employed, the FrFT method yields a higher classification accuracy than the standard deconvolution method, obtained for the linear discriminant (Tables 7.23, 7.26, 7.29 and 7.32). When the quadratic discriminant function is used, the FrFT method gives a higher accuracy than the standard deconvolution method by around 4% in the case of the Wigner distribution. For the quadratic discriminant, a better accuracy than the FrFT method has been obtained for the standard deconvolution method on most of the data sets when the Choi-Williams distribution was employed (7.23, 7.26, 7.29). The best accuracy (100%) among all nadir beams data sets with three singular values is obtained for the FrFT method when the Mahalanobis discriminant function with the Wigner distribution is used, as shown in Table 7.23. This results matches that obtained with two singular values. The classification results are illustrated as bar plots in Figures 7.10 through 7.13 and as confusion matrices in Tables 7.24, 7.25, 7.27, 7.28, 7.30, 7.31, 7.33 and 7.34.

The best combination for nadir beams data sets is the FrFT/Wigner/Mahalanobis when three singular values are used as features.

Table 7.23: Testing results for data set 1 (three dimensional case)

Discriminant Function	Accuracy			
	Standard deconvolution method		FrFT method	
	Wigner	Choi-Williams	Wigner	Choi-Williams
Linear	**86%**	81%	**86%**	**86%**
Quadratic	81%	**90%**	86%	81%
Mahalanobis	90%	90%	**100 %**	90%

Table 7.24: Confusion matrix for the classes mud and sand, for data set 1 (three dimensional case) using deconvolution method

Discriminant Function		Wigner		Choi-Williams	
		True sand	True mud	True sand	True mud
Linear	Predicted sand	8	0	7	0
	Predicted mud	3	11	4	11
Quadratic	Predicted sand	7	0	10	1
	Predicted mud	4	11	1	10
Mahalanobis	Predicted sand	10	1	11	2
	Predicted mud	1	10	0	9
Mahalanobis	Predicted sand	46	5	46	8
	Predicted mud	25	66	25	63

Table 7.25: Confusion matrix for the classes mud and sand, for data set 1(three dimensional case) using FrFT method

Discriminant Function		Wigner		Choi-Williams	
		True sand	True mud	True sand	True mud
Linear	Predicted sand	8	0	8	0
	Predicted mud	3	11	3	11
Quadratic	Predicted sand	8	0	8	1
	Predicted mud	3	11	3	10
Mahalanobis	Predicted sand	11	0	10	1
	Predicted mud	0	11	1	10

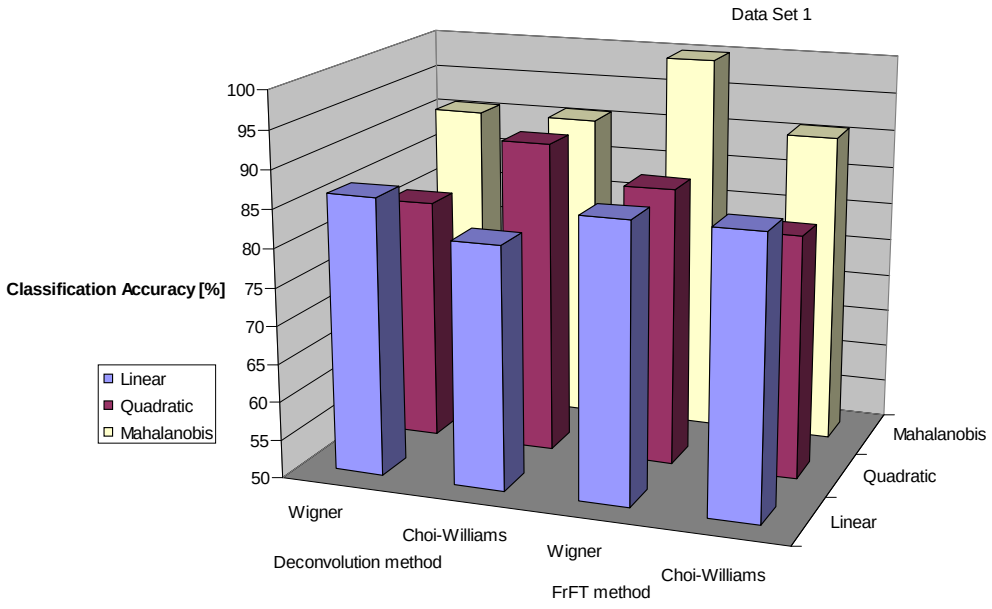

Figure 7.10: Classification accuracy data set 1 (three dimensional case)

Table 7.26: Testing results for data set 2 (three dimensional case)

Discriminant Function	Accuracy			
	Standard deconvolution method		FrFT method	
	Wigner	Choi-Williams	Wigner	Choi-Williams
Linear	**83%**	80%	**83%**	**83%**
Quadratic	80%	**86%**	83%	76%
Mahalanobis	83%	86%	**90%**	86%

Table 7.27: Confusion matrix for the classes mud and sand, for data set 2 (three dimensional case) using deconvolution method

Discriminant Function		Wigner		Choi-Williams	
		True sand	True mud	True sand	True mud
Linear	Predicted sand	10	0	9	0
	Predicted mud	5	15	6	15
Quadratic	Predicted sand	9	0	12	1
	Predicted mud	6	15	3	14
Mahalanobis	Predicted sand	12	2	13	2
	Predicted mud	3	13	2	13

Table 7.28: Confusion matrix for the classes mud and sand, for data set 2 (three dimensional case) using FrFT method

Discriminant Function		Wigner		Choi-Williams	
		True sand	True mud	True sand	True mud
Linear	Predicted sand	10	0	10	0
	Predicted mud	5	15	5	15
Quadratic	Predicted sand	10	0	10	2
	Predicted mud	5	15	5	13
Mahalanobis	Predicted sand	13	1	13	2
	Predicted mud	2	14	2	13

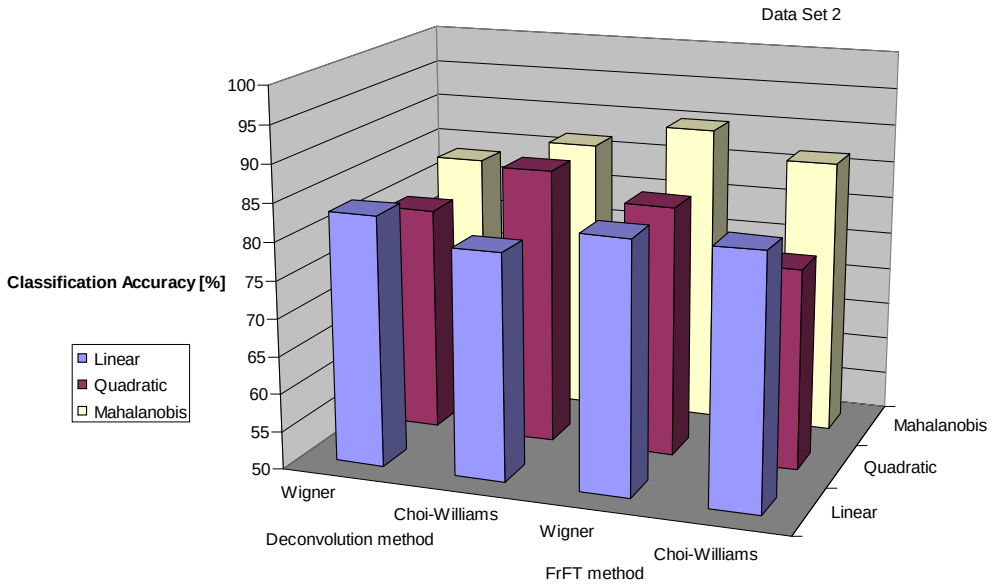

Figure 7.11: Classification accuracy data set 2 (three dimensional case)

Table 7.29: Testing results for data set 3 (three dimensional case)

Discriminant Function	Accuracy			
	Standard deconvolution method		FrFT method	
	Wigner	Choi-Williams	Wigner	Choi-Williams
Linear	**82%**	80%	**82%**	**82%**
Quadratic	80%	**87%**	85%	80%
Mahalanobis	87%	90%	**92%**	90%

Table 7.30: Confusion matrix for the classes mud and sand, for data set 3 (three dimensional case) using deconvolution method

Discriminant Function		Wigner		Choi-Williams	
		True sand	True mud	True sand	True mud
Linear	Predicted sand	13	0	12	0
	Predicted mud	7	20	8	20
Quadratic	Predicted sand	12	0	16	1
	Predicted mud	8	20	4	19
Mahalanobis	Predicted sand	17	2	18	2
	Predicted mud	3	18	2	18

Table 7.31: Confusion matrix for the classes mud and sand, for data set 3 (three dimensional case) using FrFT method

Discriminant Function		Wigner		Choi-Williams	
		True sand	True mud	True sand	True mud
Linear	Predicted sand	13	0	13	0
	Predicted mud	7	20	7	20
Quadratic	Predicted sand	14	0	14	2
	Predicted mud	6	20	6	18
Mahalanobis	Predicted sand	18	1	18	2
	Predicted mud	2	19	2	18

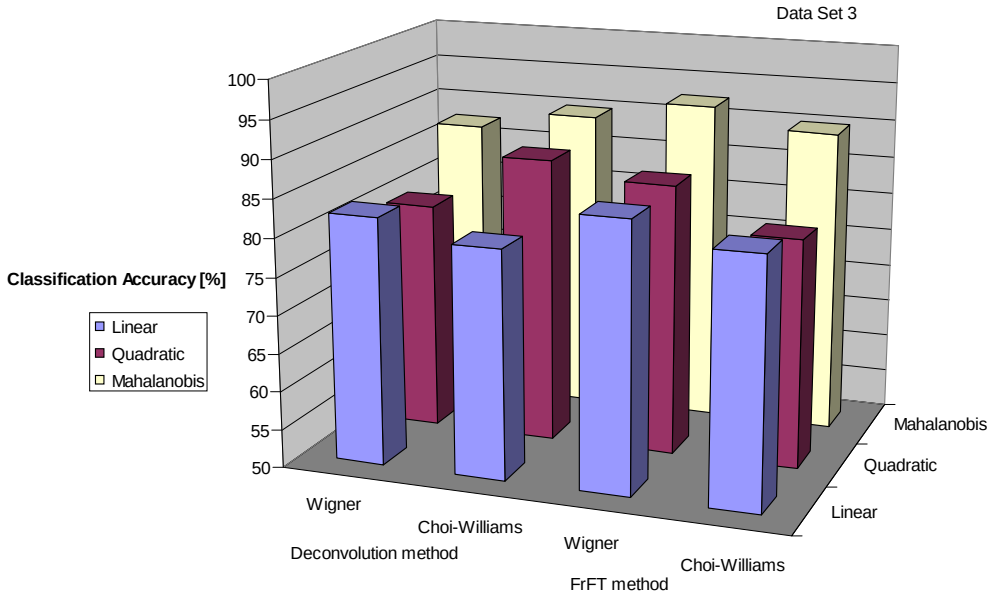

Figure 7.12: Classification accuracy data set 3 (three dimensional case)

Table 7.32: Testing results for data set 4 (three dimensional case)

Discriminant Function	Accuracy			
	Standard deconvolution method		FrFT method	
	Wigner	Choi-Williams	Wigner	Choi-Williams
Linear	77%	72%	70%	**82%**
Quadratic	82%	77%	**85%**	82%
Mahalanobis	85%	80%	**92%**	90%

Table 7.33: Confusion matrix for the classes mud and sand, for data set 4 (three dimensional case) using deconvolution method

Discriminant Function		Wigner		Choi-Williams	
		True sand	True mud	True sand	True mud
Linear	Predicted sand	11	0	9	0
	Predicted mud	9	20	11	20
Quadratic	Predicted sand	14	1	12	1
	Predicted mud	6	19	8	19
Mahalanobis	Predicted sand	17	3	14	2
	Predicted mud	3	17	6	18

Table 7.34: Confusion matrix for the classes mud and sand, for data set 4 (three dimensional case) using FrFT method

Discriminant Function		Wigner		Choi-Williams	
		True sand	True mud	True sand	True mud
Linear	Predicted sand	8	0	13	0
	Predicted mud	12	20	7	20
Quadratic	Predicted sand	14	0	14	1
	Predicted mud	6	20	6	19
Mahalanobis	Predicted sand	17	0	18	2
	Predicted mud	3	20	2	18

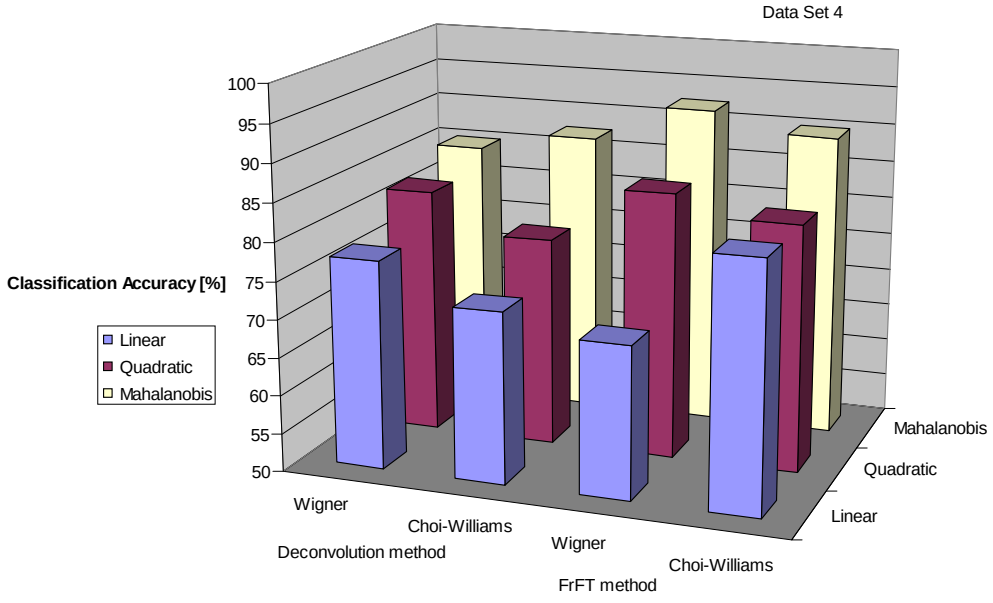

Figure 7.13: Classification accuracy data set 4 (three dimensional case)

In the three dimensional case, for sets 5 through 7, when the linear discriminant function is used, the standard deconvolution method performs better than the FrFT method for both Wigner and Choi-Williams distributions, as shown in Tables 7.35, 7.38 and 7.41. The FrFT method shows a better performance than the standard deconvolution method when the quadratic discriminant function is employed with the Wigner distribution (Tables 7.35, 7.38 and 7.41). Applying the quadratic discriminant function with the Choi-Williams distribution, a performance similar or better than with the FrFT method has been achieved for the standard deconvolution method. The FrFT method achieved the best performance when the Mahalanobis discriminant function was employed on average on most of the data sets with central beams (Tables 7.35, 7.38 and 7.41). The classification results are shown as bar plots in Figures 7.14 through 7.16 and as confusion matrices in Tables 7.36, 7.37, 7.39, 7.40, 7.42 and 7.43.

The best combination for central beams data sets is the FrFT/ Wigner/Mahalanobis, when three singular values are used as features.

Table 7.35: Testing results for data set 5 (three dimensional case)

Discriminant Function	Accuracy			
	Standard deconvolution method		FrFT method	
	Wigner	Choi-Williams	Wigner	Choi-Williams
Linear	**68%**	**70%**	67%	65%
Quadratic	69%	**73%**	72%	**73%**
Mahalanobis	77%	75%	**77%**	**78%**

Table 7.36: Confusion matrix for the classes mud and sand, for data set 5 (three dimensional case) using deconvolution method

Discriminant Function		Wigner		Choi-Williams	
		True sand	True mud	True sand	True mud
Linear	Predicted sand	41	4	42	2
	Predicted mud	59	96	58	98
Quadratic	Predicted sand	43	4	51	5
	Predicted mud	57	96	49	95
Mahalanobis	Predicted sand	71	16	67	16
	Predicted mud	29	84	33	84

Table 7.37: Confusion matrix for the classes mud and sand, for data set 5 (three dimensional case) using FrFT method

Discriminant Function		Wigner		Choi-Williams	
		True sand	True mud	True sand	True mud
Linear	Predicted sand	35	0	30	0
	Predicted mud	65	100	70	100
Quadratic	Predicted sand	47	2	49	3
	Predicted mud	53	98	51	97
Mahalanobis	Predicted sand	72	17	76	19
	Predicted mud	28	83	24	81

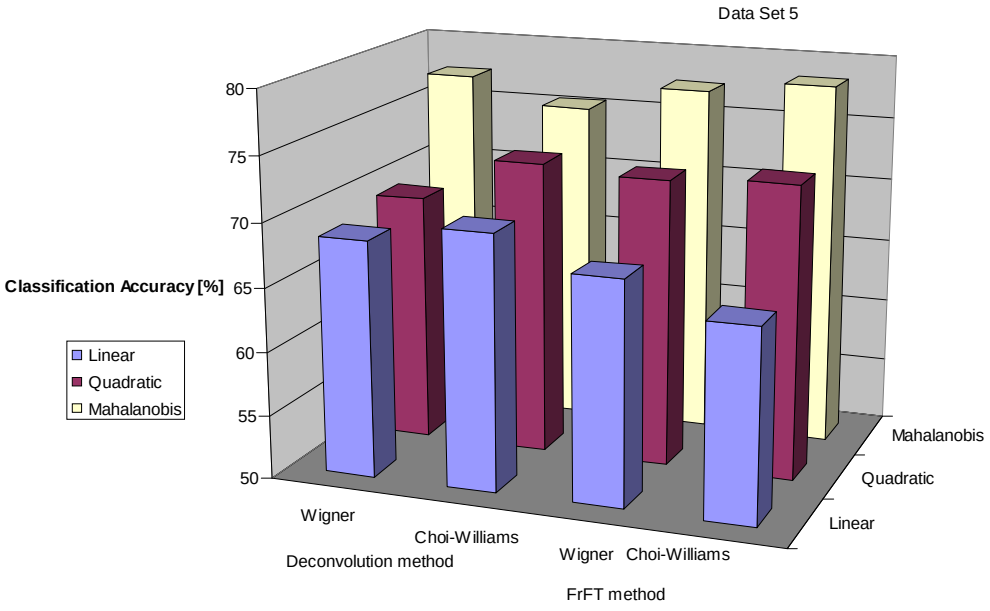

Figure 7.14: Classification accuracy data set 5 (three dimensional case)

Table 7.38: Testing results for data set 6 (three dimensional case)

Discriminant Function	Accuracy			
	Standard deconvolution method		FrFT method	
	Wigner	Choi-Williams	Wigner	Choi-Williams
Linear	**70%**	**71%**	68%	64%
Quadratic	68%	**74%**	**74%**	71%
Mahalanobis	76%	**78%**	**78%**	**78%**

Table 7.39: Confusion matrix for the classes mud and sand, for data set 6 (three dimensional case) using deconvolution method

Discriminant Function		Wigner		Choi-Williams	
		True sand	True mud	True sand	True mud
Linear	Predicted sand	22	1	23	1
	Predicted mud	29	50	28	50
Quadratic	Predicted sand	23	3	28	3
	Predicted mud	28	48	23	48
Mahalanobis	Predicted sand	37	10	36	7
	Predicted mud	14	41	15	44

Table 7.40: Confusion matrix for the classes mud and sand, for data set 6 (three dimensional case) using FrFT method

Discriminant Function		Wigner		Choi-Williams	
		True sand	True mud	True sand	True mud
Linear	Predicted sand	19	0	15	0
	Predicted mud	32	51	36	51
Quadratic	Predicted sand	26	1	23	1
	Predicted mud	25	50	28	50
Mahalanobis	Predicted sand	38	9	40	11
	Predicted mud	13	42	11	40

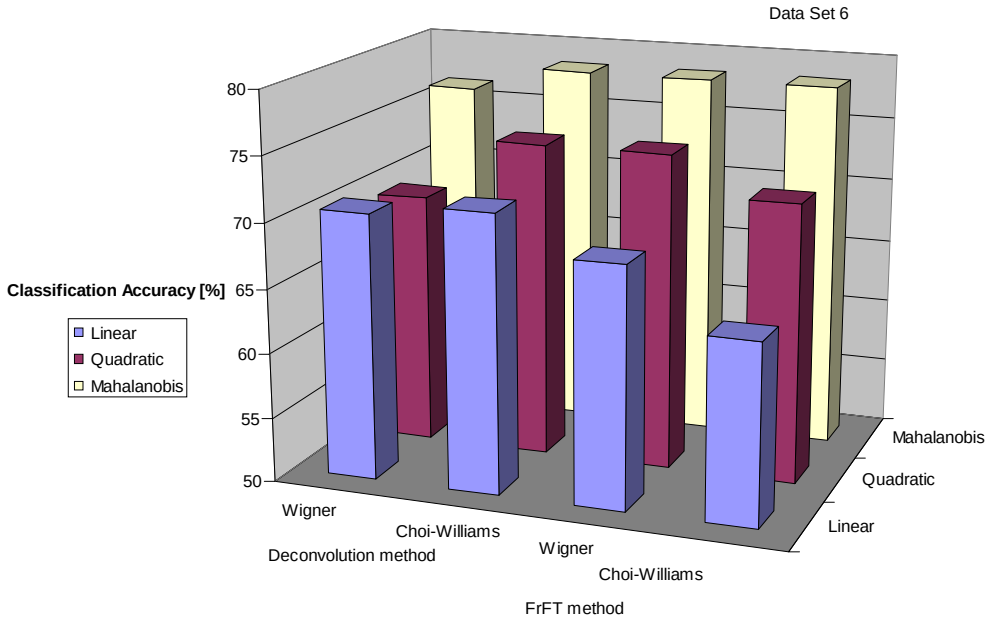

Figure 7.15: Classification accuracy data set 6 (three dimensional case)

Table 7.41: Testing results for data set 7 (three dimensional case)

Discriminant Function	Accuracy			
	Standard deconvolution method		FrFT method	
	Wigner	Choi-Williams	Wigner	Choi-Williams
Linear	**68 %**	**69%**	65%	62%
Quadratic	67%	**71%**	**71%**	**71%**
Mahalanobis	75%	**76%**	**76%**	**76%**

Table 7.42: Confusion matrix for the classes mud and sand, for data set 7 (three dimensional case) using deconvolution method

Discriminant Function		Wigner		Choi-Williams	
		True sand	True mud	True sand	True mud
Linear	Predicted sand	27	1	29	1
	Predicted mud	44	70	42	70
Quadratic	Predicted sand	28	3	34	3
	Predicted mud	43	68	37	68
Mahalanobis	Predicted sand	46	10	46	8
	Predicted mud	25	61	25	63

Table 7.43: Confusion matrix for the classes mud and sand, for data set 7 (three dimensional case) using FrFT method

Discriminant Function		Wigner		Choi-Williams	
		True sand	True mud	True sand	True mud
Linear	Predicted sand	22	0	18	0
	Predicted mud	49	71	53	71
Quadratic	Predicted sand	32	1	31	1
	Predicted mud	39	70	40	71
Mahalanobis	Predicted sand	47	9	49	11
	Predicted mud	24	62	22	60

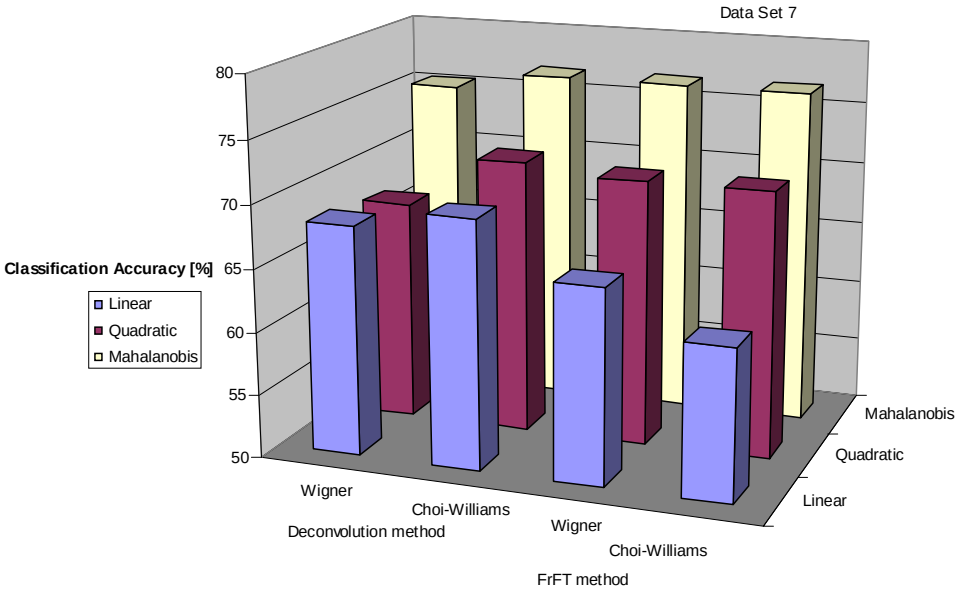

Figure 7.16: Classification accuracy data set 7 (three dimensional case)

From the experimental results shown in this chapter, one can notice that the classification accuracy is much better in the case when only nadir beams are employed (data sets 1 through 4) rather than when a larger number of beams are used (central beams and nadir beams, as in data sets 5 through 7). The signal strength intensity of the nadir beams is higher than that of any other outer beams, and hence a higher classification accuracy is expected for the data sets 1 through 4 compared to data sets 5 through 7. In addition, the presence of the sidelobe specular returns for the data sets 5 through 7 diminishes the accuracy of the sediment classification for the central beam data sets.

7.3.3 Conclusions and Recommendations

In this section a summary of the experimental results is presented and recommendations are given. The author presents the summary in a tabular format for the following cases:

Table 7.44: Summary Results nadir beams(two dimensional case)

Discriminant Function	Accuracy			
	Standard deconvolution method		FrFT method	
	Wigner	Choi-Williams	Wigner	Choi-Williams
Linear	**x**	**x**		**x**
Quadratic		**x**		
Mahalanobis			**MAX1_2D**	

a) two dimensional case, nadir beams only - Table 7.44,

b) two dimensional case, central beams - Table 7.45,

c) three dimensional case, nadir beams only - Table 7.46,

d) three dimensional case, central beams - Table 7.47.

In the Tables 7.44 through 7.47 the **x** symbol represents the maximum accuracy obtained for each type of the discriminant function. The notations **MAX1_2D, MAX2_2D, MAX1_3D, MAX2_3D** are used for the maximum classification accuracy corresponding to each case discussed in Tables 7.44 through 7.47, respectively. From the experimental results one can notice that **MAX1_2D** >**MAX2_2D,** and **MAX1_3D** >**MAX2_3D.**

When three singular values are used as features, the obtained accuracy was not higher than that achieved for the two dimensional case. Due to this fact it is recommended to use two singular values as features for sediment classification, from the time complexity computation point of view.

Finally the author recommends the following combination in order to obtain a high accuracy sediment classification (of about 100%): FrFT/ Wigner/Mahalanobis discriminant, using nadir beams only and two singular values as features. However, the same combination can also be used for central beams and a classification accuracy of around 80% can be achieved.

Table 7.45: Summary Results central beams(two dimensional case)

Discriminant Function	Accuracy			
	Standard deconvolution method		FrFT method	
	Wigner	Choi-Williams	Wigner	Choi-Williams
Linear	**x**	**x**		
Quadratic				**x**
Mahalanobis			**MAX2_2D**	

Table 7.46: Summary Results nadir beams (three dimensional case)

Discriminant Function	Accuracy			
	Standard deconvolution method		FrFT method	
	Wigner	Choi-Williams	Wigner	Choi-Williams
Linear	**x**	**x**		**x**
Quadratic		**x**		
Mahalanobis			**MAX1_3D**	

Table 7.47: Summary Results central beams (three dimensional case)

Discriminant Function	Accuracy			
	Standard deconvolution method		FrFT method	
	Wigner	Choi-Williams	Wigner	Choi-Williams
Linear		**x**		
Quadratic		**x**		
Mahalanobis			**MAX2_3D**	**MAX2_3D**

Chapter 8 A Time-Frequency Method for Underwater Target Classification

Madalina Barbu, Edit J. Kaminsky, Russell E. Trahan*

Department of Electrical Engineering, *College of Engineering,

University of New Orleans, 2000 Lakeshore Dr., New Orleans, LA, 70148

William Sanders, Naval Research Laboratory,

Code 7400, Stennis Space Center, MS 39529

Abstract

This paper introduces a pattern recognition approach for buried target classification, based on a time-frequency technique. The proposed method is evaluated on synthetic data generated according to an acoustic scattering model for seven different sizes of cylindrical targets. The model generates the characteristic response of targets acquired by a parametric sonar system. The study is carried out for various scenarios of free field response of targets as well as for buried target responses. The proposed technique is based on the singular values of time-frequency representations of the impulse response. The features thus obtained are mapped in a reduced dimensional space, where various classification approaches are considered and their performance is compared.

Keywords:Pattern classification, time-frequency analysis.

8.1 Introduction

This paper addresses a challenging classification problem: underwater buried objects classification. The complexity of the problem comes from various factors such as the propagating medium, clutter caused by biological sources in the water column and from acoustic noise which in normal incidence-reflection is frequently higher than the amplitude of echoes reflected from the buried target of interest. The underwater classification problem involves finding a robust

classification algorithm with high accuracy that will automatically assign measurements into classes by projecting the signal into a favorable space and obtaining feature vectors from that space. Among the most used projection techniques are short time Fourier transform, principal component analysis (PCA), fractal analysis and spectra. Different classification approaches have been presented in the literature such as Bayesian classifiers, nonparametric techniques (nearest neighbor), hidden Markov models and neural networks (Duda *et al.* , 2004). A pattern recognition approach for classification of buried targets like cables from parametric sonar data is reported in this work. Parametric sonars (Westerwelt, 1957) are devices that can transmit acoustic signals in the water with a very narrow beam and almost no sidelobes. These characteristics cause the echo due to the backscattering from the seafloor surface to be separated in time from the echo due to the signal transmitted through the surface backscattered by the inhomogeneity in the seafloor sediment (Caiti *et al.* , 1999). In addition, the very low sidelobes of the parametric sonar makes it attractive for shallow water measurements because it prevents interference from unwanted boundary interactions (Hines, 1999). Parametric sonars have been used in an increasing number of applications, ranging from traditional seismic processing to more complex systems for object detection and classification (Woodward *et al.* , 1994a). Woodward and Lepper (Woodward & Lepper, 2003) report a study based on an open-water trial using a parametric sonar system with the aim of detecting and classifying embedded or partially embedded objects such as pipelines, lost cargo and mines. The main finding was that both specular reflections and resonance effects could be observed. Boulinguez et al. (Boulinguez *et al.* , 1998) proposed an adapted technology for a parametric sonar for obtaining a complete identification and localization of objects embedded in sediment. The parametric sonar is used to acquire 3D data on the subbottom area; wavelets are employed for eliminating the noise and high order spectra are used both to improve the range resolution and for classification. Further on Boulinguez and Quinquis (Boulinguez &

Quinquis, 2000) investigated object classification using features extracted from the entropy of the Wavelet packet coefficients and from fractal analysis. The authors of (Azimi-Sadjadi *et al.* , 2000) proposed a classification system that consists of a feature extractor using wavelet packets in conjunction with linear predictive coding, a feature selection scheme and a backpropagation neural network classifier. A multiaspect fusion scheme was also employed for improving the classification performance. Trucco et al. (Trucco, 2001) presented a pattern recognition method for the detection of buried objects. The beamformed signals are divided into partially overlapped frames and then projected in the time-frequency space. The features extracted and fed into a multivariate Gaussian classifier. The aim of this paper is to present a method for buried target classification based on joint time-frequency domain techniques that should be robust to the bottom sediment type. Of particular interest are long targets such as cables of various diameters, which need to be identified as different from each other and from strong reflectors or point targets. Synthetic test data are used to exemplify and evaluate our technique. Our results illustrate that the proposed algorithm provides a highly accurate way to classify buried objects. We begin by presenting the acoustical model used to produce the data, and the representation of the signal in time frequency domain. The singular value decomposition of the Wigner or Choi-Williams distribution of windowed-impulse response provides the discriminant features for classification. The features are mapped into a reduced dimensional space where the classification is carried out. We use three types of discriminant functions and evaluate their performance.

8.2 Theoretical Background

8.2.1 Acoustic Scattering Model

The analysis presented in this paper is based on the acoustic scattering model for elastic cylinder presented in (Stanton, 1988). In order to estimate the scattered field due to a cylinder of finite length, the volume flow per unit length of the scattered field of an infinitely long cylinder is integrated over a finite distance. Many scatterers posses elastic properties, so conversion of

compressional waves into shear waves has to be taken into account. The assumption made for the infinite cylinder is that there is no absorption, dispersion, or nonlinearity in the cylinder or the surrounding medium (Stanton, 1988). The scattering from ends of the cylinder is ignored, and the receiver-target separation must be great enough to be in the first Fresnel zone (i.e, $L << 2\sqrt{r\lambda}$, where L is the length of the cylinder or of the insonified "spot" of a longer cylinder, λ is the acoustic wavelength and r is the range from the axis of the cylinder to the receiver or field point). Stanton (Stanton, 1988) shows that taking into account arbitrary transmitter direction, receiver position and cylinder orientation, and assuming that $r >> L$, the expression of the scattered pressure is given by 8.1:

$$P_{scatter}(k) = -P_0 \frac{e^{ikr}}{r} \left(\frac{L}{\pi}\right) \frac{\sin(\Delta)}{\Delta} \sum_{m=0}^{\infty} \varepsilon_m \sin(\eta_m) \mathrm{e}^{-i\eta_m} \cos(m\phi) \tag{8.1}$$

where k is the acoustic wavenumber; P_o is the amplitude of the incident plane wave; r is the source-target separation; $\Delta = \frac{1}{2}kL(\overrightarrow{r_i} - \overrightarrow{r_r}) \cdot \overrightarrow{r_c}$, $\overrightarrow{r_r}$ the unit direction of receiver, $\overrightarrow{r_i}$ the unit direction of incident plane wave, $\overrightarrow{r_c}$ the unit direction of cylinder axis; ε_m is Neumann's number: $\varepsilon_0 = 1, \varepsilon_{m>0} = 2$; η_m is scattering phase angle; and ϕ is the azimuth angle of the arbitrarily oriented cylinder. In equation 8.1, $\frac{\sin(\Delta)}{\Delta}$ represents the beam pattern. If it is assumed to be Gaussian, the effective length insonified is given by $\widehat{L} = \sqrt{2\pi}\sigma e^{-s_0/2\sigma^2}$ where s_0 is the distance from the maximum response on the bottom to the closest point of approach of the cylinder. The following considerations have to be incorporated in the model: spherical spreading by replacing P_o by P_1/r, and the bottom effects. Assuming a flat bottom comprising a homogeneous lossy half-space with sound speed c_s and density ρ_s, (c_w is sound speed in water and ρ_w is density in water) the pressure is reduced by $T_{ws}T_{sw}e^{-2\alpha_s z_s}$. Here, $T_{ws} = 2\rho_s c_s/(\rho_w c_w + \rho_s c_s)$ is the normal incidence plane wave transmission coefficient from water to sediment and $T_{sw} = 2\rho_w c_w/(\rho_w c_w + \rho_s c_s)$ is the normal incidence plane wave transmission coefficient from sediment to water; α_s is the attenuation coefficient in sediment, and z_s is depth of the cylinder

below surface. The scattered pressure becomes:

$$P_{scatter}(k) = -P_1 T_{ws} T_{sw} \frac{e^{i(k_w r_w + k_s r_s(1+i\delta_s))}}{(r_w + r_s)^2} \left(\frac{\widehat{L}}{\pi}\right) \sqrt{2\pi}\sigma e^{-s_0/2} \sum\nolimits^2 \sum_{m=0}^{\infty} \varepsilon_m \sin(\eta_m) e^{-i\eta_m} \cos(m\phi) \tag{8.2}$$

where k_w and k_s are the wavenumbers in the water and sediment, respectively, r_w and r_s define the path lengths in water and in the sediment, and $\delta_s = \alpha_s / k_s$. The solution is for continuous wave signals of infinite duration. For a band-limited, finite duration pulse, a time series can be created from Fourier synthesis of solutions over a discrete range of wavenumbers k_n, $n = 0, 1, ..., N$. The impulse response for the jth sample of the time series is given by:

$$h_{scatter}(t_j) = \frac{2\pi f_s}{N^2 c_s} \sum_{n=n_{\min}}^{n=n_{\max}} P_{scatter}(k_n) e^{2\pi i (j-1)(n-1)} \tag{8.3}$$

where $n_{\min}$ and $n_{\max}$ are determined from the upper and lower frequency band.

8.2.2 Time-Frequency Analysis

Time-frequency methods are powerful tools for studying variations in spectral components. The spectrum's time dependency of the return signal could be a strong indicator of the target acoustic signature. The generalized time-frequency representation can be expressed in term of the kernel $\varphi(\theta, \tau)$, which determines the properties of the distribution (Mecklenbrauker & F.Hlawatsch, 1997):

$$C(t, \varpi) = \frac{1}{4\pi^2} \int\int\int f^*(u - \tau/2) f(u + \tau/2) \varphi(\theta, \tau) e^{-j\theta t - j\tau\varpi + ju\theta} du d\tau d\theta \tag{8.4}$$

The Wigner distribution can be derived from the generalized time-frequency representation for the unity value of the kernel:

$$W(t, \varpi) = \frac{1}{2\pi} \int f^*(u - \tau/2) f(u + \tau/2) e^{-j\tau\varpi} d\tau \tag{8.5}$$

The Wigner distribution function is a time-frequency analysis tool that can be used to illustrate the time-frequency properties of a signal, and it can be interpreted as a function that indicates the distribution of the signal energy over the time-frequency space. One disadvantage of the Wigner distribution is that it sometimes indicates intensity in the regions where one would expect zero

values. This effect can be minimized by choosing a kernel that has the form $\varphi(\theta,\tau) = e^{-\theta^2\tau^2/\sigma}$, which yields the Choi-Williams distribution:

$$C(t,\varpi) = \frac{1}{4\pi^{3/2}} \int\int \frac{1}{\sqrt{\tau^2/\sigma}} f^*(u-\tau/2) f(u+\tau/2) e^{-\sigma(u-t)^2/\tau^2 - j\tau\varpi} du d\tau \qquad (8.6)$$

Choosing this kernel, the marginals are satisfied and the distribution is real. In addition, if the σ parameter has a large value, the Choi-Williams distribution approaches the Wigner distribution, since the kernel approaches one. For small σ values, it satisfies the reduced interference criterion.

8.3 Proposed Techniques and Experimental Results

The proposed technique is based on a pattern recognition approach and includes a representation of the target impulse response in the time-frequency domain. The singular value decomposition of the Wigner distribution as well as of the Choi-Williams distribution of the impulse response is next applied. This way, the discriminant features for classification are achieved due to the fact that the singular value spectrum encodes the relevant features of the signal. These features are mapped in a reduced (3D) dimensional space. Three types of discriminant functions, namely linear, quadratic and Mahalanobis, are used. Various experiments are employed for investigating the performance of the proposed target classification method. The shape of the targets is assumed to be cylindrical. In our simulation we used seven target radii: $ra_1 = 1.25$ cm, $ra_2 = 1.5$ cm, $ra_3 = 1.8$ cm, $ra_4 = 2$ cm, $ra_5 = 2.3$ cm, $ra_6 = 2.7$ cm, and $ra_7 = 3$ cm which are the seven classes, class 1 through class 7. The following parameters were initially set: the sound velocity in water $c_w = 1500$ m/s, the depth of the water 10 m, sound velocity in the sediment $c_s = 1475$ m/s, the burial depth in the sediment was 25 cm, the beam width $BW = 2^o$, and nineteen steps each of $\Delta = 0.02$ m along track. The first scenario simulated considers the free field while the next one simulates a muddy bottom. In the free field case we perform five experiments. In the first experiment we consider a cylinder for which the compressional velocity is $c_c = 3100$ m/s and then for the second experiment $c_c = 2800$ m/s. The target is assumed to be at a depth of 25

cm in water. The simulation is performed in nineteen steps for seven classes. In order to obtain a supervised classification we use a training data set of seventy vectors that correspond to ten odd steps for each of the seven classes. For the testing data set we use sixty-three vectors from the other even nine steps. Each 3-D feature vector is composed of the 3 largest singular values. The performances of the various classifiers for the first four experiments are presented in Table 8.1

Table 8.1: Classification accuracy for experiments 1 through 4

	Accuracy Linear, [%]		Accuracy Quadratic, [%]		Accuracy Mahalanobis, [%]	
	Wigner	Choi-Williams	Wigner	Choi-Williams	Wigner	Choi-Williams
Exp 1	71.4	82.25	100	100	100	100
Exp 2	74.6	57.1	100	100	100	100
Exp 3a	84.76	84.76	100	100	100	100
Exp 3b	82	80	100	100	100	100
Exp 3c	83	80	100	100	100	100
Exp 4a	82.62	87.62	100	100	100	100
Exp 4b	81.9	87.62	100	100	100	100
Exp 4c	81.9	85.71	97.14	100	97.14	100

The quadratic and Mahalanobis based classifiers show similar high accuracies comparing to the linear based classifier for both Wigner and Choi-Williams distributions. In the third experiment the classifiers were trained with 105 vectors of data from the free field at a burial depth of 25 cm and then tested with an equal size set of data corresponding for three burial depth conditions: 15 cm, 35 cm and 50 cm. The experimental results for the three burial depths are presented in Table 8.1, Exp 3a, 3b and 3c. In the fourth experiment the variation of the environmental conditions such as salinity, water temperature is reflected in the variation of the sound velocity in water c_w = 1520 m/s, 1535 m/s and 1550 m/s. The sound velocity in the water for the training data set was 1500 m/s. The sizes of training and testing data sets are equal to 105 vectors. The experimental results are shown in Table 8.1 , Exp 4a, 4b and 4c. The quadratic and Mahalanobis classifiers tested in free field presented a very good robustness comparing to the linear classifier to the changes in the environmental conditions and burial depth. The sensitivity of the algorithm

with the target material was tested in experiment 5. In this experiment, for the free field data the size of the training and testing data was 133 vectors. The target sound velocity for the training data set was c_c=2800 m/s. We use the same depth and three different types of the materials (corresponding to the sound velocities $c_c = 2775$ m/s, 2750 m/s, and 2725 m/s) for the underwater target in order to test the sensitivity to the target material. The experimental results are presented in Figure 8.1, where the quadratic based classifier achieved the best accuracy for both Wigner and Choi-Williams distributions comparing to the competing classification techniques. However, the quadratic classifier outperfoms by about 1 % the Mahalanobis classifier. An evaluation of the proposed classification technique for targets buried in sediment using free field target response data for training and mud target response data for testing are considered in the experiments 6 and 7, where the buried cylinder (corresponding to $c_c = 2800$ m/s) is positioned at two different depths: 15 cm and 25 cm, respectively. The classification results are illustrated in Figure 8.2 . Both the quadratic and the Mahalanobis based classifiers show considerably higher accuracy than the linear classifier, for both the Wigner and Choi-Williams distributions. The classification accuracy is higher for the Choi-Williams distribution versus the Wigner distribution, and degrades as the burial depth increases.

8.4 Conclusions

The classification method presented in this paper is based on feature extraction from a couple of time-frequency distributions (Wigner and Choi-Williams) of the target impulse response. The discriminant features for classification are the 3 most significant singular values of the time-frequency distribution. Three classification approaches were employed each with a different discriminant function.

The quadratic and Mahalanobis based classifiers show, on average, similar accuracy but superior to the linear classifier under various scenarios. High accuracy of the proposed method is obtained even when the environmental conditions and the depth of the buried target are varied.

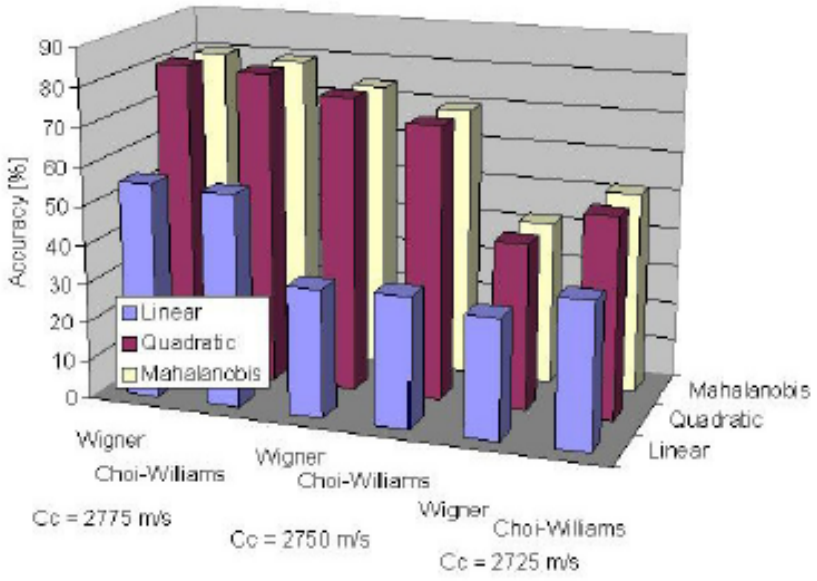

Figure 8.1: Classification accuracy for experiment 5

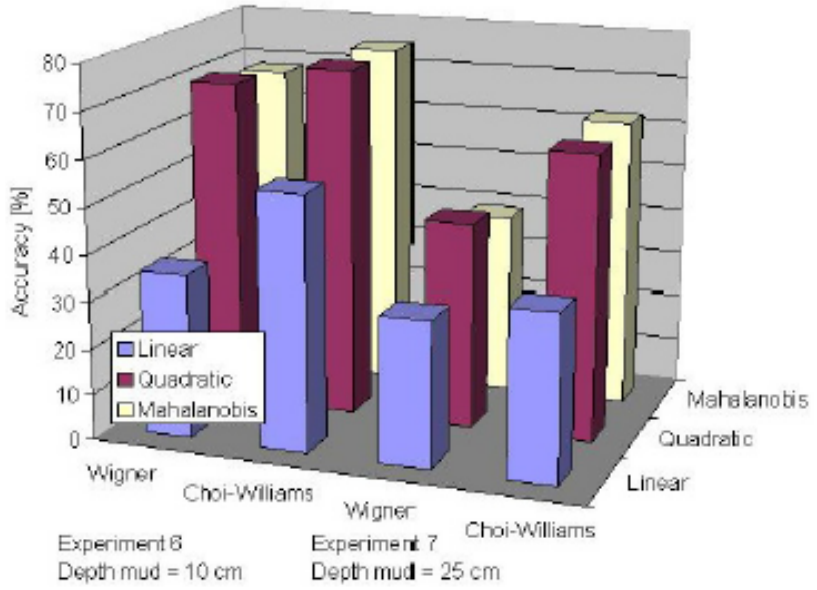

Figure 8.2: Classification accuracy for experiments 6 and 7

An important characteristic of this method is that good classification accuracy (around 75 %) of an unknown target (of various materials and buried at various depths) is achieved having only the response of a known target in the free field. A higher classification accuracy is expected for larger differences in target sizes.

Chapter 9 Conclusions

This dissertation is focused on developing an algorithm for seafloor bottom classification as well as for buried target classification using acoustic backscattered signals. The novel approach for feature extraction is based on time-frequency techniques that give a representation of the signal that lead to a good discrimination of the patterns. The technique introduced in this work employs the Fractional Fourier Transform (FrFT) in order to compute the seafloor impulse response. The FrFT is better suited for chirp sonar applications because it uses linear chirps as basis functions; it has a great potential in sonar signal processing. The work also presents the classical method for determining the bottom impulse response based on frequency domain deconvolution. The two methods are tested and compared on synthetic as well as on real data collected by the Volume Search Sonar (VSS). The final classification into sediment classes is based on singular value decomposition of the time-frequency distribution applied to the impulse response obtained using the FrFT. The set of singular values represents the desired feature vectors that describe the properties of the signal, and therefore the object being classified.

A real data set of small size is used for testing the proposed algorithm as a proof of concept. In that case, the classification has proved to be very effective for the ten central beams, five beams fore and five beams aft, near nadir. The angle between the beams across track is around 7.2 deg. The separation between the two classes, sand and mud, using our FrFT method is approximately 50% wider than when classical deconvolution and the Wigner distribution are used. When fourteen beams (seven fore and seven aft) are considered, the classification performance decreases by a small percentage. When the deconvolution method is employed, the sediment classes are not linearly separable, and the standard deviation of the class points is greater by approximately 10% compared to the case when the FrFT is used. In order to evaluate the performance of the

proposed algorithm and its dependency of transform chosen, the Choi-Williams distribution is also used. When the FrFT method is employed together with the Choi-Williams distribution, the separation between the two classes, sand and mud, is approximately 60% wider than when classical deconvolution is used. For the small data set used, the separation between the classes is wider when the Choi-Williams distribution is used than that when the Wigner distribution is employed. The new algorithm is compared to a k-means-based technique where wavelets were used for feature extraction. The accuracy of the sediment classification when k-means is used is improved by approximately 5% when the impulse response is determined via the FrFT rather than via a classical deconvolution method, again confirming the improvement produced by choosing FrFT or standard deconvolution methods

The algorithm is also evaluated for sediment classification on additional real data sets recently released by the Naval Research Laboratory. The data were collected by the same VSS sonar during a mission in the Gulf of Mexico. Three discriminant functions are compared in the final classification step of the proposed classification method: namely, Fisher's linear, quadratic and Mahalanobis discriminants. An evaluation of the algorithm's performance has been carried out for two different dimensions of the feature space (two singular values and three singular values from the time-frequency distribution extracted, respectively). The VSS field data show a large ping-to-ping variability. Therefore two structures of the data sets are used as follows: four data sets in which two nadir beams (fore and aft nadir beams) per ping are employed, and three data sets that include ten central beams (five fore beams and five aft beams) per ping.

When the two largest singular values are extracted from the time-frequency distributions and used as features, the following observations are drawn.

For data sets with nadir beams only, with a linear discriminant function, the standard deconvolution method performs better by almost 5% in terms of classification accuracy than

the FrFT when the Wigner distribution is employed. When the Choi-Williams distribution is used, both methods achieve, on average, almost the same accuracy for linear discriminants. Further, when the quadratic discriminant function is used for classification based on the Wigner distribution, the FrFt method gives better accuracy than the classical deconvolution method by about 7%. Using the Choi-Williams distribution, the deconvolution method performed best for quadratic discriminants. When the Mahalanobis discriminant function is used, the FrFT method leads if the Wigner distribution is used, and gives similar or better classification results than the deconvolution method when the Choi-Williams distribution is employed.

For the ten central beams data sets the standard deconvolution method performs better than the FrFT method for both Wigner and Choi-Williams distribution, for the linear discriminant function. The quadratic discriminant function together with the FrFT provide the best accuracy for both distributions. The FrFT method shows the best performance when the Mahalanobis discriminant function is employed for classification based on the Wigner or Choi-Williams distributions.

In conclusion, when two singular values are used, the highest classification accuracy is achieved when the combination FrFT/Wigner distribution/Mahalanobis discriminant function is employed. One can notice the following when the three highest singular values are extracted from the time-frequency distributions and used as features. For the nadir beams only, for the linear discriminant function and Wigner distribution, the standard deconvolution method gives the same or better accuracy than the FrFT method. When the Choi-Williams distribution is employed, the FrFT method produces higher classification accuracy than the deconvolution method for the linear discriminant. When the quadratic discriminant function is used the FrFT method gives a higher accuracy than the deconvolution method by around 4% in the case of the Wigner distribution. For the quadratic discriminant, a better accuracy than the FrFT method has been obtained for the deconvolution method on most of the data sets when the Choi-Williams distribution was

employed. The best accuracy among all nadir beams data sets is obtained for the FrFT method when the Mahalanobis discriminant function with the Wigner distribution is used.

For the central beams data sets, when the linear discriminant function is used, the deconvolution method performs better than the FrFT method for both the Wigner and Choi-Williams distributions. The FrFT method shows a better performance than the deconvolution method when the quadratic discriminant function is employed with the Wigner distribution. Applying the quadratic discriminant function with the Choi-Williams distribution, a similar or better performance than the FrFT method has been achieved for the standard deconvolution method.

The FrFT method achieved, on average, the best performance when the Mahalanobis discriminant function is employed on most of the data sets with central beams. The confusion matrices show that the mud sediment is easier to classify than sand. That can be explained by the fact that the sand sediment geological structure was not uniform (higher ping-to-ping variability) in the area where the data were collected. More specifically, there were mud inclusions within the sand sediment area.

The performance of the proposed classification technique is evaluated on synthetic data sets, simulated for buried targets detected by parametric sonar. Seven cylindrical targets with various diameters are considered in several different testing scenarios.

The method used for buried target classification is similar to that used for sediment classification, but in this case the target impulse response is known (simulated). High accuracy of the proposed method is obtained even when the environmental conditions and the depth of the buried target are varied. An important characteristic of this method is that good classification accuracy (around 75%) of an unknown target (of various materials and buried at various depths) is achieved having only the simulated response of a known target in the free field. Higher classification accuracy is expected for targets with large difference in sizes (radius).

A recommended procedure for *target classification* is based on a combination of the Choi-Williams distribution with either Mahalanobis or quadratic discriminant functions using the three highest singular values as features, when the target impulse response is given.

The author's recommendation for *sediment classification* is to use the combination FrFT/Wigner distribution/Mahalanobis discriminant function using two singular values as features. When only nadir beams are used the classification accuracy is, again, higher than when central beams are used.

In this dissertation the author develops a feature extraction method based on the FrFT and time-frequency representations that improve the performance of the acoustic seabed and buried target classification. The FrFT method enhances the seafloor impulse response, and hence higher classification accuracy is achieved when used in combination with Mahalanobis classifier. In addition, the novel proposed algorithm shows classification robustness under various scenarios.

References

Akay, O. 2002. Fractional Convolution and Correlation: Simulation Examples and an Application to Radar Signal Detection. *Proceedings of the 5th Nordic Signal Processing Symposium NORSIG-2002, Hurtigruten from Tromsø to Trondheim, Norway*.

Aridgides, A., Libera, P., Fernanades, M., & Dobeck, G.J. 1996. Adaptive Filter/ Feature Orthogonalization Processing String for Optimal LLRT Mine Target Classification in Side-Scan Sonar Imagery. *Proceedings of SPIE, Detection and Remediation Technologies for Mines and Mine Like Targets, Orlando, FL*, **2765**, 110–121.

Azimi-Sadjadi, M. R., Huang, Q., & Dobeck, G. J. 1998. Underwater Target Classification using Multiaspect Fusion and Neural Networks. *Proceedings of SPIE International Symposium Aerospace/Defense Sensing Controls, Orlando, FL*, 334–341.

Azimi-Sadjadi, M. R., Yao, D., Huang, Q., & Dobeck, G. J. 2000. Underwater Target Classification using Wavelet Packets and Neural Networks. *IEEE Transactions on Neural Networks*, **11**(3), 784–794.

Baan, M., & Jutten, C. 2000. Neural Networks in Geophysical Applications. *Geophysics*, **65**(4), 1032–1047.

Baggeroer, A. B., Kuperman, W. A., & Mikhalevsky, P. N. 1993. An Overview of Matched Field Methods in Ocean Acoustics. *IEEE Journal of Oceanic Engineering*, **18**(4), 401–424.

Baldacci, A., & Haralabus, G. 2006. *Signal Processing for an Active Sonar System Suitable for Advanced Sensor Technology Applications and Environmental Adaptation Schemes*. Viale San Bartolomeo 400, 19138 La Spezia, Italy: NATO Undersea Research Center.

Barad, H., Martinez, A. B., Bourgeois, B. S., & Kaminsky, E. J. Spring 2003. Acoustical Boundary Location through Texture Analysis of Multibeam Bathymetric Sonar Data. *Marine Technology Society Journal*, **27**(1), 24–30.

Barbu, M., Kaminsky, E., & Trahan, R.E. 2005a. Fractional Fourier Transform for Sonar Signal Processing. *Proceedings of the Oceans 2005 MTS/IEEE Conference, Washington, DC*.

Barbu, M., Kaminsky, E., & Trahan, R.E. 2005b. Sonar Signal Enhancement using Fractional Fourier Transform. *Proceedings of the SPIE Defense and Security Symposium, Automatic Target Recognition XV, Orlando, FL*, **5807**, 170–177.

Barbu, M., Kaminsky, E., & Trahan, R.E. 2006a. Acoustic Seabed Classification using Fractional Fourier Transform. *Proceedings of the SPIE Defense and Security Symposium, Detection and Remediation Technologies for Mines and Minelike Targets XI, Orlando, FL*, **6217**.

Barbu, M., Kaminsky, E., & Trahan, R.E. 2006b. Acoustic Seabed Classification using Fractional Fourier Transform and Time-Frequency Transform Techniques. *Proceedings of the Oceans 2006 MTS/IEEE Conference, Boston, MA*.

Barbu, M., Kaminsky, E., & Trahan, R.E. 2007. A Time-Frequency Method for Underwater Target Classification. *Submitted to the IEEE International Conference on Acoustics, Speech, and Signal Processing, Honolulu, HI*.

Bastiaans, M. J., & Alieva, T. 2005. Wigner Distribution Moments Measured as Intensity Moments in Separable First-Order Optical Systems. *EURASIP Journal on Applied Signal Processing*, **10**, 1535–1540.

Berry, M. V. 1973. The Statistical Properties of Echos Diffracted from Rough Surfaces. *Philosophical Transactions of the Royal Society of London*, **273**, 611–654.

Bing, D., Ran, T., Lin, Q., & Feng, L. 2003. A New Method of Anti-Reverberation via Fractional Fourier Transform. *Proceedings of IEEE International Conference on Neural Networks and Signal Processing, Nanjing, China*, 1379–1381.

Boulinguez, D., & Quinquis, A. 2000. Entropy and Fractal Analysis for Underwater Object Classification. *Proceedings of 5th European Conference on Underwater Acoustics, Lyon, France*, **XXIV**, 1103–1108.

Boulinguez, D., Quinquis, A., & Brussieux, M. 1998. Classification of Buried Objects using a Parametric Sonar. *Proceedings of Oceans 1998 MTS/IEEE Conference, Nice, France*, **1**, 1264–1268.

Burdic, W. S. 1984. *Underwater Acoustic System Analysis*. Englewood Cliffs, NJ: Prentice-Hall.

Caiti, A., Bergem, O., & Dybedal, J. 1999. Parametric Sonars for Seafloor Characterization. *Measurement Science and Technology*, **10**, 1105–1115.

Capus, C., & Brown, K. 2003. Fractional Fourier Transform of the Gaussian and Fractional Domain Signal Support. *IEE Proceedings - Vision Image Signal Process.*, **150**(2), 99–106.

Capus, C., Linnett, L., & Rzhanov, Y. 2000. *The Analysis of Multiple Linear Chirp Signal*. Savoy Place, London, UK: IEE.

Coetmellec, S., Brunel, M., Lebrun, D., & Ozkul, C. 2001. Characterization of Chirped Pulses with the Fractional-Order Fourier Transformation. *Journal of Optical Society of America*, **18**(11), 2754–2759.

Cohen, L. 1995. *Time Frequency Analysis*. NY: Prentice Hall.

Cook, J. C., Goodson, A. D., Lepper, P. A., & Woodward, B. 1997. The Design and Evaluation of a Phase - Steering Parametric Sonar Systems intended for Sediment Characterisation. *Underwater Technology*, **22**(2), 43–54.

de Moustier, C. 1986. Beyond Bathymetry: Mapping Acoustic Backscattering from the Deep Seafloor with Sea Beam. *Journal of Acoustic Society of America*, **79**(2), 316–331.

de Moustier, C. 2000. Seafloor Classification. *OMG Coastal Multibeam Training Course*.

Djurovic, I., Stankovic, S., & Pitas, I. 2001. Digital Watermarking in the Fractional Fourier Transform Domain. *Journal of Network and Computer Applications*, **24**, 167–173.

Dobeck, G.J. 2005. A Probabilistic Model for Score based Algorithm Fusion. *Proceedings of Oceans 2005 MTS/IEEE Conference, Washington, DC*, 212–219.

Dobeck, G.J., Hyland, J. C., , & LeDrrick, S. 1997. Automated Detection / Classification of Sea Mines in Sonar Imagery. *Proceedings of SPIE, Detection and Remediation Technologies for Mines and Mine Like Targets, Orlando, FL*, **3079**, 90–108.

Donghui, L., Azimi-Sadjadi, M. R., & Robinson, M. 2004. Comparison of Different Classification Algorithms for Underwater Target Discrimination. *IEEE Transactions on Neural Networks*, **15**(1), 189–194.

Duda, R. O., Hart, P. E., & Stork, D. G. 2004. *Pattern Classification*. China Machine Press.

Dybedal, J. 1993. TOPAS: Parametric End-Fire Array used in Offshore Applications. *Advances in Nonlinear Acoustics, Singapore: World Scientific*.

Erden, M. F., Kutay, M. A., & Ozaktas, H. M. 1999. Repeated Filtering in Consecutive Fractional Fourier Domains and Its Application to Signal Restoration. *IEEE Transactions on Signal Processing*, **47**(5), 1458–1462.

Feranadez, J. E., & Christoff, J. T. 2000. Multi-aspect Synthetic Aperture Sonar. *Proceedings of Oceans 2000 MTS/IEEE Conference, Providence, RI*, **1**, 177–184.

Foote, K. G., & Francis, D. T. I. 2005. Scheme for Parametric Sonar Calibration by Standard Target. *Proceedings of Oceans 2005 MTS/IEEE Conference, Washington, DC*, **2**, 1409–1414.

Guyonic, S. 2000. Buried Objects Detection and Classification with a 3-D Parametric Sonar. *Journal of Acoustic Society of America*, **108**(5), 2649–2658.

Heald, G. J., & Pace, N. G. 1996. An analysis of 1st and 2nd Backscatter for Seabed Classification. *Proceedings of 3rd European Conference on Underwater Acoustic, Heraklion, Greece*, 649–654.

Heald, G. J., & Pace, N. G. June, 1998. Implications of Bi-static Treatment for the Second Echo from a Normal Incidence Sonar. *Proceedings 16th International Congress on Acoustics and 135th Meeting Acoustical Society of America, Seattle, WA*, **IV**, 3009–3010.

Hennelly, B., & Sheridan, J. T. 2003a. Fractional Fourier Transform - based Image Encryption: Phase Retrieval Algorithm. *Optics Communications*, **226**, 61–80.

Hennelly, B., & Sheridan, J. T. 2003b. Image Encryption and the Fractional Fourier Transform. *Optik*, **114**, 251–265.

Hines, P. C. 1999. Quantifying Seabed Properties in Shelf Water using a Parametric Sonar. *Measurement Science and Technology*, **10**(12), 1127–1134.

Hlawatsch, F., & Bourdeaux-Bartels, G. F. 1992. Linear and Quadratic Time-Frequency Signal Representations. *IEEE Signal Processing Magazine*, **9**, 21–67.

Jackson, D. R., & Nesbitt, E. 1988. Bottom Classification using Backscattering at Vertical Incidence. *Journal of Acoustic Society of America*, **83**(S1), S80.

Jackson, D. R., Winerbrener, D., & Ishimaru, A. 1986. Application of the Composite Roughness Model to High-Frequency Bottom Backscattering. *Journal of Acoustic Society of America*, **79**(5), 1410–1422.

Kaminsky, E. J. 2002. *Processing VSS Data for Ocean Bottom Sediment Classification*. Stennis Space Center, MS: ASEE Fellowship Technical Report, Naval Research Laboratory.

Kaminsky, E. J. 2005. *Accurate Detection and Classification Algorithms for PARADISE*. Stennis Space Center, MS: Technical Report, NRL Grant N00573-06-01-G902,Naval Research Laboratory.

Kundu, A., Chen, G. C., & Persons, C. E. 1994. Transient Sonar Signal Classification using Hidden Markov Models and Neural Nets. *IEEE Journal of Oceanic Engineering*, **19**(1), 87–99.

Kutay, M. A., & Ozaktas, H. M. 1998. Optimal Image Restoration with the Fractional Fourier Domain. *Journal of Optical Society of America*, **15**, 825–833.

Kutay, M. A., Ozaktas, H. M., Onural, L., & Arikan, O. 1995. Optimal Filtering in Fractional Fourier Domain. *Proceedings IEEE International Conference on Acoustics, Speech, Signal Processing, Piscataway, NJ*, 937–940.

Kutay, M. A., Ozaktas, H. M., Arikan, O., & Onural, L. 1997. Optimal Filtering in Fractional Fourier Domain. *IEEE Transactions on Signal Processing*, **45**, 1129–1143.

LeBlanc, L. R., Mayer, L., Rufino, M., & King, J. 1992. Marine Sediment Classification using the Chirp Sonar. *Journal of Acoustic Society of America*, **91**(1), 116–126.

Lenon, M., & McLaughlin, S. 2002. Analyzing Sonar Data using Fractional Fourier Transform. *Proceedings of the 5th Nordic Signal Processing Symposium NORSIG-2002, Hurtigruten from Tromsø to Trondheim, Norway*.

Levenon, M.J., & McLaughlin, S. 2002. Analysing Sonar Data Using Fractional Fourier Transform. *Proceedings of the 5th Nordic Signal Processing Symposium NORSIG-2002, Hurtigruten from Tromsø to Trondheim, Norway*.

Lin, Q., Ran, T., Siyong, Z., & Yue, W. 2004. Detection and Parameter Estimation of Multicomponent LFM Signal based on the Fractional Fourier Transform. *Science in China Series F-Information Sciences*, **47**(2), 184–198.

Lurton, X. 2002. *An Introduction to Underwater Acoustics - Principles and Applications*. Springer.

Lurton, X., & Pouliquen. 1992. Sea-bed Identification using Echosounder Signal. *Proceedings*

of European Conference on Underwater Acoustic, **Elsevier Applied Science, New York, NY**, 317–321.

Mahale, V., Chakraborty, B., Navelkar, G., & Desai, R. P. 2005. Seafloor Classification using Artificial Neural Network Architecture from Central Western Continental Shelf of India. *Acoustical Society of America Journal*, **117**(4), 2441–2442.

Marinovich, N.M., & Eichmann, G. 1985. An Expansion of the Wigner Distribution and its Applications. *Proceedings of IEEE International Conference on Acoustics, Speech and Signal Processing, Tampa, FL*, **3**, 1021–1024.

Mecklenbrauker, W., & F.Hlawatsch. 1997. *The Wigner Distribution. Theory and Applications in Signal Processing*. Elsevier.

Miao, X., Azimi-Sadjadi, M. R., Tian, B., Dubey, A. C., & Witherspoon, N. H. 1998. Detection of Mine and Minelike Targets using Principal Component and Neural-Network Methods. *IEEE Transactions on Neural Networks*, **9**(3), 454–463.

Muir, T. G. 1974. Nonlinear Parametric Transduction in Underwater Acoustics. *Proceedings of Ultrasonics Symposium, Milwaukee, WI*, 603–612.

Musha, T., Uchida, H., & Nagashima, M. 2002. Self-Monitoring Sonar Transducer Array with Internal Accelerometers. *IEEE Journal of Oceanic Engineering*, **27**(1), 28–34.

Namias, V. 1980. The Fractional Order Fourier and its Application to Quantum Mechanics. *J. Inst. Math. Applicat.*, **25**, 241–265.

Neudorfer, M., Kosalos, J., & Bonneau, R. 2000. Results of Synthetic Amperture Sonar Experiments. *Proceedings of Oceans 2000 MTS/IEEE Conference, Providence, RI*, **1**, 323–330.

Nielsen, R. O. 1991. *Sonar Signal Processing*. London: Artech House.

Novarini, J. C., & Caruthers, J. W. 1998. A Simplified Approach to Backscattering from a Rough Seafloor with Sediment Inhomogeneities. *IEEE Journal of Oceanic Engineering*, **23**(3), 157–199.

Ozaktas, H. M., Barshan, B., & Mendlovic, D. 1994. Convolution and Filtering in Fractional Fourier Domain. *Optics Review*, **1**, 15–16.

Ozaktas, M. H, & Arikan, O. 1996. Digital Computation of the Fractional Fourier Transform. *IEEE Transactions on Signal Processing*, **44**(9), 2141–2149.

Ozaktas, M. H, Zalevsky, Z., & Kutay, M. A. 2001. *The Fractional Fourier Transform with Applications in Optics and Signal Processing*. NY: John Wiley Sons.

Pace, N. G., & Ceen, R. V. 1982. Seabed Classification using the Backscattering of Normally Incident Broadband Acoustic Pulses. *Hydrographic Journal*, **26**, 9–16.

Pace, N. G., & Gao, H. 1988. Swathe Seabed Classification. *IEEE Journal of Oceanic Engineering*, **13**(2), 83–90.

Pei, S. C., & Ding, J. J. 2001. Relations between Fractional Operations and Time-Frequency Distributions, and Their Applications. *IEEE Transactions on Signal Processing*, **49**(8), 1638–1655.

Petillot, Y. R., Reed, S. R., & Bell, J. M. 2002. Real Time AUV Pipeline Detection and Tracking using Side Scan Sonar and Multi-Beam Echosounder. *IEEE*, 1234–1239.

Preston, J. M. 2005. Acoustic Seabed Classification with Multibeam and Sidescan Images. *Tutorial Oceans 2005 MTS/IEEE Conference, Washington, DC*.

Quinquis, A., Ioana, C., Frezza-Boin, K., & LeGac, J. C. 2003. On the Use of Time-Frequency Methods in the Oceanic Passive Tomography Context. *Proceedings of Oceans 2003 MTS/IEEE Conference, San Diego, CA*, **2**, 917–921.

Raytheon. 1999. *AN/WLD-1(V) Variable Depth Sensor (VDS) Subsystem*. 1847 West Main Road, Portsmouth, RI 02871: Raytheon, Defense Systems Segment, Naval and Maritime Systems, Portsmouth Operations.

Roitblat, H. L., Au, W. W. L., Nachtigall, P. E., Shizumura, R., & Moons, G. 1995. Sonar Recognition of Targets Embedded in Sediments. *Neural Networks*, **8**(7/8), 1263–1273.

Runkle, P. R., Bharadwaj, P. K., Couchman, L., & Carin, L. 1999. Hidden Markov Models for Multiaspect Target Classification. *IEEE Transactions on Signal Processing*, **47**(7), 2035–2040.

Schock, S. 2004. A Method for Estimating the Physical and Acoustic Properties of the Sea Bed Using Chirp Sonar Data. *IEEE Journal of Oceanic Engineering*, **29**(4), 145–149.

Schock, S. G., LeBlanc, L. R., & Mayer, L. 1989. Chirp Subbottom Profiler for Quantitative Sediment Analysis. *Geophysics*, **54**(4), 445–450.

Schock, S. G., A.Tellier, Wulf, J., Sara, J., & Ericksen, M. 2001. Buried Object Scanning Sonar. *IEEE Journal of Oceanic Engineering*, **26**(4), 677–689.

Shin, F. B., & Kil, D. H. 1996. Full-Spectrum Signal Processing using a Classify-Before-Detect Paradigm. *Journal of Acoustic Society of America*, **99**(4), 2188–2197.

Stanley, Z., Satrino, J. H., & Geneva, A. 1996. Development of the Physically-based Ocean Bottom Classification Analysis System using Multibeam Sonar Backscatter. *Proceedings of Oceans 1996 MTS/IEEE Conference, Fort Lauderdale, FL*, Sep, 1058–1063.

Stanton, T. K. 1984a. Sonar Estimates of Seafloor Microroughness. *Journal of Acoustic Society of America*, **75**(3), 809–818.

Stanton, T. K. 1984b. Volume Scattering: Echo Peak PDF. *Journal of Acoustic Society of America*, **75**(S1), 551–560.

Stanton, T. K. 1988. Sound Scattering by Cylinders of Finite Length. II. Elastic cylinders. *Journal of Acoustic Society of America*, **83**(1), 64–67.

Sternlicht, D., & de Moustier, C. P. 2003a. Remote Sensing of Sediment Characteristics by Optimized Echo-Envelope Matching. *Journal of Acoustic Society of America*, **114**(5), 2727–2743.

Sternlicht, D., & de Moustier, C. P. 2003b. Time dependent Seafloor Acoustic Backscatter (10-100kHz). *Journal of Acoustic Society of America*, **114**(5), 2709–2725.

Sternlicht, D., Lemons, D. W., Dikeman, R. D., Ericksen, M., & Schock, S. 2001. Detection and Classification of Buried Object by an Adaptive Acoustic Mine-Hunting System. *Proceedings of Oceans 2001 MTS/IEEE Conference, Honolulu, HI*, **3079**, 212–219.

Sternlicht, D., Thompson, A. W., Lemons, D. W., Dikeman, R. D., & Korporall, M. T. 2002. Image and Signal Classification for a Buried Object Scanning Sonar. *Proceedings of Oceans 2002 MTS/IEEE Conference, Biloxi, MS*, **3079**, 485–490.

Stewart, W., Chu, D., Malik, S., Lerner, S., & Singh, H. 1994. Quantitative Seafloor Characterization using Bathymetric Sidescan Sonar. *IEEE Journal of Oceanic Engineering*, **19**(4), 599–610.

Taroudakis, M., Tzagkarakis, G., & Tsakalides, P. 2006. Classification of Shallow-Water Acoustic Signals via Alpha-Stable Modeling of the One-dimensional Wavelet Coefficients. *Journal of Acoustical Society of America*, **119**(3), 1396–1405.

Trucco, A. 2001. Detection of Objects Buried in the Seafloor by a Pattern Recognition Approach. *IEEE Journal of Oceanic Engineering*, **26**(4), 769–782.

Trucco, A., & Pescetto, A. 2000. Acoustic Detection of Objects Buried in the Seafloor. *Electronics Letters*, **36**(18), 1595–1596.

Urick, R. J. 1975. *Principles of Underwater Sound*. New York, NY: McGraw-Hill.

Voronin, V. A., & Timoshenko, I.V. 1994. Location by Nonlinear Interaction of the Reflection Signals. *Proceedings of MTS/IEEE Oceans 1994 Conference, Brest, France*, **1**, 741–744.

Voronin, V. A., Tarasov, S. P., Timoshenko, I. V., & Anasov, V. I. 1994. Investigation of Hydrophysical Inhomogeneities by Parametric Acoustic Equipment. *Proceedings of MTS/IEEE Oceans 1994 Conference, Brest, France*, **1**, 741–744.

Westerwelt, P. J. 1957. Scattering of Sound by Sound. *Journal of Acoustic Society of America*, **29**(2), 199–203.

Wood, J. C., & Barry, D. T. 1994. Linear Signal Synthesis Using the Radon-Wigner Transform. *IEEE Transactions on Signal Processing*, **42**(8), 2107–2111.

Woodward, B., & Lepper, P. A. 2003. Acoustic Detection and Classification on Fluid filled Cylinders Embedded in Sediments. *Proceedings of Oceans 2003 MTS/IEEE Conference, San Diego, CA*, 1912– 1916.

Woodward, B., Goodson, A. D., Cook, J. C., & Lepper, P. A. 1994a. Acoustic Seabed Characteristics using Non -linear Acoustics. *Proceedings of 2nd European Conference on Underwater Acoustics, Copenhagen, Denmark*, **2**, 875–880.

Woodward, B., Goodson, A. D., Cook, J. C., & Lepper, P. A. 1994b. A Phase Steered Parametric Array for Sub Bottom Profiling. *Proceedings of 6th International Conference on Electronic Engineering in Oceanography, Cambridge, MA*, 77–82.

Yang, X., Tan, Q., Wei, X., Xiang, Y., Yan, Y., & Jin, G. 2004. Improved Fast Fractional Fourier Transform Algorithm. *Journal of Optical Society of America*, **21**(9), 1677–1681.

Yetik, I. S., & Nehorai, A. 2003. Beamforming using Fractional Fourier Transform. *IEEE Transactions on Signal Processing*, **51**(6), 1663 – 1668.

Yetik, I. S., Kutay, M. A., & Ozaktas, H. M. 2001. Image Representation and Compression with the Fractional Fourier Transform. *Optics Communications*, **197**, 275–278.

Appendix

Wednesday, November 22, 2006

William M. Sanders
NRL Code 7433
Stennis Space Center, MS 39529

To: Dr. Russell E. Trahan
Dean of Engineering
College of Engineering
University of New Orleans
New Orleans, LA 70148

Dear Dr. Trahan,

I hereby, grant approval for the article: "A TIME-FEQUENCY METHOD FOR UNDERWATER TARGET CLASSIFICATION", submitted to the *International Conference on Acoustics, Speech, and Signal Processing (ICASSP'07)* and co-authored with Madalina Barbu, to be used in her Ph D dissertation.

Sincerely, William M Sanders

Date: 11-22-06

Vita

The author was born in Ploiesti, Romania in 1969. She received a dual B.S. / M.S. degree in Physics in 1993 from the University of Bucharest. She has held a faculty position in the Department of Physics at the "Petroleum-Gas" University of Ploiesti in the period 1995 – 1997. She graduated with an M.S. degree in Electrical Engineering from the University of New Orleans in Fall, 2001.She received two summer internship awards from Office of Naval Research in 2003 with Naval Research Lab (Stennis Space Center, MS) and in 2005 with NAVAIR (Orlando, FL), respectively. She was enrolled as a gradute student with University of New Orleans, where she worked as a Research Assistant or Teaching Assistant during her Ph.D studies. Her research interests include sonar signal processing, image processing, pattern recognition and optics engineering.